Prevention of Medical Implant Infection through Self-Assembled Engineered Peptides as Surface Active Bio-Agents

By
E. Cate Wisdom
B.S. Chemical Engineering, University of New Mexico, 2011

Submitted to the graduate degree program in Bioengineering and the Graduate Faculty of the University of Kansas in partial fulfillment of the requirements for the degree of Doctor of Philosophy.

_____
Chair: Dr. Candan Tamerler, Ph.D.

_____
Cory Berkland, Ph.D.

_____
Suzanne Shontz, Ph.D.

_____
Malcolm Snead, D.D.S, Ph.D.

_____
Paul Arnold, M.D.

_____
Gibum Kwon, Ph.D.

Date Defended: 16 December 2019

The dissertation committee for E. Cate Wisdom certifies that this is the approved version of the following dissertation:

Prevention of medical implant associated infection through self-assembly of engineered bifunctional peptides with antimicrobial and titanium binding functions as surface active bio-agents

_____

Chair: Dr. Candan Tamerler

Date Approved: 16 December 2019

Abstract

Titanium medical implants have revolutionized health care in treating bone and joint degeneration, neoplasms and inflammation[1]. Due to their biocompatibility, mechanical strength, and non-corrosive properties, titanium and titanium alloys are among the most common materials used in medical and dental implants[2-5]. Despite improvements in implant technology, including prophylactic therapy, failure attributed to infection is as high as 7.5% of total hip arthroplasty, 14.8% of total knee arthroplasty[6,7], and 8% of dental implants[8-10]. In the first hours following surgery the implant surface is most vulnerable to bacterial colonization and the bacterial pathogens are also most susceptible to antimicrobial treatment[11,12]. We demonstrate the design and application of a bifunctional peptide film composed of a titanium anchoring domain linked to an antimicrobial peptide domain through an engineered spacer for prevention and treatment of medical implant infections. To overcome challenges with preserving anchoring and antimicrobial domain function, we propose a spacer design to reduce inter-domain interference and improve function based on understanding the peptide structure/function relationship. This innovative approach overcomes challenges faced with rising numbers of antibiotic resistance bacterial strains, by providing a localized and robust antimicrobial and antifouling effect. Our studies aim to enhance the bifunctional peptide design by incorporating different functional domains using a predictive design approach. Along with these studies, we designed peptides based upon structure-function relationship, characterized their individual functions, and proposed design criteria for effective surface functionalization of the peptide films. Finally, we test the proposed approach as a retreatment option for various stages of peri-implant disease, which is a major unsolved problem in dentistry leading to dental implant failure.

Table of Contents

CHAPTER 1 - Introduction to Thesis 1

CHAPTER 2 - Controlling the Biomimetic Implant Interface: Modulating Antimicrobial Activity by Spacer Design 4

Abstract 4

Introduction 6

Materials And Methods 9

Chimeric Peptide Design 9

Molecular Structure Modeling 10

Antimicrobial “Rule Induction” Method 10

Circular Dichroism (CD) Analysis 11

Bacterial Maintenance and Culturing 12

Antimicrobial Activity in Solution 12

Titanium Surface Preparation 13

Chimeric Peptide Coating on Surfaces 14

Antimicrobial Activity on Substrates 14

Host Cell Response 15

Results and Discussion 16

Computational structure and function predictions 18

Structure determination with CD 21

Chimeric Peptide Function 23

Antimicrobial Effect in Solution 23

Antimicrobial Effect on Surfaces 25

Host Cell Attachment and Viability 29

Conclusion 33

Supplementary Information 35
CHAPTER 3 – Mitigation of Peri-Implantitis by Design and Stability of Bifunctional Peptides with Antimicrobial Properties 38
Abstract 38
Introduction 40
Materials and Methods 45
Peptide Synthesis, Purification, and FITC-Derivatization 45
Peptide Property Calculations 46
Peptide CD Data Collection and Secondary Structure Prediction 46
Peptide Structure Analysis 47
Titanium Implant Disc Preparation 48
Peptide Binding to Implant Discs 49
Determination of Surface Coverage 49
Serum Competition Assay 50
Mechanical Durability Assay 50
Bacteria Culture 51
Visualizing Bacteria on Implant Discs 51
Statistical Analysis 51
Results and Discussion 52
Design by Structure Prediction from Amino Acid Sequence 52
Design by Hydrophobicity and Amphipathicity 55
Dynamics Prediction in Bifunctional Peptide Design 57
Secondary Structure Modeling and Analysis 58
Experimental Determination of Secondary Structure 60

Theoretical Surface Coverage Determination 63
Evaluation of Binding, Stability and Durability 64
Bifunctional Activities of the Designed Peptides 67
Conclusion 72
Supplementary Information 74
CHAPTER 4 - Repeatedly Applied Peptide Film Kills Bacteria on Dental Implant 76
Abstract 76
Introduction 78
Materials and Methods 81
Synthesis and Purification of Bifunctional Peptides 81
Minimum Inhibitory Concentration (MIC) 82
Titanium Implant Disc Preparation 82
Bacterial Culture and Maintenance 82
Bifunctional Peptide Binding on Titanium Discs 83
Fluorescent Imaging for Peptide Binding 83
Peptide Film Antibacterial Function on Titanium Discs 83
Implant Disc Cleaning for Rebinding 84
Retreatment Cycle Binding and Reapplication 84
Surface Profilometry 85
De Novo Peptide Structure Prediction and 3D Model Generation 85
3D Model Visualization and Recoloring 86
Results 86
Antibacterial Activity in Solution 86
Implant Disc Preparation and Cleansing 87

Binding and Re-binding of the Bifunctional Peptide 88
Antibacterial Functionalization on Implant Discs 88
Retreatment Cycle Binding and Reapplication 88
De Novo Secondary Structure Generation 90
Titanium Disc Surface Topography 91
Discussion 94
In Solution Antibacterial Activity 94
Binding and Re-binding of the Bifunctional Peptide 95
Antibacterial Functionalization on Implant Discs 96
Retreatment Cycle Binding and Reapplication 97
De Novo Secondary Structure Generation 97
Titanium Disc Surface Topography 98
Conclusion 98
CHAPTER 5 – Conclusion 100
References 108
Appendix A - Publications, Patents, and Presentations 117
Publications 117
Patents 117
Conferences and Presentations 118

List of Figures

Figure 2-1: Lowest energy structures modeled in solution 19

Figure 2-2: CD spectrum for TiBP-Spacer5-AMP 22

Figure 2-3: Fluorescent microscope images of *S. mutans* bacteria 26

Figure 2-4: Fluorescent microscope images of *S. epidermidis* bacteria 27

Figure 2-5: Fluorescent images of NIH/3T3 fibroblast attachment on titanium foils 31

Figure 2-6: Fluorescent images of NIH/3T3 fibroblast attachment on titanium implants 32

Figure 2-7: NIH/3T3 fibroblast metabolism on titanium foils and implants 33

Figure 2-8: Ramachandran Plot of TiBP-Spacer3-AMP 35

Figure 2-9: Ramachandran Plot of TiBP-Spacer5-AMP 36

Figure 3-1: Helical wheel predictions of bifunctional peptides. 56

Figure 3-2: DynaMine classification for backbone dynamics 57

Figure 3-3: Secondary structure models and structural similarity analysis 59

Figure 3-4: Theoretical and experimental CD spectra 62

Figure 3-5: Fluorescent microscopy images of binding 66

Figure 3-6: Visualization of FITC labeled bifunctional peptides 68

Figure 3-7: Fluorescence microscopy images and quantification 69

Figure 3-8: Bifunctional peptide hydrophobicity analysis 74

Figure 4-1:MIC of TiBP-AMP 87

Figure 4-2: Fluorescence microscopy images of bifunctional peptide binding and antimicrobial activity 90

Figure 4-3: Fluorescence microscopy images of binding/rebinding 92

Figure 4-4: De novo secondary structures of the bifunctional peptides 93

Figure 4-5: Surface topography characterization by optical profilometry 94

List of Tables

Table 2-1: Physical chemical properties and amino acid sequences 17

Table 2-2: “Rule Induction" method predictions 20

Table 2-3: MIC of TiBP-Spacer5-AMP, TiBP-Spacer3-AMP, and AMP 24

Table 2-4: Fold improvement calculated from fluorescent microscopy image analysis 28

Table 2-5: Minimum Inhibitory Concentrations of TiBP-Spacer5-AMP 37

Table 3-1: Chou-Fasman secondary structure predictions 54

Table 3-2: Physicochemical properties of peptides 54

Table 3-3: Theoretical “footprint” calculation and concentrations 64

Table 3-4: The minimum inhibitory concentration 75

Table 3-5: Fluorescence image quantification for percentage surface coverage 75

Table 4-1: Quantitative results for the binding and rebinding 91

Table 4-2: Quantitative results from the live/dead images 91

Table 4-3: Fluorescence microscopy image quantification 93

CHAPTER 1 - INTRODUCTION TO THESIS

The overall objective of this thesis is to develop a bio-enabled peptide film approach to combat implant failure by designing an engineered bifunctional peptide film that anchors to titanium and brings antimicrobial function to the implant surface as a treatment for orthopedic and dental implant infections and resulting diseases such as peri-implantitis. We note bifunctional design has a tremendous effect on the overall function of the peptide film when an implant binding peptide is combined to a bioactive peptide domain such as an antimicrobial peptide (AMP). Development of an understanding of the sequence-structure-function relationship of bifunctional peptides represents a significant addition to the current body of work and the opportunity to advance the development of biointerfaces on medical implants that are effective at combating bacterial colonization leading to infection while supporting host cell attachment and viability.

The overall progression of this thesis was accomplished in three specific aims. These aims were published in three peer-reviewed articles that are reproduced in this thesis as Chapter 2, Chapter 3, and Chapter 4. Chapter 5 summarizes the key findings of this body of work as a whole.

The first aim was to design and engineer the spacer in bifunctional peptides. Peptide secondary structure is closely linked to function. Thus, preservation of the secondary structure of the functional domains is critical for peptide engineering. In Chapter 2, we build upon the work on bifunctional peptides previously reported by our group and incorporate a novel spacer design engineered to improve the antimicrobial domain function while maintaining attachment of the titanium binding peptide (TiBP) to the implant surface. In this chapter we report an improvement of antimicrobial function of the bifunctional peptide film applied to titanium foils and orthopedic implants against two bacterial strains,

S. mutans and *S. epidermidis*. Further, the bifunctional peptide film was evaluated for host cell response using fibroblast cells. The improved function associated with the novel spacer design was related to "rules" developed by our group for bifunctional peptide design.

The second aim was the design of novel bifunctional peptides. The body of literature identifying naturally occurring AMP domains, as well as efforts to computationally search for novel sequences is rapidly growing. Several databases have been assembled to house AMP sequences. Deploying these antimicrobials to combat implant infection requires engineering of the bifunctional peptide platform to demonstrate the feasibility of incorporating additional AMPs. Incorporation of additional AMPs offers the opportunity to improve antimicrobial function of the bifunctional peptide film with the potential to further extend the bifunctional peptide film efficacy to a broad spectrum of bacteria. In Chapter 3, we report a design approach for bifunctional peptides using less resource intensive methods to evaluate the bifunctional peptide contributions of amino acids in the sequence, peptide secondary structure features, and backbone dynamics. This design approach was used to design two additional bifunctional peptides by incorporating AMP sequences from the literature and available databases. We report computational and experimental structural analysis, bifunctional peptide binding on a clinically relevant time scale and in the presence of competing serum proteins, quantify the antimicrobial effect and evaluate the durability of the bifunctional peptide film. This is done while relating the sequence-structure-function relationships in the bifunctional peptide engineering.

The third aim was to demonstrate *in vitro* the treatment and retreatment of peri-implant disease using a bifunctional peptide film. Delivery of a bifunctional peptide film to dental implants represents a non-surgical, green technology approach to improve oral health and reduce peri-implant disease progression. In Chapter 4, we demonstrated the

bifunctional peptide film as a water-based, non-surgical strategy that can be reapplied during recall appointments for treatment of peri-implant disease. We demonstrate the reapplication of the bifunctional peptide film with effective antimicrobial function following four successive bacterial fouling and cleaning cycles.

In Chapter 5, we provide concluding remarks and summarize key findings from the thesis as a whole. This work represents a paradigm shift in the prevention of implant failure while adding to the range of bioactive molecules that can be anchored to implant surfaces to improve implant longevity and effectiveness in restoring function to the body. Further efforts in this direction have great promise in providing treatment alternatives to traditional antibiotic therapies as the number of antibiotic resistant bacterial strains are increasing, while allowing for local antibiotic efficacy by anchoring bioactivity to the implant surface.

CHAPTER 2 - CONTROLLING THE BIOMIMETIC IMPLANT INTERFACE: MODULATING ANTIMICROBIAL ACTIVITY BY SPACER DESIGN *

ABSTRACT

Morbidity progressing to failure remains a challenge for surgical placement of titanium implants due to surface bacterial infection that initiates a host inflammatory response leading to implant loosening and ultimately requiring revision surgery. Since implant failure starts at the implant surface, creating and controlling the bio-material interface will play a critical role in reducing infection while improving host cell-to implant interaction. Here, we engineered a biomimetic interface based upon a chimeric peptide that incorporates a titanium binding peptide (TiBP) with an antimicrobial peptide (AMP) into a single molecule to direct binding to the implant surface and deliver an antimicrobial activity against *S. mutans* and *S. epidermidis*, two bacteria which are linked with clinical implant infections. To optimize antimicrobial activity, we investigated the design of the spacer domain separating the two functional domains of the chimeric peptide. Lengthening and changing the amino acid composition of the spacer resulted in a 3-fold MIC improvement against *S. mutans*. Surfaces coated with the chimeric peptide showed dramatically reduced bacteria numbers, with up to a 9-fold reduction for *S. mutans* and a 48-fold reduction for *S. epidermidis*. *Ab initio* predictions of antimicrobial activity based

---

* **Wisdom C**, VanOosten, S.K., Boone, K.W., Khvostenko, D., Arnold, P.M., Snead, M.L., and Tamerler, C. Controlling the Biomimetic Implant Interface: Modulating Antimicrobial Activity by Spacer Design. Journal of Molecular and Engineering Materials. 2016

on structural features were confirmed. Host cell attachment and viability at the biomimetic interface were also improved compared to the untreated implant surface. Biomimetic interfaces formed with this chimeric peptide offer interminable potential by coupling antimicrobial and improved host cell responses to implantable titanium materials, and peptide-based approach offers this approach to be extendable for various biomaterials surfaces.

INTRODUCTION

Bone and joint implants have revolutionized the healthcare of aging patients whose life expectancy has been increasing.[1] Implants have been intensively used during the last 40 years in treating bone and joint degeneration, neoplasms and inflammation.[1] Titanium and titanium alloys are used as implant biomaterials due to their biocompatibility, mechanical strength, and non-corrosive properties.[2-5] However, nosocomial microbial attachment to the implant surface can result in infection and inflammation with loosening that requires surgical revision. In the first hours following surgery the implant surface is most vulnerable to bacterial colonization and the bacterial pathogens are also most susceptible to antimicrobial treatment.[11,12] With time, bacteria populations multiply and cooperate to form biofilms that function as natural barriers against antibiotic effectiveness.[13] Treatment for infection of this type is difficult and the revision surgery is more complex, adding to patient morbidity. Despite improvements in implant technology including prophylactic therapy, most implant failures can be attributed to either infection or aseptic loosening resulting from poor integration with host tissue.[6,7] Failure requiring revision surgery is caused by infection in 7.5% of total hip arthroplasty (THA) and 14.8% of total knee arthroplasty (TKA) and by aseptic loosening in 55.2% of THA and 29.8% of TKA.[14] Immediate prevention of bacterial attachment on the implant surface is critical in prevention of infection related failure. However, host cell attachment and viability at the interface is also critical to host bone integration to prevent implant loosening. Therefore, an imperative clinical need exists to prevent bacterial colonization on the implant surface while not negatively affecting host cell response that could lead to poor integration of the implant material with the host. An implant surface with a fast-acting, broad-spectrum

antimicrobial function prevents bacterial attachment to reduce biofilm formation while maintaining implant integration with the host tissue would prove to be a paradigm shift.

Multiple strategies have been developed with the aim of eliminating microbial attachment on the implant surface. Among them, the use of antibiotics has been commonly employed in daily practice. However the rise of antibiotic resistance is becoming a major concern in dealing with bacteria, which also led to an increase in efforts to find alternative strategies.[2-5] Silver, polyethylene glycol (PEG), or quaternary ammonia based compounds (QACs) have been among the well-studied examples to bring the antimicrobial property by attaching them to the biomaterials using covalent chemical bonds.[15-20] Another strategy is to improve the antibacterial properties of metals by doping them with elements such as bismuth and zinc.[21,22] While promising, chemistry based immobilizations require complex steps, which may be not favorable within the biological environment due to their harshness. Additionally, uniform coatings where bioactivity is both preserved and homogenously distributed throughout the biomaterial surface following their coupling onto the biomaterials are challenging to obtain.

Another strategy is to coat the surface with antimicrobial peptides (AMPs). AMPs are abundant in nature and employed as natural innate immune system defense fighters. AMPs are fast-acting antimicrobial agents that are effective against a broad spectrum of gram-positive bacteria, gram-negative bacteria, viruses and fungi.[23-25] AMPs offer an alternative to conventional antibiotics to which some pathogens develop resistance more readily.[26] However, with the current technologies available, AMPs can be covalently immobilize onto the implant surfaces, and covalently immobilization of biomolecules have also proven to be less effective due to lack of control over the conformation of the biomolecules, which is critical to their biofunctionality. In our previous studies, we

demonstrated that AMPs can be immobilized on titanium implant surfaces through the engineering of chimeric peptides that use molecular recognition to attach and self-assemble on the implant surface as a novel biomolecular-coatings.[27-29] A chimeric peptide is a bifunctional single relatively short peptide chain compared to polypeptides and it joins two functional domains through an engineered spacer. The functional domain joined to the AMP for immobilization on implant surface is a peptide that is identified using combinatorial biology based molecular libraries, i.e. phage and cell surface display libraries. These genome-based screening process of the peptides allows for finding the potential candidates that can interact with the solid materials building upon molecular recognition, a feature similar to Nature. Due to phenotype-genotype based relations obtained for inorganic materials throughout the combinatorial biology-based selection process, these peptides are generally referred as genetically engineered peptide for inorganics (GEPIs). GEPIs offer the ability to use molecular recognition to self-assemble active peptide-based agents selectively on inorganic materials including titanium implants.[30,31] Previous work has identified several titanium binding peptides (TiBP) that assemble onto the titanium surface with high affinity appropriate for the surface of titanium and titanium alloy based implants.[28,32] Peptide based self-immobilization strategies therefore offer an opportunity to overcome the limitations and challenges associated with covalent immobilization of antibacterial agents on implant surfaces.

The current paper builds upon our studies suggesting that the function of an engineered chimeric peptide can be further improved through a spacer region that is placed in between the individual functional domains, i.e. TiBP and AMP. This novel design employed here allows retention of AMP secondary structural features responsible for the antimicrobial activity without jeopardizing the implant self-assembling domain of the

peptide. The changes offered in the spacer design induce enough structural alterations in the chimeric peptide to be more effectively displayed at the bio-materials interfaces. Herein, we demonstrate that engineering the length and composition of the spacer led to improved antimicrobial function and favorable host cell response. Chimeric peptides offer a simple unifying strategy to immobilize AMPs as a uniform bio-coating on titanium implant surfaces to combat implant failure due to infection.

MATERIALS AND METHODS

Chimeric Peptide Design

Titanium binding peptide (TiBP) and antimicrobial peptide (AMP) domains previously demonstrated as viable in a chimeric peptide (TiBP-Spacer3-AMP) were selected for this work.[32] Briefly, TiBP was selected by screening a bacterial surface display system, FliTrx (Invitrogen, Carlsbad, CA) against a titanium surface.[30,31,33] After four rounds of biopanning, 60 clones were selected and characterized based on their surface binding affinity using fluorescence microscopy techniques. The strongest binding sequence determined through these experiments was used in our chimeric peptide to bind to the titanium surface, anchoring the chimeric peptide. The AMP domain used in our chimeric peptide was computationally designed by data mining the literature.[28,34,35] A novel spacer, Spacer5 was designed as an elongated link, joining TiBP with AMP to form the chimeric peptide, TiBP-Spacer5-AMP. TiBP-Spacer5-AMP was synthesized using solid phase peptide synthesis by KanPro (Lawrence, KS). Physical chemical data including, molecular weight, isoelectric point, charge and GRand AVerage of hydropathY (GRAVY) scores based on amino acid sequences for AMP, TiBP, TiBP-Spacer3-AMP, and TiBP-Spacer5-AMP were obtained using the ExPasy Proteonomics Server.[36]

Molecular Structure Modeling

To understand how the secondary structure of the chimeric peptides change in solution depending on the spacer sequence, we generated ensembles of 1,000 likely structures using the PyRosetta project software and identified secondary structures with the DSSP program.[37,38] Structure generation is stochastic using a knowledge-based energy scoring function. An ensemble of structures was generated for each full chimeric peptide and each peptide domain to sample likely structural variations. Ramachandran plots were generated for the lowest energy structures for TiBP-Spacer3-AMP and TiBP-Spacer5-AMP structures. Chimera Software version 1.9 from University of California at San Francisco was used to visualize the structures.[39]

Antimicrobial "Rule Induction" Method

A "rule induction" method was used to correlate the generated secondary structures with the probability of antimicrobial function. Rule induction is a data mining approach to learn associations between paired sets of data made of sets of cases. As previously published, our paired data is the computationally generated structure decoys for both chimeric antimicrobial peptides and antimicrobial peptides paired with the minimum inhibitory concentration (MIC) of the peptides in solution.[32] Each structural decoy represents a single case in a set of cases. Given a list of cases where each case has a list of features and a selected outcome, rough-set theory approaches rule induction by looking for features which apply to the maximum number of cases and are selective for the selected outcome.[40] For our project, the cases are structure decoys and the list of features are the secondary structure features found. The paired distinct outcome is the MIC result from the

in-solution assay. The rough set theory implementation is based on MLEM2.[41] Two secondary structure features, 4-amino-acid right-handed alpha helices and 5-amino-acid alpha helices were key features for rules inducted from our previous work.[27] These rules associated with strong antimicrobial activity for the bacteria tested (*S. epidermidis and S. mutans)*. The secondary structure feature frequencies of these two rules were compared against TiBP-Spacer3-AMP and TiBP-Spacer5-AMP. Higher frequencies of these secondary structure features associate with stronger antimicrobial activity.

Circular Dichroism (CD) Analysis

A solution containing 50 μM TiBP-Spacer5-AMP in phosphate buffered saline (PBS) at pH 7.4 was prepared for circular dichroism analysis. The spectrum is the average of four scans from 190—239 nm using a Jasco J-810 spectrometer (Easton, MD). Appropriate background buffer subtraction was performed and the instrument carefully calibrated. The averaged spectrum was subtracted from background and smoothed with the Savitzky-Golay algorithm. The spectrum was transformed for mean residue ellipticity in degrees·cm^2/dmol. Two methods were used to estimate the secondary structure features from the CD spectra. The CAPITO method makes a comparison to reference spectra for helix (α-helix, 3_{10}-helix and π-helix), β-strands (β-sheets, β-bridge) and irregular secondary structures (bonded turns, bends and loops) using a liner regression method.[42] The Raussens method is a concentration-independent estimation of α-helix, β-sheets and irregular secondary structure proportions.[43]

Bacterial Maintenance and Culturing

The antimicrobial activity of TiBP-Spacer5-AMP was evaluated against two bacterial strains, *Streptococcus mutans* (American Type Culture Collection (ATCC) 25175, Manassas, VA) and *Staphylococcus epidermidis* (ATCC 29886). *S. mutans* cultures were prepared using Brain Heart Infusion Broth (BHI, BD Difco, Franklin Lakes, NJ) and *S. epidermidis* using Nutrient Broth (NB, BD Difco) according to ATCC protocols. Bacterial pellets obtained from ATCC were rehydrated in appropriate media of which several drops were used to streak either BHI or NB agar plates. Bacteria streaked agar plates were subsequently incubated for 24 hours. Agar plates and cultures were incubated at 37 ^{o}C in the presence of five-percent CO_2-supplemented atmosphere for *S. mutans* and in aerobic atmosphere and 200rpm shaking for *S. epidermidis*. Overnight cultures were made by aseptically transferring a single-colony forming unit (CFU) into 10mL of appropriate broth media followed by incubation in appropriate conditions for 16 hours. Bacteria from overnight cultures were used to inoculate fresh media and grown to mid-log phase.

Antimicrobial Activity in Solution

The minimum inhibitory concentration (MIC) of TiBP-Spacer5-AMP against *S. mutans* and *S. epidermidis* in solution was evaluated in 96 well plates (Corning Costar 3370, Corning, NY) spectrophotometrically over a period of 24 hours by obtaining a measurement for the optical density at 600 nm (OD_{600}) every two hours. Optical density at 600nm was measured using a Cytation3 microplate reader (Bio Tek Instruments, Winooski, VT). Bacteria grown to mid-log phase at a density of 10^7 CFU/mL were cultured at appropriate growth conditions in appropriate broth media only as a control or in broth

media containing a range from 5-70μM of TiBP-Spacer5-AMP for *S. mutans* and 1-10μM for *S. epidermidis*. The OD_{600} measurements obtained, relating optical density to bacteria CFUs/mL, were plotted versus time to generate standard growth curves. The minimum concentration of TiBP-Spacer5-AMP at which no increase in optical density measurement, corresponding to no bacterial growth occurring was designated as the MIC. AlamarBlue assay (Invitrogen, Carlsbad, CA) was used for determination of a minimum bactericidal concentration of TiBP-Spacer5-AMP. Bacteria in broth media only and with the TiBP-Spacer5-AMP concentrations described in the MIC experiments were prepared in 96 well plates. AlamarBlue reagent was added to experimental wells and incubated for two hours at 37ºC. Experimental wells were observed and evaluated for color change. Wells corresponding to concentrations of TiBP-Spacer5-AMP where no color change occurred were determined to have bactericidal concentrations of the chimeric peptide.

Titanium Surface Preparation

Two surfaces, 99% pure titanium foil (Alfa Aesar 43677, Ward Hill, MA) and titanium implant discs cut from orthopedic bar material (University of Kansas Medical Center Department of Neurosurgery, Kansas City, MO) were used for evaluation of TiBP-Spacer5-AMP bio-coating antimicrobial activity. Titanium foils were cut into squares measuring 0.5 mm thick x1 cm x 1 cm and 6 mm diameter implant rods were cut by the University of Kansas Medical Center Department of Neurosurgery with a standard orthopedic surgical rod cutter into 3 mm long disc segments. Surfaces were sterilized by soaking overnight in 70% bleach, followed by sonication for 15 minutes in each 1:1 acetone:methanol, isopropanol and filtered deionized water, dried under UV light in a biosafety cabinet and then autoclaved.

Chimeric Peptide Coating on Surfaces

Sterilized titanium surfaces were transferred to sterile 24 well plates (Costar 3738) with the bactericidal concentrations (60μM for *S. mutans* and 10μM for *S. epidermidis*) of TiBP-Spacer5-AMP dissolved in phosphate buffered saline (PBS) at pH 7.4 and incubated at 37ºC, constant agitation (200rpm) for 4 hours.[27] Following incubation substrates were washed twice by pipetting with PBS to remove unbound peptide and transferred to sterile 24 well plates to be used in experiments.

Antimicrobial Activity on Substrates

Antimicrobial activity of TiBP-Spacer5-AMP bio-coated titanium surfaces against each bacterial strain was evaluated by culturing bacteria in 24 well plates containing bio-coated surfaces or bare, untreated control surfaces. Bacteria grown to mid-log phase at a concentration of 10^7 CFU/mL were harvested by centrifugation at 2000xg for five minutes followed by resuspension in 500μL of appropriate media, transferred to sterile 2 mL centrifuge tubes, and then centrifuged at 2000xg for three minutes.[27] The supernatant was carefully removed from the pellet and the pellet resuspended in PBS at final concentration of 10^8 CFU/mL and 500μL of suspension was added to wells containing foil surfaces and 1000 μL to wells with implants. Well plates with TiBP-Spacer5-AMP bio-coated surfaces were incubated for two hours at 37 ºC in the presence of five-percent CO_2-supplemented atmosphere for *S. mutans* and in aerobic atmosphere and 200rpm shaking for *S. epidermidis*. Following incubation all surfaces were washed with PBS to remove unbound bacteria. Bacteria were fixed with 1 mL of 2% gluteraldehyde solution for 30 minutes and then dehydrated in 50, 70, 90 and 100% ethanol baths, 10 minutes for each ethanol

concentration. Bacteria were stained with SYTO 9 green fluorescent dye (Life Technologies L7012, Carlsbad, CA), incubated for 15 minutes at room temperature protected from light and excess dye was removed by washing twice with PBS. Stained bacteria were imaged with a fluorescence microscope (Olympus Spin Disk Epifluorescent microscope, Richmond Hill, Ontario, Canada) at an excitation/emission wave number provided by the manufacturer. Five representative fluorescence images were taken for each sample (n=3) and the bacteria were quantified using ImageJ Software and then subjected to statistical analysis.

Host Cell Response

Host cell response was evaluated with a fibroblast cell line (NIH/3T3 ATCC CRL-1658). The fibroblast cells were cultured following the ATCC protocol. Briefly, cells were grown in DMEM media (Gibco 11995073, Carlsbad, CA) supplemented with 10% fetal bovine serum (Gibco 10437036) and 1% penicillin-streptomycin (Gibco 15070063) and incubated at 37ºC in a five-percent CO2 atmosphere. Fibroblasts were passaged using 0.25% Trypsin-EDTA (Gibco 25200072) and cells were counted to ensure correct seeding concentrations.

Fibroblast cell response to 60µM TiBP-Spacer5-AMP bio-coating, 200 µg/mL collagen (Sigma C7661, St. Louis, MO) coating (positive control) and bare, untreated (negative control) titanium foil and implant surfaces was studied. Fibroblast cells at a concentration of 8x105 cells/mL were added to sterile 24 well plates containing TiBP-Spacer5-AMP coated, collagen coated, or bare, untreated foils or implants and incubated for 24 hours at 37ºC in a five-percent CO2 atmosphere. Fibroblast attachment and spreading were evaluated by fixing fibroblasts on titanium surfaces with 2% gluteraldehyde

solution, followed by dehydration in 10, 30, 60, 90 and 100% ethanol. Fixed fibroblasts on titanium surfaces were washed twice with PBS, permeabilized with TritonX (Sigma T8787), sealed with BSA (Fisher BioReagents BP671-10, Carlsbad, CA), and stained with Alexa Fluor488-Phalloidin dye (Invitrogen). Unbound dye was removed by washing with PBS and substrates were imaged with a fluorescent microscope at 4, 10, and 20 times magnification. Five representative images of each surface (n=3) were obtained and analyzed with ImageJ Software and then subjected to statistical analysis. Cell attachment was determined as number of cells per square millimeter and the percentage of the image surface covered by attached cells. Another measure of viability, metabolic activity was determined using a MTT Assay (Sigma M5655). Following incubation of fibroblasts with TiBP-Spacer5-AMP, collagen, or bare, untreated titanium surfaces for 24 hours at 37ºC in a five-percent CO2 atmosphere, one tenth of the well liquid volume was removed and replaced by the same volume of 5 mg/mL MTT reagent. The substrates with MTT reagent were incubated for 3 hours then transferred to a sterile 24-well plate. The formazan crystals were dissolved in the detergent reagent according to the manufacture's protocol. Absorbance was measured at 570 nm.

RESULTS AND DISCUSSION

Here, we engineered and evaluated a chimeric peptide composed of a titanium binding and an antimicrobial domain linked by a novel spacer design (TiBP-Spacer5-AMP). Our objective was to preserve the secondary structural features of both the titanium binding peptide and the antimicrobial peptide so as to impart an effective antimicrobial activity against two bacteria commonly associated with nosocomial implant infections, *S. mutans* and *S. epidermidis*.[44,45] Data from a similar chimeric peptide with identical

functional domains, but a shorter spacer sequence (TiBP-Spacer3-AMP) and the AMP peptide alone were used to evaluate the effect of the new engineered spacer design.[27-29]

Table 2-1: Physical chemical properties and amino acid sequences for TiBP, AMP, and two chimeric peptides TiBP-Spacer3-AMP and TiBP-Spacer5-AMP. Notes: MW, molecular weight; pI, isoelectric point; GRAVY, GRand Average Value of hydropathicitY; and _", gap inserted for sequence alignment. Despite chimeric peptide similarity to one another, we observed improved antimicrobial activity with the altered amino acid composition of the longer peptide spacer, Spacer5.

Name	Sequence	Spacer length	MW (kDa)	PI	Charge	GRAVY
TiBP	RPRENRGRERGL	N/A	1.4956	11.82	+3	−2.633
AMP	LKLLKKLLKLLKKL	N/A	1.6923	10.70	+6	0.500
TiBP-Spacer 3-AMP	RPRENRGRERGL–GGG LKLLKKLLKLLKKL	3	3.3411	11.85	+9	−0.890
TiBP-Spacer 5-AMP	RPRENRGRERGLGSGGG LKLLKKLLKLLKKL	5	3.4852	11.85	+9	−0.871

Table 2-1 contains the sequences and physical chemical properties for each chimeric peptide and their functional domains. Despite the physical chemical similarity to one another, we observed improved antimicrobial activity with the altered amino acid composition designed into the longer linker called Spacer5. The interfacial activity model suggests that antimicrobial activity depends on amino acid composition and physical chemical properties.[46] Interfacial activity is the electrostatic and hydrophobic interactions between peptides and the lipid surface of the bacterial cell wall. Literature suggests several mechanisms leading to cell death following interaction between the peptide and the lipid surface including a compromised bacterial cell wall which initiates a cascade of effects including cellular respiration, DNA damage and altered gene expression. Recent publications indicate the production of reactive oxygen species (ROS) when AMPs attack bacteria.[47,48 49] Much of the literature characterize AMP activity based on either structure-function relationships or physical chemical properties.[46] The effect of the engineered spacer design was evaluated through independent, but corroborating approaches, including: computational and direct structural analysis coupled with measurement of antimicrobial activity of the chimeric peptide in solution, as well as when bound to titanium

substrates against common nosocomial microorganisms allowing us to suggest that the restored antimicrobial activity is due to the preserved structure associated with the Spacer5 design.

Computational structure and function predictions

Computational molecular structures were generated using the PyRosetta structural ensemble generation method.[37] One thousand likely energy minimized structures were generated for each chimeric peptide, for each spacer sequence, and for each functional domain. The lowest energy structure for each is depicted in Figure 2-1 with TiBP, spacer domain, and AMP designated with blue-, black-, and red-shading, respectively. The images shown in Figure 2-1 represent likely structures that are modeled in solution. Ramachandran plots were generated for the lowest energy chimeric peptide structures and are shown in the supporting information for TiBP-Spacer3-AMP and TiBP-Spacer5-AMP. The Ramachandran plots simulates the contribution of hydrogen bonding among backbone atoms and can be interpreted to correlate the contribution of the alpha helix or beta sheet structural features depicted in the energy minimized structures.

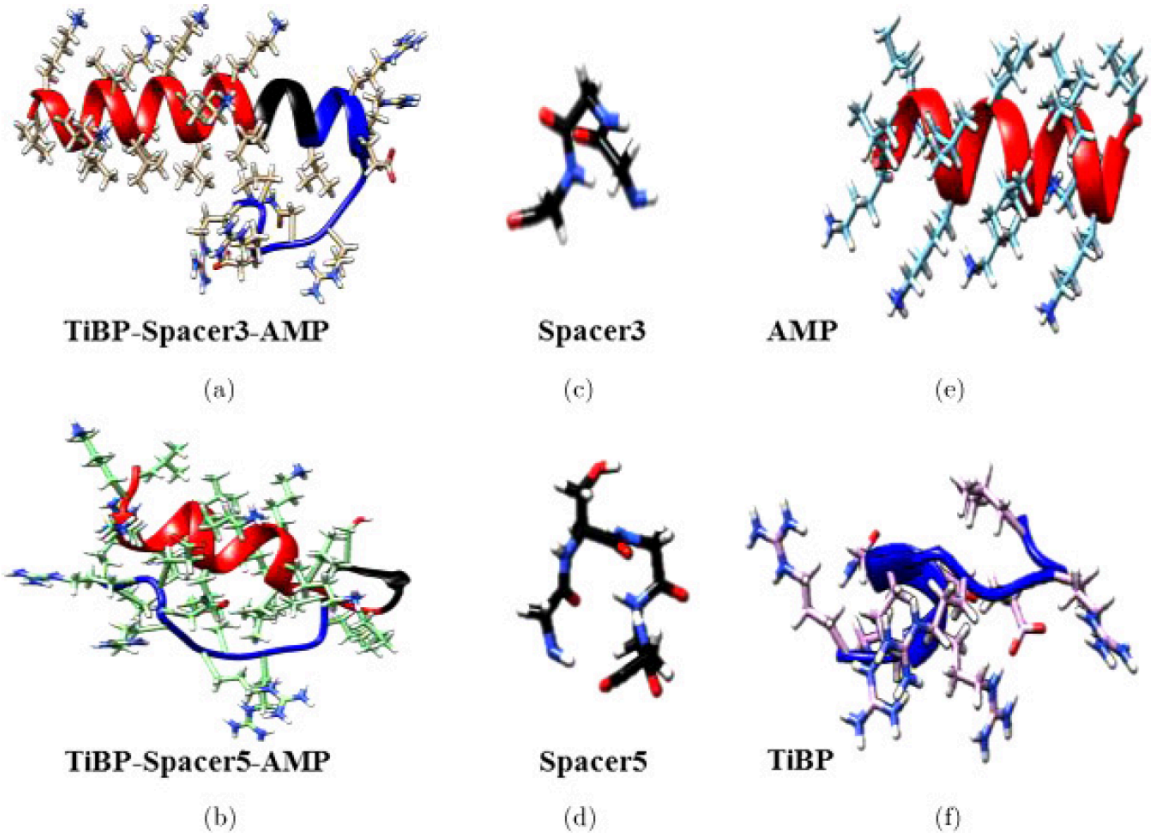

Figure 2-1: Lowest energy structures modeled in solution for (a) TiBP-Spacer3-AMP chimeric peptide; (b) TiBP-Spacer5-AMP chimeric peptide; (c) Spacer3 (GGG); (d) Spacer5 (GSGGG); (e) AMP; (f) TiBP. The peptide backbone is represented as a ribbon to show secondary structure for peptides with side chains represented by full atoms. TiBP domains, spacer domains, and AMP domains are designated with blue-, black-, and red-shading, respectively. The. TiBP-Spacer3-AMP (a) has an _-helix feature beginning with the AMP domain and preserved through Spacer3, whereas TiBP-Spacer5-AMP (b) has a shorter _-helix ends at Spacer5. Both functional domains, AMP (e) and TiBP (f) have _-helix secondary structure, with a stronger prominence in the AMP domain.

Previous published analysis using the "rule induction method" suggest that increasing the number of short alpha helices is associated with antimicrobial activity, therefore we first examined the structure of the chimeric peptides.[27] The computational structures in Figure 2-1 show the secondary structure features for the chimeric peptides and their component parts. The structure of both TiBP and AMP peptides show features of alpha helicity with a stronger helicity prominence in the AMP domain (Figure 2-1, E). TiBP-Spacer3-AMP (Figure 2-1, A) has an alpha helix feature beginning within the AMP domain and preserved through Spacer3. From the Ramachandran plot we conclude the

alpha helix feature is approximately 26 amino acids long and confirm that backbone angles consistent with alpha helix features are present though AMP, Spacer3, and almost the entire TiBP. All but three amino acids correspond to psi/phi angles (-90^0, -60^0) consistent with alpha helix. Spacer3 consists of but three glycine amino acid residues; therefore the minimal side chain size of glycine in Spacer3 could allow the alpha helix feature to be preserved across the spacer domain and into the TiBP, producing longer alpha helices. The alpha helix feature in TiBP-Spacer5-AMP is comparatively much shorter. The Ramachandran plot for TiBP-Spacer5-AMP shows the psi/phi angles (-90^0, -60^0) corresponding to alpha helicity are assigned to the AMP domain, while psi/phi angles (-90^0, $+120^0$) corresponding to beta sheet/random coil secondary structures are observed in the rest of the molecule. We interpret these finding to suggest that the Spacer 5 segregates the AMP domain from the rest of the chimeric peptide, allowing its antimicrobial activity to be preserved.

Table 2-2: "Rule Induction" method predictions of antimicrobial activity based on secondary structure features of four and five amino acid alpha helicity present in computationally generated structures.[50] Increasing antimicrobial activity is associated with increasing percent of helix frequency over either a four or five amino acid average. The "rule induction method" predicts that TiBP-Spacer5-AMP possesses a secondary structure associated with antimicrobial activity to a greater extent than the secondary structure of the TiBP-Spacer3-AMP.

Peptide	4 aa α-helix frequency (%)	5 aa α-helix frequency (%)
TiBP-Spacer3-AMP	10.4	5.6
TiBP-Spacer5-AMP	17.6	8.0

The Spacer5 (GSGGG) is composed of four glycine and a single serine amino acid residues, and the presence of a polar serine residue could produce a slight "ST staple" feature in the spacer region producing a backbone bend that prevents the continuity of the alpha helix feature observed in TiBP-Spacer3-AMP. The alpha helix property that most accurately predicts antimicrobial activity by the "rule induction method" against *S. mutans*

and *S. epidermidis* is the number of five amino acid- and four amino acid-right-handed-helices. The "rule induction method" also predicts antimicrobial function based on the percentage of these features present in the energy minimized PyRosetta generated structures. The "rule induction method" was used to predict the antimicrobial activity of TiBP-Spacer5-AMP and TiBP-Spacer3-AMP with the results shown in Table 2-2. Of the one thousand structures generated in the ensembles for each chimeric peptide, TiBP-Spacer5-AMP had a larger percentage of structural topologies represented with four or five amino acid residue alpha helix features. This is consistent with what we observed with the detailed structure analysis conducted for the lowest energy structure of each chimeric peptide. Based on previously published data validating the "rule induction method", we predict that TiBP-Spacer5-AMP should have greater antimicrobial activity in solution against *S. mutans* and *S. epidermidis*.[27] To further corroborate our analysis, we next turned to circular dichroism (CD) analysis which can directly measure secondary structure of TiBP-Spacer5-AMP.

Structure determination with CD

The chimeric peptide was prepared at a concentration of 50μM in phosphate buffered saline at pH of 7.4 for secondary structure analysis by CD.

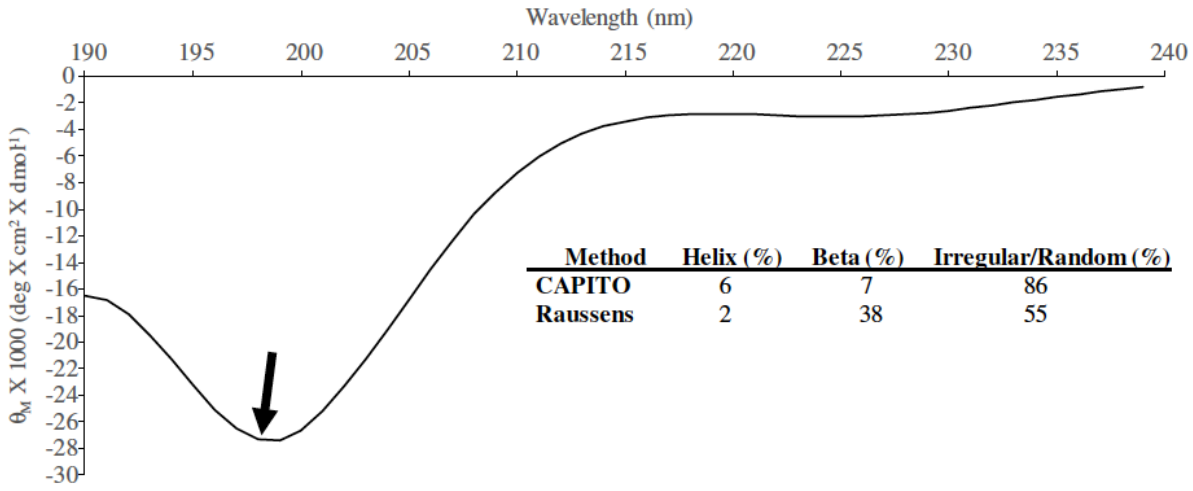

Figure 2-2: CD spectrum for TiBP-Spacer5-AMP chimeric peptide at a concentration of 50 μM in PBS, pH 7.4. The feature designated by the arrow indicates a greater preference for right-circularly polarized light absorbance compared to the previously published spectrum for chimeric peptide with Spacer3.[29] The CAPITO and Raussens methods indicates a predominance of irregular and random coil features in the spectrum consistent with what is observed in the computationally generated secondary structure for TiBP-Spacer5-AMP shown in Figure 2-1(b).[42,43]

Two complementary methods, the CAPITO and the Raussens method were used to quantify the results obtained from the CD spectra.[42,43] We applied both the concentration dependent CAPITO method and the concentration independent Raussens method for these predictions to corroborate outcomes. Both approaches are regression methods used to transform CD spectral data in order to identify corresponding structural information from a protein database.

The CD spectrum for TiBP-Spacer5-AMP is depicted in Figure 2-2 with inset table containing results from analysis with the regression methods. The spectrum for the chimeric peptide with Spacer5 indicates a greater preference for right-circularly polarized light absorbance compared to the previously published spectrum for Spacer3, indicating that the predominance of alpha helix secondary structure present in TiBP-Spacer3-AMP is not preserved through the newly designed Spacer5.[29] The CD structural prediction results are consistent with the computationally predicted secondary structure analysis, indicating

that a majority of the secondary structure of TiBP-Spacer5-AMP is beta sheet or random coil. Moreover, both the CAPITO and Raussens method assigns 86% and 55% secondary structure to irregular or random coil features, for TiBP-Spacer5-AMP, respectively. In addition to random coil features, the Raussens method assigns 38% of TiBP-Spacer5-AMP secondary structure to beta sheet features. The Raussens method also corroborates the Ramachandran plot prediction for analysis computationally generated structures. These secondary structure features are predicted by the "rule induction method" to also produce a greater antimicrobial activity for TiBP-Spacer5-AMP. These structural analyses are related only to the in solution secondary structure of the chimeric peptides not their structures when bound to titanium surfaces. Currently, a computational model for proteins bound to a titanium surface does not exist. While this limits our ability to describe the exact structural contributions to antimicrobial activity on the titanium implant surface, we can however measure the antimicrobial activity of the chimeric peptides in solution and empirically apply those findings to titanium surfaces.

Chimeric Peptide Function

Antimicrobial Effect in Solution

Antimicrobial activity in solution was elucidated by determining the minimum inhibitory concentration (MIC) of TiBP-Spacer5-AMP required to inhibit growth for two bacterial strains commonly recovered from infected implants, *S. mutans* and *S. epidermidis*.[44,45]

Table 2-3: MIC of TiBP-Spacer5-AMP, TiBP-Spacer3-AMP, and AMP alone in solution against *S. mutans* and *S. epidermidis*. There is a three-fold decrease in TiBPSpacer5-AMP MIC against *S. mutans*.

Peptide	*S. mutans* (μM)	*S. epidermidis* (μM)
AMP	38	4
TiBP-Spacer3-AMP	153	5
TiBP-Spacer5-AMP	50	8

Previously published MIC values for TiBP-Spacer3-AMP and AMP alone were used for comparison.[27] MIC data for AMP, TiBP-Spacer3-AMP, and TiBP-Spacer5-AMP are depicted in Table 2-3. The MIC value of TiBP-Spacer5-AMP against *S. mutans* and *S. epidermidis* are 50µM and 8 µM, respectively. We observed a remarkable three-fold improvement of MIC antimicrobial activity for the TiBP-Spacer5-AMP against *S. mutans*. This can be attributed to the increased frequency of secondary structural features corresponding to antimicrobial activity as predicted by the "rule induction method", corroborating the importance of secondary structure features in antimicrobial peptide design. The design of the spacer offers an opportunity to fine-tune the structural properties of the chimeric peptide so as to improve its antimicrobial potential. The use of the Spacer5 results in a chimeric peptide displaying shorter alpha helix structural features compared to Spacer3 and yields improved antimicrobial activity. In contrast however, the antimicrobial activity of TiBP-Spacer5-AMP against *S. epidermidis* appears to be slightly diminished compared to TiBP-Spacer3-AMP. We cannot yet account for why TiBP-Spacer5-AMP was less effective against *S. epidermidis*, than *S. mutans* and we are conducting further experiments to investigate this observation.

The bactericidal concentration for TiBP-Spacer5-AMP against each bacteria was also determined using the AlamarBlue assay.[51] The bactericidal concentration for TiBP-

Spacer5-AMP was found to be 60μM for *S. mutans* and 10μM for *S. epidermidis*. These concentrations are only slightly higher than the observed MIC values indicating that TiBP-Spacer5-AMP corroborating these complementary methods of killing bacteria. Next, we used the bactericidal concentrations determined from the AlamarBlue assay to assess the antimicrobial activity of medical implants coated with TiBP-Spacer5-AMP by assessing bacterial growth on their surfaces.

Antimicrobial Effect on Surfaces

TiBP-Spacer5-AMP at 60μM for *S. mutans* and 10μM for *S. epidermidis* were permitted to self-assemble on selected titanium surfaces and evaluated for their antimicrobial activity. Titanium foils were selected for their ease of use, while discs cut from stock titanium orthopedic bar material were used to ascertain their effectiveness directly on a clinically relevant surface. For both surfaces, infectious organisms common to clinical infections, *S. mutans* and *S. epidermids*, were used to evaluate the antimicrobial activity of the bio-coating. Previous published investigation had established the binding characteristics and affinity for the titanium binding peptide as part of a chimeric molecule.[27] Following incubation, the unbound peptide was removed by repeated washing, suggesting the antimicrobial activity observed for either titanium surface was the result of the chimeric peptide bound to the surface and presenting an antimicrobial activity. The observed effectiveness of TiBP-Spacer5-AMP antimicrobial effect against *S. mutans* is shown in Figure 2-3 and against *S. epidermidis* in Figure 2-4.

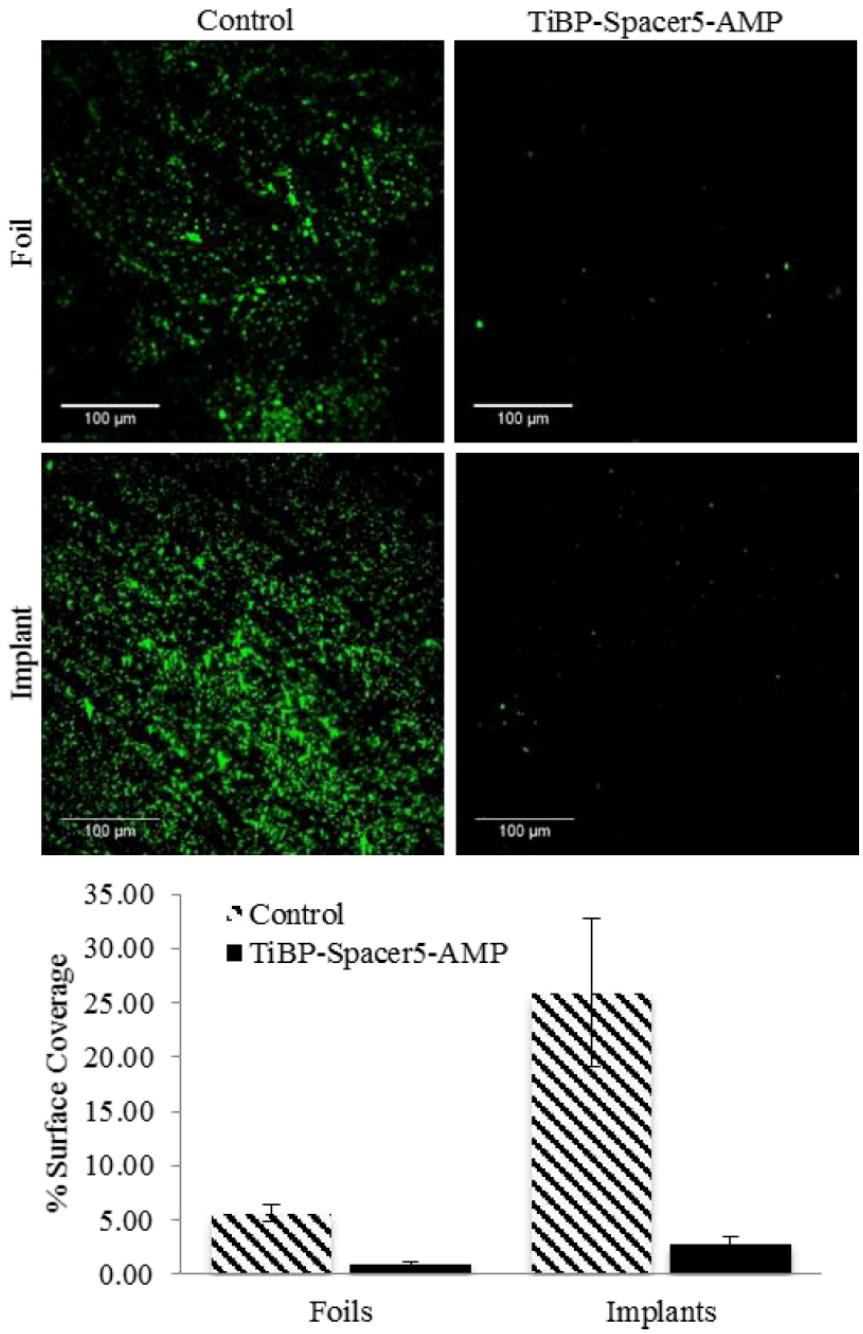

Figure 2-3: Fluorescent microscope images of *S. mutans* bacteria on 99% pure titanium foils and orthopedic implant discs with TiBP-Spacer5-AMP bio-coating and bare, bare untreated controls. (Scale Bar is 100 µm) Chart depicts the percent surface coverage quantified by ImageJ of bacteria on the titanium surfaces.

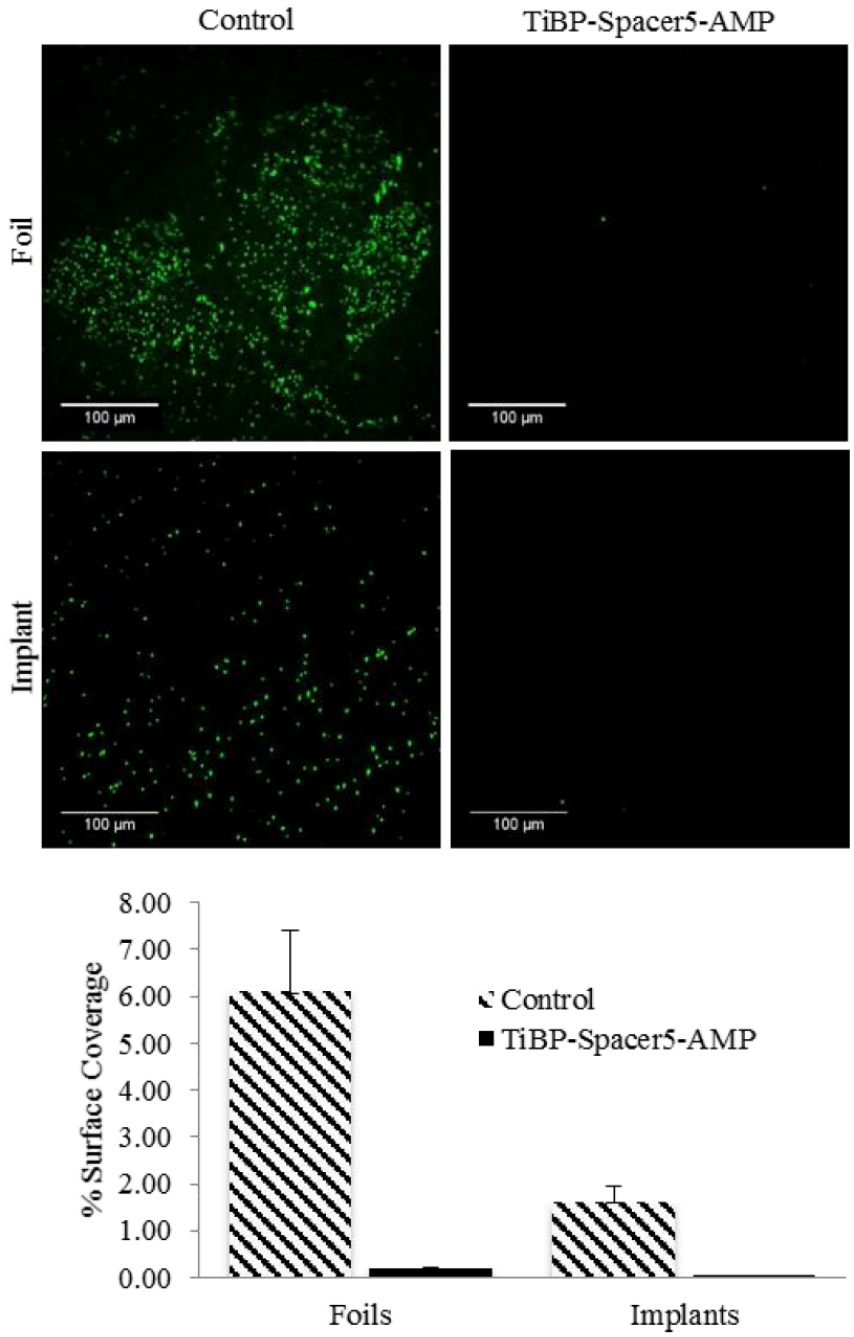

Figure 2-4: Fluorescent microscope images of *S. epidermidis* bacteria on 99% pure titanium foils and orthopedic implant discs with TiBP-Spacer5-AMP bio-coating and bare, bare untreated controls. (Scale Bar is 100 µm) Chart depicts the percent surface coverage quantified by ImageJ of bacteria on the titanium surfaces.

The images are representative areas, and the percent of the total surface area covered by bound bacteria was identified by bacterial staining and quantified by analysis with ImageJ. In all cases, TiBP-Spacer5-AMP bio-coating reduced the number of bacteria attached to the surface compared to uncoated control surfaces. The fold reduction for the number of bacteria on titanium surfaces with TiBP-Spacer5-AMP bio-coating is depicted in

Table 2-4. There is a 6- to 9-fold reduction for *S. mutans*, with a 33- to 48-fold improvement noted for *S. epidermidis* on foil or implant surfaces, respectively, due to the presence of the TiBP-Spacer5-AMP bio-coating. These data suggest that the TiBP-Spacer5-AMP bio-coating is an effective strategy to combat infections and consequential implant failure by reducing bacterial colonization which ultimately transform to a complex biofilm that can resist systemic administration of antibiotics and lead to implant failure.[52] Alternatively, the coating formed by the TiBP-Spacer5-AMP may interfere with bacterial attachment by forming a biomimetic surface that is less fouling than the bare titanium or titanium alloy surface.[35] The increasing frequency of antibiotic resistant bacteria in hospital settings contributing to nosocomial infections and the increasing number of patients with co-morbidities can both contribute to a diminished ability of the host to resist and clear bacteria at surgical sites which lead to implant failure. Whether by antimicrobial activity or reduced attachment, the reduction in the number of pathogenic bacterial by the TiBP-Spacer5-AMP would result in improved patient outcomes. Lastly, we evaluated host cell response on titanium surfaces coated with the TiBP-Spacer5-AMP chimeric peptide.

Table 2-4: Fold improvement calculated from fluorescent microscopy image analysis of *S. mutans* and *S. epidermidis* bacteria on titanium foil and implant surfaces with TiBPSpacer5-AMP bio-coating, compared

to bare, uncoated control surfaces. There is in resistance to bacteria as a result of the TiBP-Spacer5-AMP bio-coating on foil and implant surfaces.

Fold improvement compared to uncoated Ti surfaces		
	Foils	Implants
TiBP-Spacer5-AMP against *S. mutans*	6	9
TiBP-Spacer5-AMP against *S. epidermidis*	33	48

Host Cell Attachment and Viability

Host cell attachment and viability was evaluated *in vitro* using a fibroblast cell line (NIH/3T3) by measuring cell attachment, morphology/spreading, and viability response to TiBP-Spacer5-AMP coated substrates. The results are shown in Figure 2-5 for titanium foils and those for orthopedic implants are shown in Figure 2-6. The number of fibroblasts that attached to the TiBP-Spacer5-AMP bio-coated foils was not statistically different compared to an untreated control surface. However, the cells attached on the chimeric peptide bio-coated foil surface did demonstrate greater coverage, suggesting they spread more effectively compared to cells grown on untreated control surfaces. As expected, collagen-coated surfaces, the gold-standard used as a positive control, did out-perform the TiBP-Spacer5-AMP chimeric peptide bio-coating. Interestingly, for studies with fibroblasts seeded onto titanium implant surfaces, the chimeric peptide bio-coated surfaces showed statistically greater cell attachment and spreading properties than observed for the unmodified implant substrates. Additionally, the TiBP-Spacer5-AMP bio-coated implant surfaces showed adhesion and spreading results that were statistically comparable to the positive collagen controls. These results suggest that bio-coating orthopedic medical

implants with TiBP-Spacer5-AMP would result in an improved host cell response at the implant-tissue interface.

The MTT assay was used as a live-dead discrimination assay for fibroblasts grown on various surfaces. We found that cell viability on either titanium foils or implant surfaces treated with chimeric peptide were similar to values observed for the positive control collagen coated surfaces (Figure 2-7), with approximately 50% greater cell viability observed compared to untreated surfaces.

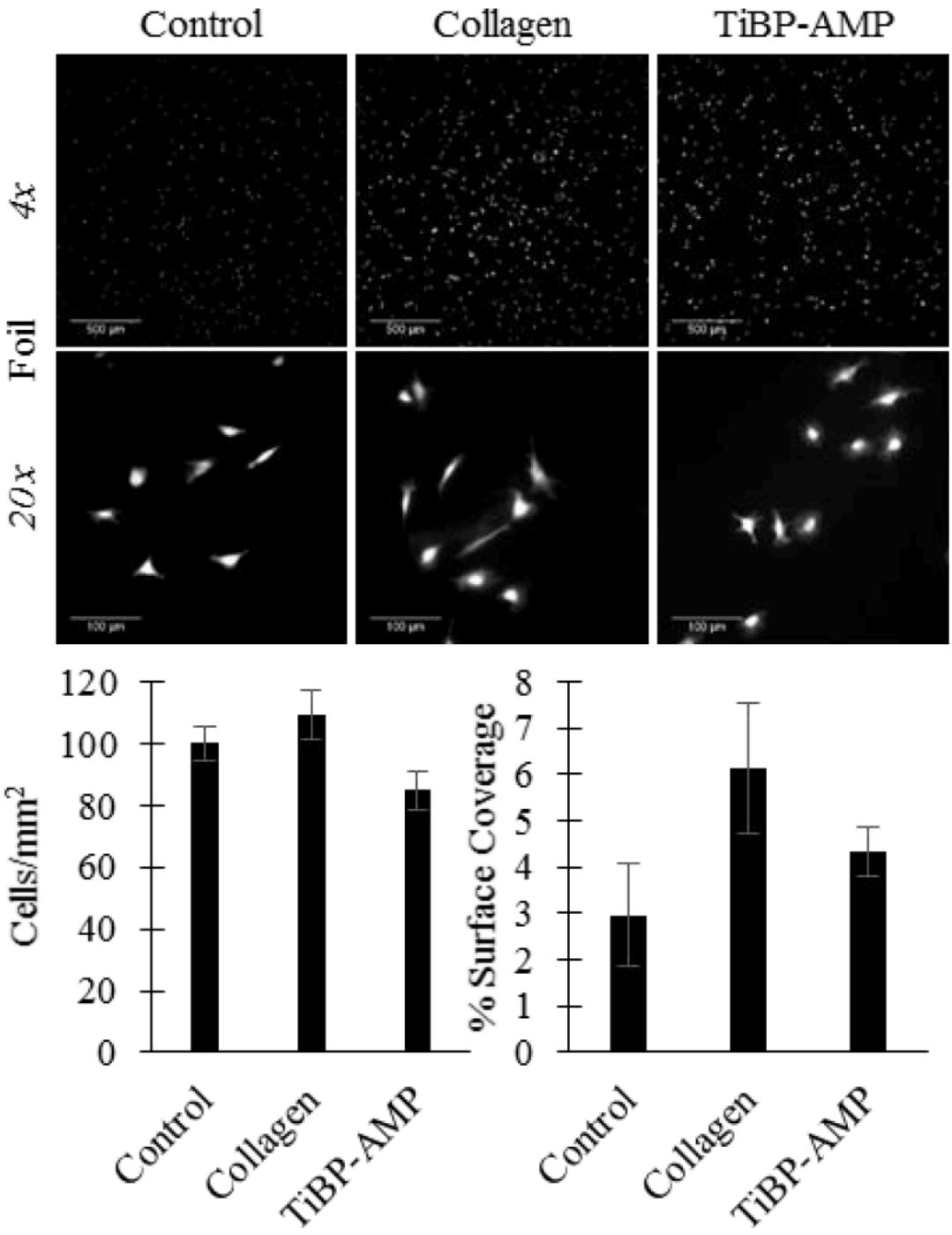

Figure 2-5: Fluorescent images of NIH/3T3 fibroblast attachment on titanium foils : Control (no treatment), Collagen (200 µg/mL collagen coating positive control), or TiBP-AMP (60 _M TiBPSpacer5-AMP bio-coating). Scale bar represents 500 µm for 4X images and 100 µm for 20X images. TiBP-Spacer5-AMP biocoated foils had fewer ¯broblasts attach compared to untreated control, however the ¯broblast surface coverage for TiBPSpacer5-AMP was greater indicating the cells spread more.

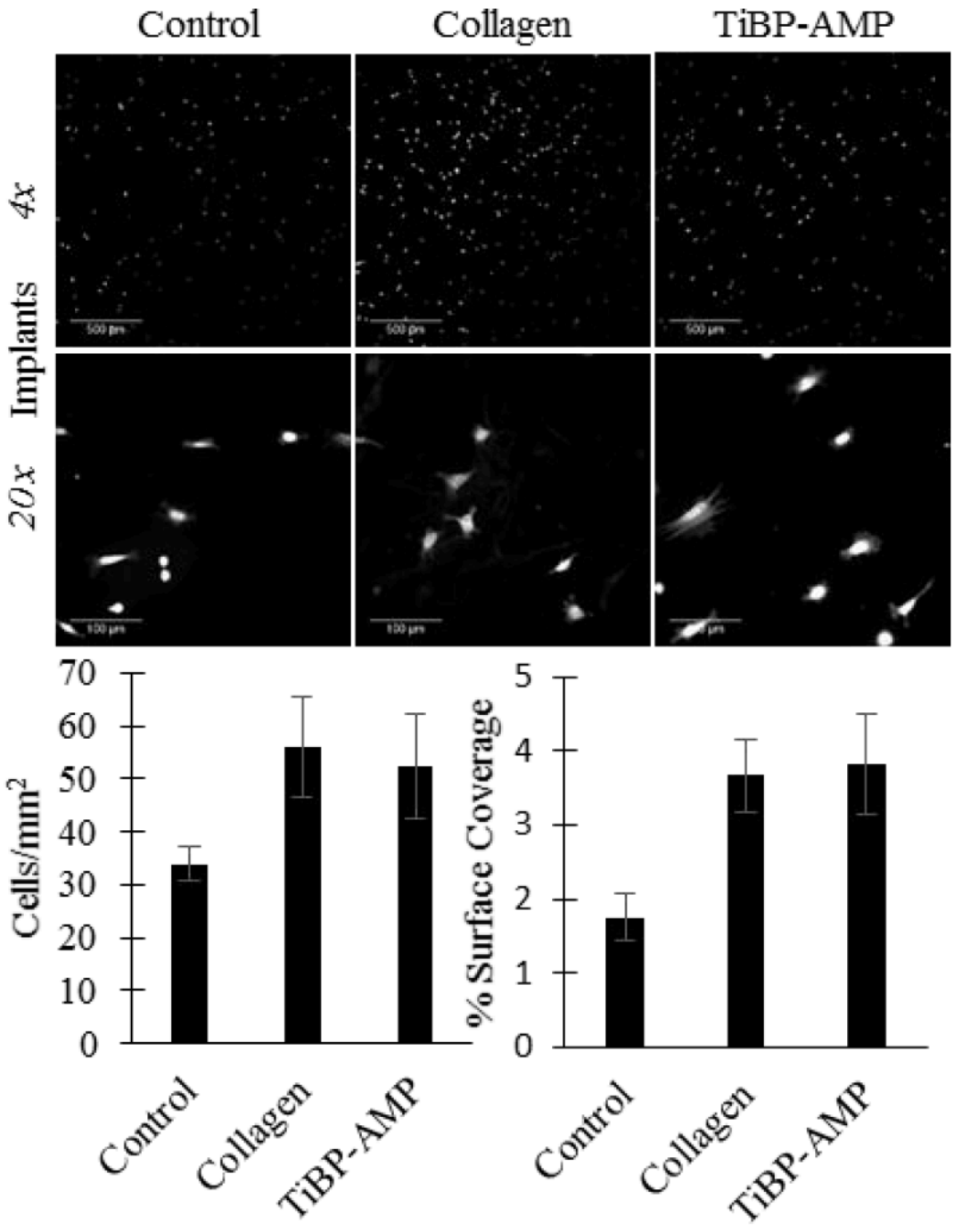

Figure 2-6: Fluorescent images of NIH/3T3 fibroblast attachment on titanium implants : Control (no treatment), Collagen (200 µg/mL collagen coating positive control), or TiBP-AMP (60 µM TiBP-Spacer5-AMP bio-coating). Scale bar represents 500 µm for 4X images and 100 µm for 20X images. TiBP-Spacer5-AMP bio-coated implants showed greater cell attachment and spreading compared to untreated controls and attachment and spreading were comparable to collagen positive

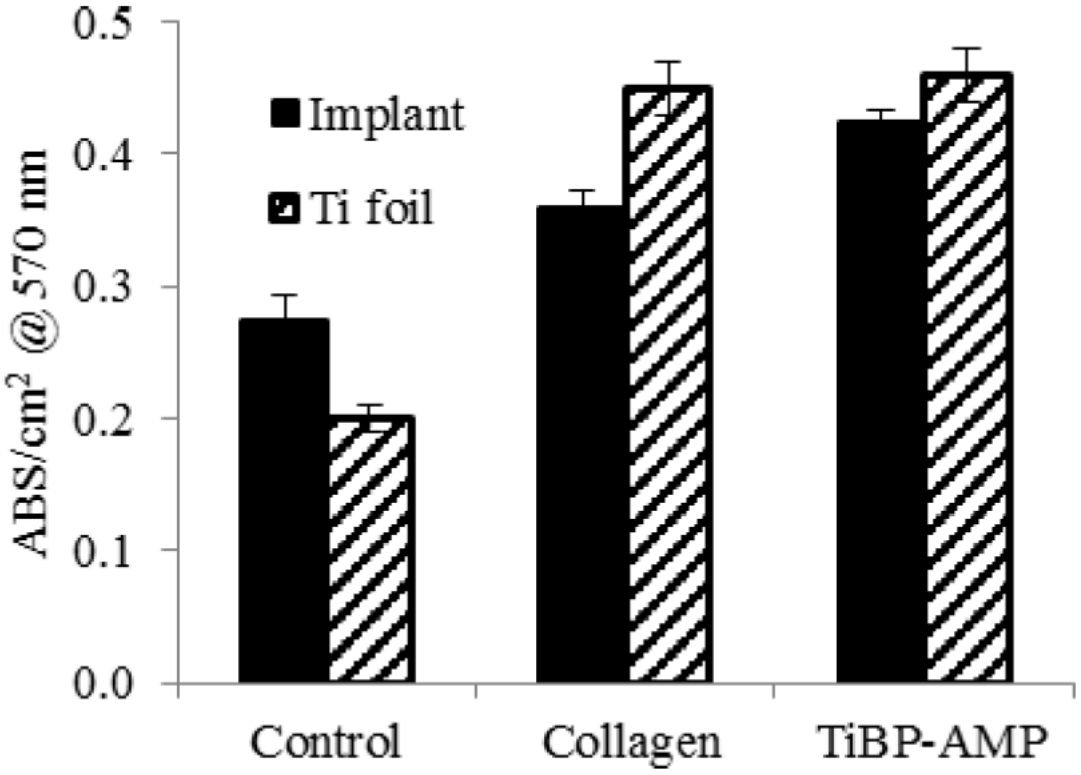

Figure 2-7: NIH/3T3 fibroblast metabolism on titanium foils and implants measured by MTT assay. Control (no treatment), collagen (coated with 200 μg/mL collagen), TiBP-AMP (coated with TiBP-Spacer5-AMP at 60 μM).

CONCLUSION

A titanium binding, antimicrobial chimeric peptide with novel spacer design (TiBP-Spacer5-AMP) was rationally engineered. Computational structure analysis revealed secondary structural features that were dependent on the length and composition of the spacer. These features were confirmed through direct evaluation with circular dichroism (CD). Specifically, TiBP-Spacer5-AMP has a multiple short alpha helix features with predominately irregular or random coil secondary structure corroborated by Ramachandran plot analysis of energy minimized structures and CD. The previously developed “rule induction method” was applied and predicted the beneficial effect of structural features induced by the spacer that resulted in greater antimicrobial activity. In fact, a three-fold

decrease in MIC that indicates increased antimicrobial activity was observed against bacteria common to nosocomial implant infection. TiBP-Spacer5-AMP was assembled on titanium foils and orthopedic implant surfaces as a biomimetic coating which reduced bacterial numbers nine-fold against *S. mutans*,a bacteria common to dental implant infections, and 48-fold against *S. epidermidis* bacteria common to orthopedic implant infections. The potential of the chimeric peptide bio-coating to promote host cell attachment was evaluated using a fibroblast cell line. On chimeric peptide bio-coated surfaces, the cells attached, spread and exhibited 50% greater viability measured by a metabolic assay compared to identical cells on bare, untreated titanium surfaces. Data from the TiBP-Spacer5-AMP point to the importance of optimal design of the spacer between two functional domains within the chimeric peptide in order to optimize the function of each domain, namely binding and self-assembling onto titanium surfaces and the displayed antimicrobial activity on the biomaterial surface. The ability to create an antimicrobial bio-coating on titanium medical implants that serve to overcome complications associated with implant failure due to nascent infection and their eventual loss by infection that contributes to increasing medical costs and patient morbidity has interminable value.

SUPPLEMENTARY INFORMATION

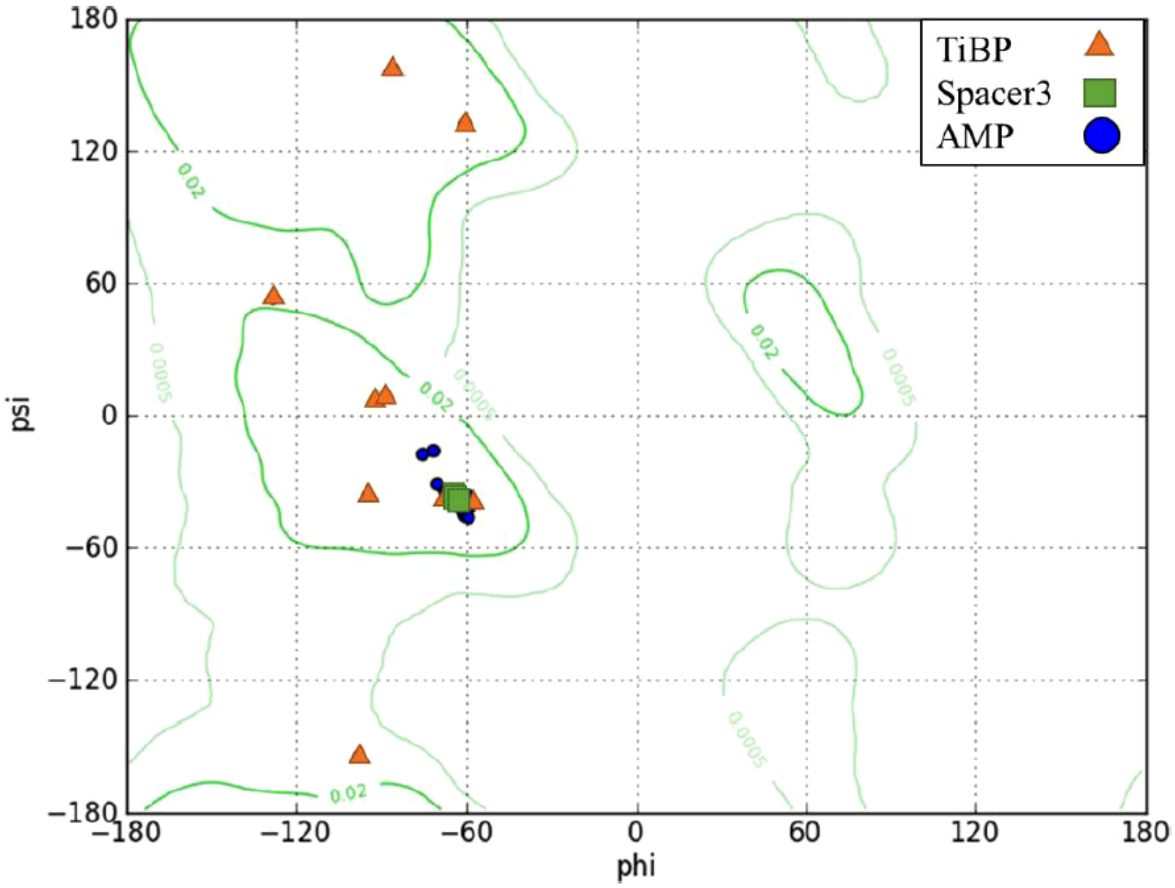

Figure 2-8: Ramachandran Plot of TiBP-Spacer3-AMP generated from the lowest energy computationally generated structure. Orange triangles, green squares, and blue circles, designate contributions from TiBP, Spacer3, and AMP domains, respectively. Psi/phi angles (-90°,-60°) predicting prominent α-helix structure involving most amino acid residues in TiBP-Spacer3-AMP chimeric peptide.

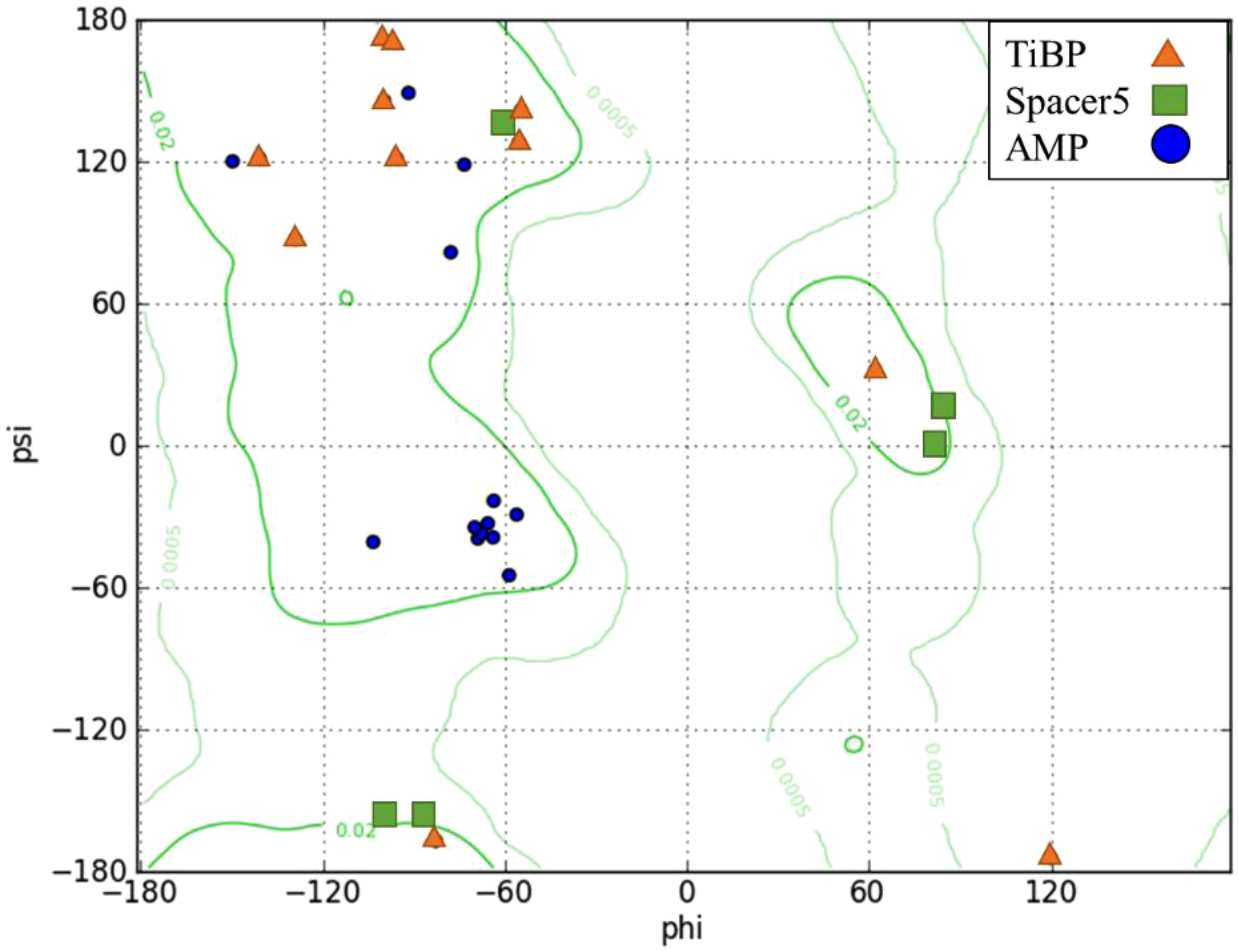

Figure 2-9: Ramachandran Plot of TiBP-Spacer5-AMP generated from the lowest energy computationally generated structure. Orange triangles, green squares, and blue circles, designate contributions from TiBP, Spacer5, and AMP domains, respectively. Psi/phi angles (-90°, -60°) corresponding to α-helicity are assigned to the AMP domain, while psi/phi angles (-90°, +120°) corresponding to β-sheet/random coil secondary structures are observed in the rest of the molecule.

Table 2-5: Minimum Inhibitory Concentrations of TiBP-Spacer5-AMP evaluated against *S. mutans* and *S. epidermidis* in solution. Growth was monitored every two hours for 24 h by measuring the optical density at 600nm (OD600) corresponding to bacterial CFU/mL. Entries with a "+." indicate bacterial growth did occur at that concentration of TiBP-Spacer5-AMP, whereas entries with a "-" indicate inhibition of bacterial growth. The MIC of TiBP-Spacer5-AMP against *S. mutans* and *S. epidermidis* is 50 µM and 8 µM, respectively.

S. mutans									
TiBP-Spacer5-AMP	0 μM	5 μM	10 μM	20 μM	30 μM	40 μM	50 μM	60 μM	70 μM
Growth	+	+	+	+	+	+	−	−	−
							MIC is 50 μM		
S. epidermidis									
TiBP-Spacer5-AMP	0 μM	1 μM	2 μM	3 μM	4 μM	5 μM	6 μM	7 μM	8 μM
Growth	+	+	+	+	+	+	+	+	−
							MIC is 8 μM		

CHAPTER 3 – MITIGATION OF PERI-IMPLANTITIS BY DESIGN AND STABILITY OF BIFUNCTIONAL PEPTIDES WITH ANTIMICROBIAL PROPERTIES[1]

ABSTRACT

The integration of molecular and cell biology with materials science has led to strategies to improve the interface between dental implants with the surrounding soft and hard tissues in order to replace missing teeth and restore mastication. More than 3 million implants have been placed in the US alone and this number is rising by 500,000/year. Peri-implantitis, an inflammatory response to oral pathogens growing on the implant surface threatens to reduce service life leading to eventual implant failure, and such an outcome will have an adverse impact on public health and significant health care costs. Here we report a predictive approach to peptide design, which enabled us to engineer a bifunctional peptide to combat bacterial colonization and biofilm formation, reducing the adverse host inflammatory immune response that destroys the tissue surrounding implants and shortens their lifespans. This bifunctional peptide contains a titanium-binding domain that recognizes and binds with high affinity to titanium implant surfaces, fused through a rigid spacer domain with an antimicrobial domain. By varying the antimicrobial peptide domain, we were able to predict the properties of the resulting bifunctional peptides in their entirety by analyzing the sequence-structure-function relationship. These bifunctional peptides

---

[1] * **Wisdom C**, Zhou, Y., Chen, C., Tamerler, C., and Snead, M.L. Mitigation of peri-implantitis by design and stability of bifunctional peptides with antimicrobial properties. ACS Biomaterials Science & Engineering. 2019

achieve: 1) nearly 100% surface coverage within minutes, a timeframe suitable for their clinical application to existing implants; 2) nearly 100% binding to a titanium surface even in the presence of contaminating serum protein; 3) durability to brushing with a commercially available electric toothbrush; and 4) retention of antimicrobial activity on the implant surface following bacterial challenge. A bifunctional peptide film can be applied to both new implants and/or repeatedly applied to previously placed implants to control bacterial colonization mitigating peri-implant disease that threatens dental implant longevity.

INTRODUCTION

There is a continuing need to improve patient treatment to ensure the longevity of the therapeutic advantages offered by titanium dental implants [53-60]. The creative fusion of molecular and cell biology with materials science and engineering has resulted in improved understanding of implant-tissue interfaces [61]. These advances have been translated clinically to improve oral and systemic health through the replacement of diseased teeth by titanium dental implants, among numerous examples [35,62,63]. Titanium and its alloys have the requisite toughness needed to resist the repeated loading that occurs with food mastication. Titanium is biocompatible, and more importantly, inherently promotes its own integration into host bone by activating the Wnt/integrin signaling pathway for osteogenesis [64].

In recent years, increased reliance on dental implants to restore missing teeth has resulted in a concomitant rise in the prevalence of peri-implant disease, a host-mediated immune response to bacteria which can shorten implant life and culminate in the loss of the implant [65,66]. A growing consensus suggests that peri-implant disease is similar to periodontal disease: bacterial plaque accumulation and microbiome dysbiogenesis trigger a host immune inflammatory response that destroys soft- and hard-peri-implant tissues [67-69]. Within weeks after implant placement, a biofilm develops consisting of the typical subgingival bacterial species, including keystone periodontal pathogens such as *A. actinomycetemcomitans, P. gingivalis, T. forsythia, T. denticola,* and *P. intermedia* [70-72]. Dysbiosis shifts the relative abundance of commensal species to pathogens. For many patients, this shift induces the host to mount an inflammatory response leading to peri-implant disease, starting with peri-implant mucositis and progressing to peri-implantitis, which is accompanied by dramatic bone loss that can necessitate implant removal [73]. A

treatment protocol that can slow and/or prevent bacterial infection may help to mitigate the host immune response and slow peri-implant disease progression.

The incidence of peri-implantitis is reported to be as high as 14.5% after 9 years of service although clinically significant, non-linear loss of bone support around the implants may be present as early as after 3 years after placement in more than 80% of patients [74]. With over 3 million implants placed in the US alone and growing by 500,000 implants/year [59], a reduced service life ending in implant failure will adversely impact public health, trigger increased health care costs and precipitate a loss of public confidence in the dental profession. Furthermore, this outcome may dissuade many patients to avoid this therapy who would benefit from the health benefits of implants. Currently, the goal of implant disease treatment is to control bacterial infection through mechanical debridement and bacterial plaque control, in order to mitigate the host immune response, in order to slow disease progression [75]. However, debridement, which is often performed with titanium brushes [76], results in implant surface damage and loss of biocompatibility. This hastens inevitable apical movement of the implant-supporting tissues and worsens the loss of supporting hard and soft tissue.

An additional challenge associated with prevention of implant infection is the increased incidence of bacterial resistance, which represents a major public health concern [77-80]. Novel antibacterial agents and strategies are needed to ensure future therapeutic efficacy [81]. While systemic antibiotics can treat infections that result from non-resistant bacteria, the peri-implant environment poses many challenges. Implant surfaces are susceptible to biofilm development as bacteria attach to the surface and synthesize an extracellular biofilm matrix [52]. An estimated 80% of human infections are associated with biofilms [82]. Biofilms respond differently to antibiotics than planktonic bacteria and are

difficult for antibiotics to penetrate [52,83]. Poor antibiotic penetration into biofilms results in subtherapeutic antibiotic concentrations and increases the likelihood of developing antibiotic resistance [84]. Preventing the attachment of planktonic bacteria to the implant surface, while killing them via antimicrobial agents that do not lead to the development of resistance represents a novel strategy for reducing biofilm formation and preventing persistent infection that leads to implant failure [11,12]. One approach to addressing bacterial resistance is the use of antimicrobial peptides (AMPs). AMPs are natural antimicrobials that form part of the innate immune defense peptides of both invertebrates and vertebrates. Most AMPs contain fewer than 50 amino acids and more than 2800 AMPs have been discovered from natural resources [80]. Integration of computer-assisted peptide design methods has increased the number of *in silico* designed antimicrobial peptides. The mechanisms of AMP action on bacteria includes membrane perturbation, disruption and/or translocation affecting diverse physiological events such as cell wall biosynthesis, pore formation, and cell division, as well as non-membrane-based pathways. The mechanism for GL13K action on bacterial membranes involves localized removal of lipid from the membrane through peptide induced micellization. The mechanism for action of AMPA is not yet fully explored, it is also considered to have its action through membrane permeation [85,86]. Furthermore, their antimicrobial affects can mitigate biofilm formation when used alone or in combination with other AMPs, or even with antibiotics, to achieve the desired antimicrobial effect and preserve the health of the host tissues without triggering resistance.

Systemic delivery of AMPs has been a major limiting factor in their wider use as therapeutics because a high AMP concentration is required to achieve effective antimicrobial activity and such levels can potentially result in *in vivo* damage to host cells

[87]. Local delivery of AMPs may overcome this challenge by reducing and focusing the required therapeutic concentration and thereby decrease the potential for deleterious effects on eukaryotic cells [87]. The advantages of delivering AMPs locally have been explored using a variety of methods for their retention on implant surfaces, including physical adsorption and chemical immobilization strategies. Chemical immobilization strategies include covalently attaching AMPs to the implant surfaces using silane-, catechol- and phosphate-groups [88-91]. Structural constraints introduced to the AMP during covalent coupling are known to limit antimicrobial activity, more so, the covalent coupling procedure can only be performed prior to implantation as they are generally performed under harsh conditions which prevents their intraoral application. To this point, investigators recently demonstrated that amphipathic GL13K antimicrobial peptide can be used to coat dentin to resist recurrent caries around resin bonded dental restorations [92,93].

Combinatorial screening of peptide sequences with affinity for various materials has identified hundreds of peptides with the ability to self-assemble on metal-, metal oxide, mineral- and polymer-surfaces. As the number of the biocombinatorially selected peptides increased, computational methods have provided an understanding for the peptide-solid materials interactions, as well as for their self-assembly and molecular recognition mechanism(s) on nanostructured materials including metals, metal oxides, ceramics and others [94-98]. By merging biocombinatorial and computationally methods, we have developed high affinity inorganic binding peptides for titanium and titanium alloys. Furthermore, we have engineered these peptides into bifunctional peptide molecules that incorporate biologically instructive signaling functions in order to create novel, bioactive biomaterial interfaces [31,99-102]. We demonstrated that titanium binding peptides (TiBP) can be used to design a biomimetic interface for enhancing bioactivity in osteoblast and

fibroblast cells when coupled with RGD peptides [103]. We have further demonstrated that TiBP is an effective anchor for AMPs on implant surfaces, serving to localize the molecule effectively for repeated intraoral applications [104]. When a TiBP anchor was combined with a Wnt signaling peptide [105,106], the resulting bifunctional peptide produced a peptide film on implant surfaces that led to enhanced osteogenesis in human stem cells, consistent with directed bone regenerative capacity [35]. We next combined the TiBP with antimicrobial peptides and demonstrated their effective use against *E. coli, S. epidermis* and *S. mutant* strains [29 50]. While our earlier studies utilized a simple flexible spacer of amino acids, e.g., "GGG", to combine two distinctive AMPs, we have now analyzed sequence-structure-function relationships for optimal design of the spacer. By computationally studying the Dictionary of Protein Secondary Structure (DSSP) features and observed patterns, we proposed secondary structure “rules” to enhance antimicrobial activity of bifunctional peptides. By designing a rigid and longer amino acid spacer domain, "GSGGG", between the TiBP and the AMP domains, we significantly improved the antibacterial efficacy against *S. mutans* bacteria [107]. We demonstrated the TiBP as an effective anchor for the AMPs on implant surfaces serving to localize the molecule effectively for repeated intraoral applications [104].

Here, we report a novel antimicrobial medicinal approach to slowing or halting the progression of peri-implant disease by furthering the design of bifunctional peptides that deliver a local antimicrobial peptide. This film can be applied in two minutes and can be repeated at follow up appointments. The renewable effects of the bifunctional peptides upon successive reapplication were evaluated on bacteria-fouled and -cleaned dental implant surfaces, mimicking the re-treatment of implants affected by peri-implant disease in a dental office [104]. We systematically studied the sequence-structure-function

relationships of two bifunctional peptides that incorporated structurally distinctive antimicrobial peptides combined with the same anchoring domain using a newly developed longer, more rigid peptide spacer. Our secondary structure prediction suggested that greater helical content could improve antimicrobial activity while preserving the intrinsically disordered behavior of TiBP for effective surface binding. The resulting bifunctional peptides were evaluated for their suitability for clinical deployment using tests of peptide binding, stability, antimicrobial function and durability *in vitro* on titanium implant discs. Our computational predictions were merged with experimental structural analyses and showed enhanced design of bifunctional peptides with the best candidate molecules outperforming other peptides in promoting antimicrobial film activity. Overall, we demonstrate that our engineered small bifunctional peptide selectively binds to titanium/titanium alloy implant surfaces to deliver an antimicrobial peptide film in as little as two minutes. This non-surgical approach has the potential to improve oral health by controlling microbial dysbiogenesis and reducing peri-implant disease progression. This approach could be more widely beneficial for the design of a range of bioactive biomaterials interfaces that could for the basis for next generation therapeutics.

MATERIALS AND METHODS

Peptide Synthesis, Purification, and FITC-Derivatization

Peptides were synthesized by standard solid phase peptide synthesis technique using Fmoc chemistries and Wang resins (AAPPTec Focus XC solid phase peptide synthesizer, Louisville, KY). Fmoc protecting groups were removed by 20% piperidine in dimethylformamide (DMF). Following deprotection, piperidine was removed by DMF and the samples were solubilized in DMF at a concentration of 0.2M and added in 7-fold

excess. The amino acids were activated with 0.4M O-benzotriazole-N,N,N',N'-tetramethyl-uronium-hexafluoro-phosphate (HBTU) and 1M 4-methyl morpholine (NMM) in DMF. Reactions were performed with mechanical mixing under nitrogen gas. Resin-bound peptides were dried with ethanol and cleaved using a cleavage cocktail. Reagent K (TFA/thioanisole/phenol/ethanedithiol at a ratio of 87.5:5:5:2.5) was used to deprotect side-chain and peptides were precipitated with cold ether. The crude peptides were purified using reverse phase-HPLC to greater than 98% purity, lyophilized and stored at -20°C.

Fluorescein 5(6)-isothiocyanate (FITC) was used to fluorescently derivatize bifunctional peptides on their free C'-termini for experiments requiring visualization of bifunctional peptide molecules bound to the surface of titanium implant discs.

Peptide Property Calculations

Peptide CD Data Collection and Secondary Structure Prediction

Secondary structure estimation was accomplished using a Jasco J-810 circular dichroism (CD) spectrophotometer. Solutions of 40μM peptide in 100mM Tris-HCL buffer with varying volumes of 2,2,2-trifluoroethanol (TFE) were prepared for CD analysis. A minimum of 8 scans over wavenumber 190-260nm with a scan rate of 0.5 nm/min were collected on a calibrated spectrophotometer and averaged. The background was subtracted, and the spectra smoothed using the Savitzky-Golay algorithm. The resulting CD spectra were deconvoluted using the BeStSel web server for accurate prediction of protein secondary structure and folding [108].

Predicted secondary structure contents for helical (α, and π-helix), beta (β-bridge, bonded turn), and irregular (bend and loop) features were determined using the Chou-

Fasman algorithm. The Chou-Fasman algorithm was applied for each bifunctional peptide after uploading their CD spectra and amino acid sequences using the online server available through the CD Analysis and Plotting Tool (CAPITO) [109].

Peptide Structure Analysis

The *de novo* 3D structural modeling algorithm, PEP-FOLD 3.5, was implemented to generate Protein Data Base (PDB) models for a minimum of five of the best predictions for each bifunctional peptide sequences [110,111]. PEP-FOLD 3.5 was used to generate 3D-structural conformations of linear peptides. PEP-FOLD 3.5 generates peptide structures by assigning one of 27 structural alphabets where fragments of four amino acid residues overlap with three residues. The structural alphabet generalizes the secondary structure by assigning geometric descriptors created by the Hidden Markov model as described by Maupetit, et. al., [112]. 3D models were ultimately generated from the fragments using a coarse-grained representation and refined by 30,000 Monte-Carlo steps using the PEP-FOLD 3.5 online service on an average of 200 simulations executed assuming aqueous conditions and neutral pH. Once generated, the models were clustered and sorted using sOPEP (Optimized Potential for Efficient Structure Prediction) with non-biased modeling.

*S*imilarity among the predicted secondary structure models for the bifunctional peptides was compared for each of the constituent domains: titanium binding domain (TiBP), spacer, and each of two unique antimicrobial domains using the MatchMaker tool. The individual constituent domain structures were superimposed on the corresponding segments of the bifunctional peptide structure. The Match-Align tool was used with a 5Å threshold and the percent identity or degree of relatedness was recorded. Backbone rigidity of the bifunctional peptides was predicted using the DynaMine webserver

following their amino acid sequence in FASTA format [113]. The server segmented the sequence and the fragments were used as the input for the DynaMine predictor for the given segment length. The predictions for each segment were reassembled to produce a dynamics profile from the amino acid sequence.

Protein Data Bank files containing the secondary structure models generated by PEP-FOLD 3.5 were visualized and further analyzed by the UCSF Chimera program [114]. The theoretical "footprint" for each bifunctional peptide was calculated using the measure tool in Chimera. The footprint was determined by obtaining the distance from the α-carbon of amino acid residues to obtain length and width values. These measurements were converted to corresponding area and the number of peptide molecules required to saturate a 10 mm disc surface area serving as an implant mimic was determined. The number of peptides was converted to a molecular mass required to deliver the corresponding surface coverage to the titanium implant disc surface.

A web interface program DichroCalc [115] was used to predict the theoretical circular dichroism spectra from secondary structures models predicted with PEP-FOLD 3.5. Spectra were requested in ellipticity units [(deg cm^2)/dmol] over wavenumber 190nm to 260nm and compared to the corresponding experimentally collected spectra. The Hirst *ab initio* parameter set was used for backbone chromophores.

Titanium Implant Disc Preparation

Coin-shaped titanium implant discs were punched from grade 4 titanium by the USC Engineering Shop. The discs were 10mm in diameter and 0.5mm thick, lap-polished and air-blasted with 180-220 micron titanium dioxide particles. Following manufacturing, the discs were cleaned as stated in a published protocol used for producing surfaces optimal

for osseous integration [56]. The protocol included sonication in DI H_2O for 5 minutes, ethanol for 30 seconds, DI H_2O for 30 seconds, 40% sodium hydroxide for 10 minutes, washed in DI H_2O for 5 minutes, 50% nitric acid for 10 minutes followed by rinsing with DI H_2O for 5 minutes. The discs were autoclaved prior to use.

Peptide Binding to Implant Discs

Titanium implant disc functionalization with bifunctional peptides was accomplished by incubating 100μL of a specified fold concentration of the theoretical "footprint" concentration ontoclean, sterile discs for different time periods at 37°C for 2 minutes. Following incubation, the discs were transferred to a sterile well in a 24-well plate containing 500μL of DI H_2O and washed multiple times to remove unbound peptide. The discs were transferred to a clean glass microscope slide for imaging using a fluorescent microscope. All experiments were repeated a minimum of three times and images were recorded at 10X magnification.

Determination of Surface Coverage

A custom MatLab script was developed to determine the percent surface coverage of fluorescently labeled bifunctional peptides on the implant disc surface. The color fluorescent images were read into MatLab using the *imread* function. The images were converted to black and white and the total number of black and white pixels quantitated. The number of white pixels corresponding to the fluorescently labeled peptides, was divided by the total number of pixels to determine the percent surface coverage. The theoretical footprint was used solely to determine an *ab initio* concentration for achieving

an optimal bifunctional peptide interface in a clinically relevant time interval and did not include lateral resolution.

Serum Competition Assay

Serum competition binding assay was completed with 1.0wt%, and 5.0wt% of bovine serum albumin (BSA) at selected theoretical "footprint" concentrations of FITC-labeled bifunctional peptide. Prior to functionalization of sterile titanium implant discs, a solution of BSA and the bifunctional peptide was made in a sterile centrifuge tube. In a sterile 24 well plate, 100μL of the BSA/bifunctional peptide solution was pipetted onto a titanium implant disc and incubated at 37°C for 2 minutes. The discs with BSA/bifunctional peptide were transferred to a new well containing 500μL sterile deionized water for 1 minute and washed to remove unbound peptide. The discs were transferred onto a clean glass microscope slide and imaged as previously described [104].

Mechanical Durability Assay

Sterile titanium implant discs were functionalized with FITC-labeled bifunctional peptides and brushed using a commercially available electric toothbrush, as previously described [63, 78-79]. Deionized water was applied to the functionalized discs and an electric toothbrush with a round head the same size as the implant disc was applied to the disc for 1 minute. A 100g weight was secured to the toothbrush 10cm from the brush head to ensure consistent force during brushing. Following brushing the implant disc was imaged.

Bacteria Culture

Streptococcus mutans bacteria (ATCC 700610) were cultured according to an ATCC protocol. Frozen stocks were streak plated on agar and incubated for 24 hours at 37°C in atmosphere with 5% CO_2. A single bacterial colony was used to inoculate 5mL of Brain Heart Infusion (BHI) broth in a sterile 50mL conical tube and incubated overnight in the same conditions. Following incubation, 1mL of culture was added to 9mL of fresh media and grown to mid-log phase with a final concentration of 10^5 CFU/mL.

Visualizing Bacteria on Implant Discs

Following the functionalization of titanium discs, they were transferred to a sterile well in a 24-well plate and 400 µL of *S. mutans* bacteria at a concentration of 10^3 CFU/mL was added to the wells containing the discs and incubated for 24 hours at 37°C in atmosphere with 5% CO_2. Following incubation, discs were imaged with a fluorescent microscope to visualize FTIC-labeled bifunctional peptides on the disc surface after bacterial challenge. The dead bacteria were stained with propidium iodide and imaged using a fluorescent microscope. Experiments were repeated in triplicate and images were recorded at 10X magnification.

Statistical Analysis

For all experimental groups, values are reported as mean ± standard deviations. One-way analysis of variance (ANOVA) was performed to assess statistical significance. Statistical significance was set at $p<0.05$.

RESULTS AND DISCUSSION

We explored the structure-function relationship of bifunctional peptides designed with two distinct antimicrobial peptide domains. Each bifunctional peptide molecule incorporated three peptide domains: an implant anchoring domain provided by the TiBP, an antimicrobial domain provided by the AMP, and a spacer domain to ensure the functionality of each of the two other domains when constrained within a single peptide chain. Computationally derived rules for predicting performance of antimicrobial bifunctional peptide films and experimentally evaluated for antimicrobial activity, extent of film coverage and binding, binding under competition from an interloper contaminant, and mechanical durability within clinically relevant parameters needed by dentists to treat peri-implant disease.

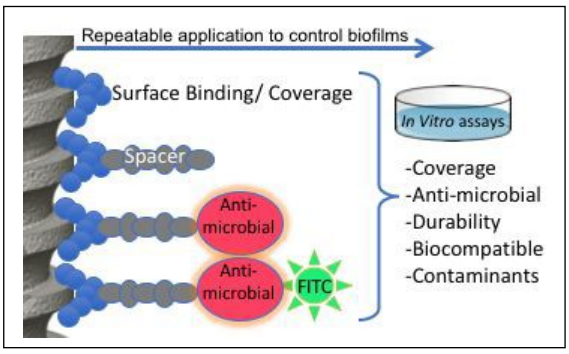

Schematic 1: Our approach includes an antimicrobial peptide film based upon an engineered bifunctional peptide composed of peptide domains for implant binding and antimicrobial activity separated by a spacer. The peptide was tested using a variety of *in vitro* assays to demonstrate its suitability.

Design by Structure Prediction from Amino Acid Sequence

In our earlier work, we identified secondary structure rules that associate greater antimicrobial property with α-helix features adopted over 4- and 5-amino acid residues [50]. Based on this, we screened the CAPITO webserver provided in the Antimicrobial Peptide Database (APD) that contains the cationic AMPs identified with low minimum inhibitory concentrations (MIC) based on their percentage of α-helix secondary structure [109]. The

method implemented in CAPITO uses the Chou-Fasman algorithm to analyze the relative frequencies of amino acids adopting a specific secondary structure conformation based on protein structures previously solved by X-ray crystallography. The secondary structure prediction mainly relies on the probability parameters obtained for the occurrence of α-helix, β-sheet and turns. The Chou-Fasman method is roughly 60% accurate in predicting secondary structures compared to 80% accuracy achieved by some of the recent machine learning approaches [116]; however computationally Chou-Fasman remains a simple and efficient method for approximating secondary structure content starting from an amino acid sequence. Chou-Fasman was used as an initial estimation tool in developing rules for the antimicrobial peptide film property. We identified two AMPs with low MIC: AMPA[117], comprised of 60% predicted α-helix forming amino acids and GL13K[118] containing no predicted α-helix forming amino acids (Table 3-1). The MIC for each AMP is given in Supplemental Information Table 3-4.

Titanium binding peptides were selected using phage display and characterized for their binding affinity using Quartz Crystal Microbalance Spectroscopy (QCM) [50,103]. Based upon this earlier work, we selected one of the strong titanium binding peptides as a promising candidate for the bifunctional peptide film [103]. When AMPA was combined with a spacer to the titanium binding peptide (TiBP) domain, the α-helix content of the resulting bifunctional TiBP-AMPA increased to 69%. Whereas combining TiBP with GL13K resulted in a drastic change to the α-helix content for the bifunctional TiBP-GL13K molecule, with α-helix content as low as 50%.

Native chimeric proteins containing multiple functional domains often are separated by inter-domain sequences called "spacers" that enable multiple domains to

coexist on a single polypeptide chain. Inspired by this, we studied different spacer sequences when designing the bifunctional peptides described here. The goal of the spacer design was to preserve and enhance the function of each of the functional domains within the molecule. We previously tested the effects of spacers on the overall bifunctional peptide by testing them with a single antimicrobial peptide, AMP1, linked with a strong titanium binding peptide sequence (TiBP) [29,50,103,119]. Here, a five-amino-acid spacer, GSGGG, resulted in drastic improvement of the antimicrobial efficacy against *S. mutans*, compared to a three amino acid, GGG spacer [120]. We therefore elected to combine the TiBP domain to each of the two selected AMPs using the GSGGG spacer.

Table 3-1: Chou-Fasman secondary structure predictions from amino acid sequences for the bifunctional peptide and its constitutive domains. Secondary structure features including helix (α, 310 and π-helix), beta (β-bridge, bonded turn), and irregular (bend and loop) features.

	α-helix	β-strand	irregular
TiBP	0%	0%	100%
AMPA	60%	0%	40%
GL13K	0%	0%	100%
TiBP-AMPA	69%	0%	31%
TiBP-GL13K	50%	0%	50%

Table 3-2 provides the physicochemical properties for AMPs and the related bifunctional peptide. Both of the AMPs selected are cationic with net positive charge of 5 and 4, respectively for AMPA and GL13K. In contrast, the net charges of the corresponding bifunctional peptides, TiBP-AMPA and TiBP-GL13K increased to 8 and 7, respectively.

Table 3-2: Physicochemical properties of peptides .

		# AA	MW	pI	Charge	GRAVY
TiBP	*RPRENRGRERGL*	12	1496	12	+3	-2.6
AMPA	*KWKLWKKIEKWGQGIGAVLKWLTTW*	25	3085	10	+5	-0.4
GL13K	*GKIIKLKASLKLL*	13	1429	11	+4	0.7
TiBP-AMPA	*RPRENRGRERGL GSGGG KWKLWKKIEKWGQGIGAVLKWLTTW*	43	4991	12	+8	-1
TiBP-GL13K	*RPRENRGRERGL GSGGGG KIIKLKASLKLL*	30	3218	12	+7	-0.8

The Chou-Fasman secondary structure algorithm predicted greater helical content in the bifunctional peptides compared to either of the AMP domains in isolation. Further, the distribution of secondary structure between the AMPs in isolation compared to the bifunctional peptides suggested that the AMPA domain retained a greater percentage of secondary structure than GL13K. Thus, we predicted that a design with AMPA would have greater antimicrobial potential than one containing GL13K. We recognize the limitations of Chou-Fasman in predicting secondary structure; however, the GL13K α-helix prediction differed only by 10% from a recently reported estimate on the secondary structure of GL13K using a complementary approach [92,93].

Design by Hydrophobicity and Amphipathicity

Hydrophobicity and amphipathicity are believed to allow the AMP to penetrate a bacterial lipid bilayer and disrupt the cell membrane [121,122]. Using the Calculate and Predict tool from the Antimicrobial Peptide Database (APD), it was determined that TiBP-AMPA has a hydrophobic ratio of 30% with 10 hydrophobic residues aligned along the same surface of the α-helix. TiBP-GL13K revealed a hydrophobic ratio of 26%, slightly less than that of TiBP-AMPA, with only 5 hydrophobic residues aligned on the same surface (Supplementary Information Figure 3-8). This sequence analysis revealed that the majority of the hydrophobic amino acids in both bifunctional peptides were located in the AMP

region. The TiBP region contains only one hydrophobic residue on the C'-terminus of the binding peptide, immediately before the spacer. The hydrophobic nature of the bifunctional peptide is attributed to the AMP portion, which may increase the likelihood of the AMP interacting with the bacterial membrane while the binding domain remains anchored on the implant surface. To visually demonstrate this distribution of residues, we generated helical wheels using an online tool (http://rzlab.ucr.edu/scripts/wheel/wheel.cgi). The helical wheel diagrams represented in Figure 3-1 show that 10 hydrophobic residues reside on the same surface of the α-helix for TiBP-AMPA compared to only 5 for TiBP-GL13K.

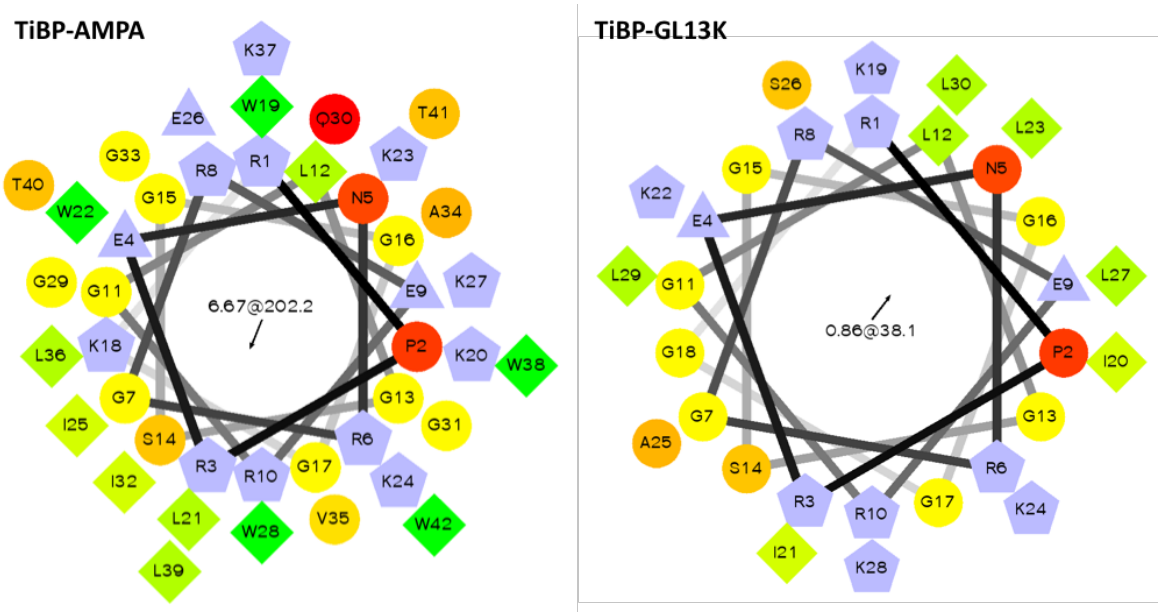

Figure 3-1: Helical wheel predictions of bifunctional peptides. Hydrophilic amino acid residues are represented as circles, hydrophobic amino acid residues as diamonds, potentially negatively charged residues as triangles, and potentially positively charged residues as pentagons. The most hydrophobic amino acid residue is shown in green with the chroma intensity decreasing proportionally to hydrophobicity, with zero hydrophobicity coded as yellow. Hydrophilic residues are coded red with intense red chroma being the most hydrophilic (uncharged) residue, and the chroma decreasing proportionally to the hydrophilicity. Potentially charged residues are shown as blue.

Dynamics Prediction in Bifunctional Peptide Design

Next, the dynamics of the peptide backbone were studied to determine the disorder of the regions within the whole bifunctional peptide relative to their constitutive binding, spacer, and AMP domains. DynaMine, a tool that leverages chemical shift data to make predictions about backbone dynamics at the amino acid residue level, was used for this purpose. The dynamics of the residues are essential for peptide function, so evaluating the backbone dynamics in relation to the bifunctional peptide function is important in considering the design of these peptides [123]. Given a protein sequence, DynaMine predicts backbone flexibility at the level of amino acid residue in the form of backbone N-H S2 order parameter values. These S2 values represent how restricted the movement of the atomic bond vector is with respect to the molecular reference frame. The results from the DynaMine analysis are depicted in Figure 3-2.

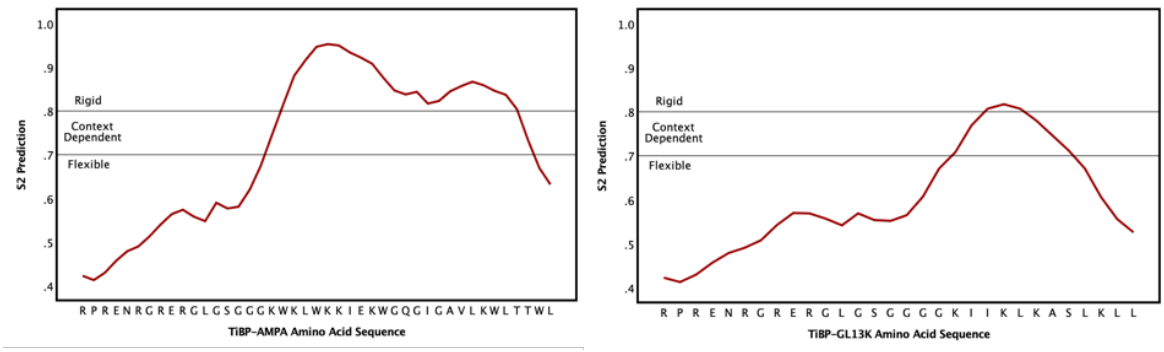

Figure 3-2: DynaMine classification for backbone dynamics of amino acids comprising each bifunctional peptide. The AMP domains located on the C'-terminus represent a more ordered region relative to the TiBP binding domain located on the N'-terminus. The TiBP domain is an intrinsically disordered peptide. AMPA has more order than GL13K, which could contribute to its greater predicted antimicrobial function.

The more hydrophilic amino acids located in the AMP domain of the bifunctional peptide correspond to the more ordered region of the bifunctional peptide. The Gly and Ser residues comprising the spacer region, are known to be more disordered, serving to

promote the propensity for a more dynamic backbone that improves overall function of the tethered molecule, namely binding to the implant surface while presenting an active antimicrobial domain. This is important for dental implants as the accumulation of a biofilm on the implant is believed to lead to an adverse host immune response to the bacterial antigens, resulting in host directed inflammatory destruction of soft and hard tissues surrounding the implant [69,73,124,125]. Consistent with this interpretation, the binding domain for the bifunctional peptides showed the least variation in order. Intrinsically disordered proteins (IDPs) function in a wide spectrum of biological situations due to their ability to adapt their structure by adopting conformation over a small number of amino acid residues [113,126-128]. Thus, it would be expected that the dynamics of the binding domain may resemble the range of conformational structure observed within IDPs.

Secondary Structure Modeling and Analysis

A more in depth secondary structure prediction was accomplished by developing structural models from the amino acid sequences using PEP-FOLD 3.5 [129]. Secondary structure models generated for the individual domains and the bifunctional peptide appear in Figure 3-3. Secondary structural analysis of the antimicrobial peptide domains, AMPA and GL13K, revealed that the AMPA domain is composed of two short α-helixes joined by a turn while GL13K is composed of one short α-helix. The Chou-Fasman analysis did not identify helicity exclusive to the GL13K domain, although helicity was predicted for the bifunctional peptide, TiBP-GL13K.

The mechanism by which amphipathic α-helical AMPs kill bacteria may involve their creation of trans-bilayer pores which serve to disrupt the bacterial membrane by separating the polar from the non-polar parts[130]. Thus, we predicted TiBP-AMPA would

have greater antimicrobial activity than TiBP-GL13K due to the greater number of membrane-disrupting helical features present in AMPA (two features) compared to GL13K (one feature).

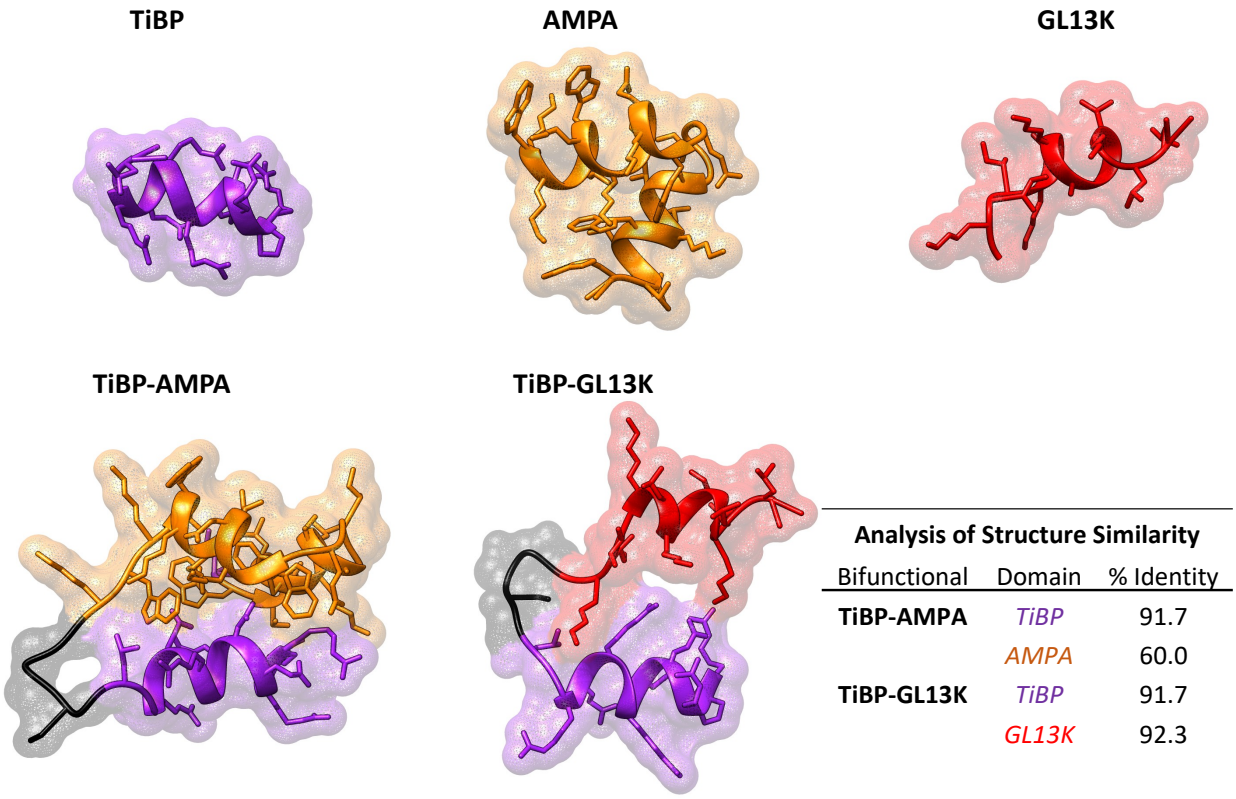

Analysis of Structure Similarity

Bifunctional	Domain	% Identity
TiBP-AMPA	*TiBP*	91.7
	AMPA	60.0
TiBP-GL13K	*TiBP*	91.7
	GL13K	92.3

Figure 3-3: Secondary structure models and structural similarity analysis . Each TiBP domain is colored purple, the AMPA domain is colored orange and the GL13K domain is colored red, while the spacer domain linking the antimicrobial and binding domains is colored black. The chart depicts the structural similarity determined by superimposing the domain models over the bifunctional models and calculating the percent identity.

Using Chimera, the PDB file could be compared using the MatchMaker tool and the structure models superimposed [39]. Similarity among the individual functional domains was evaluated by superimposing the structural model for the AMP and TiBP domain alone on the corresponding portion of the bifunctional peptide. The superimposed structures were further studied to determine the percent identity or the degree of relatedness. This was

useful in determining the preservation of the TiBP domain and each antimicrobial domain when linked by the spacer in the whole bifunctional peptide. This analysis revealed that 91.7% of the TiBP domain identity was preserved when combined with either AMPA or GL13K through the GSGGG spacer. The GL13K domain retained 92.3% identity, while the AMPA domain retained only 60% identity. This suggests that most of the secondary structure of the TiBP and GL13K domain are preserved by the GSGGG spacer, while further engineering of the spacer could improve the antimicrobial activity of TiBP-AMPA. Preservation of the TiBP domain is postulated to be critical for binding to the implant surface in the presence of competing proteins while contributing to the durability of the bifunctional peptide in the oral environment both of which are an essential property for effective clinical deployment.

Experimental Determination of Secondary Structure

Next, secondary structures of the bifunctional peptide were experimentally determined using CD spectroscopy in an aqueous environment with increasing concentrations of TFE to mimic peptide film behavior. Theoretical spectra were determined using DichroCalc from the PDB files generated from the secondary structure models. Secondary structures of the bifunctional peptides were evaluated experimentally using CD spectroscopy in an aqueous environment. The presence of ordered or disordered conformational state was assayed for each bifunctional peptide. We next evaluated the folding propensity of the peptide sequences in the presence of increasing TFE concentration. TFE is used as a structure stabilizing solvent to mimic the restricted mobility of the peptides due to inherited function of the bifunctional peptide. As the bifunctional peptide interacts with the titanium surface through its anchoring domain it also interacts

with the bacterial membrane via the antimicrobial domain. Theoretical spectra were determined using DichroCalc from the PDB files generated from the secondary structure models [90]. Analysis performed by the Dynamine program for dynamic behavior of the TiBP domain suggest the TiBP behaves as an intrinsically disordered peptide. While these structural states are representatives of the peptide in aqueous environments, circular dichroism data supported this behavior. In the absence of the TFE, both of the peptides exhibited a strong negative ellipticity band around 198nm representing the pi-pi* transition. This is a characteristic band for random coil conformation which is in equilibrium with other secondary structures. Based upon our prior TiBP related work, we conclude that the titanium binding features of the bifunctional peptide was preserved. Overall, addition of TFE to each peptide resulted in reduced intensity of the pi-pi* transition ellipticity band and an observed ~10nm red shift in absorption wavelength. These results suggest a shift in secondary structure population and both peptides undergoing some degree of conformational reordering in the presence of TFE. Relating such transitions to the bifunctionality of the peptide may provide insights for rational design for bioactive interactions at the interfaces by the peptide.

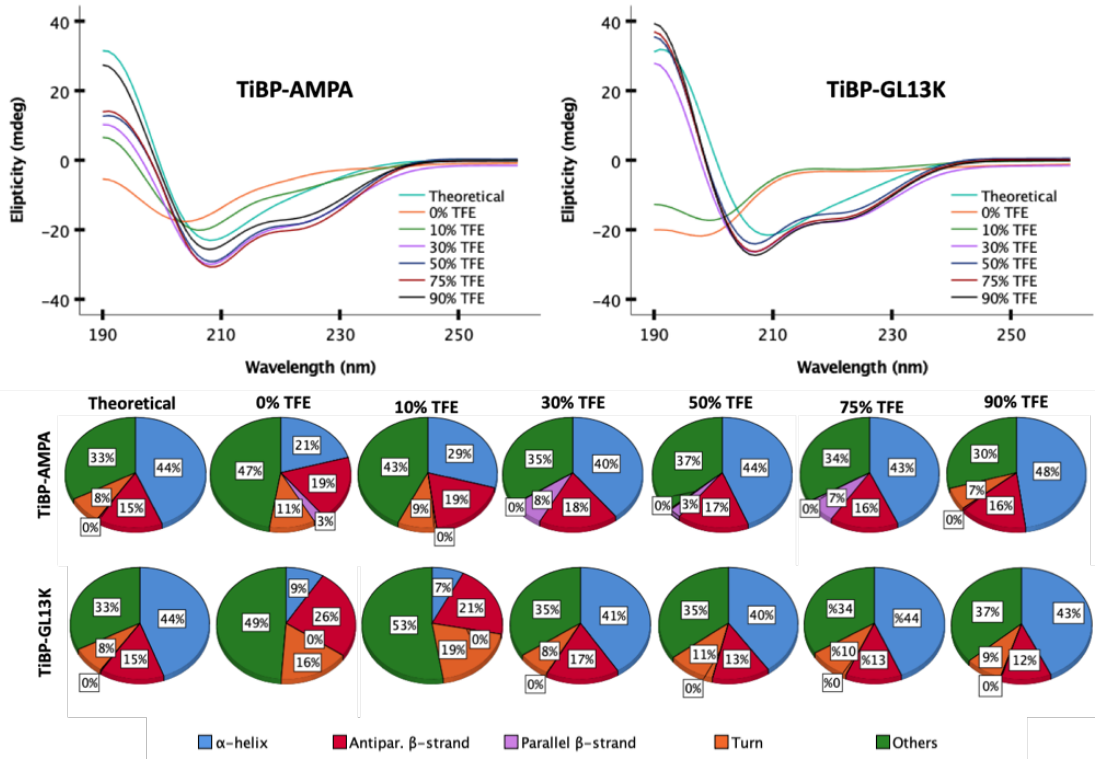

Figure 3-4: Theoretical and experimental CD spectra with deconvolution using Beta Sheet Selection (BeStSel). Experimental CD spectra were collected in aqueous environment and increasing concentrations of 2,2,2-trifluoroethanol. The pie charts represent BeStSel's deconvolution of the CD spectra.

The CD spectra were deconvoluted using Beta Sheet Selection (BeStSel), a method for secondary structure determination from CD spectra [108]. BeStSel links the CD spectra structural findings to the computational Dictionary of Protein Secondary Structure (DSSP) patterns [131]. Our previously described "Rule Induction" method also relied on DSSP structure patterns and identified a pattern of 4- and 5- amino acid α-helix structures as being linked to antimicrobial activity in bifunctional peptides [50,120]. The BeStSel tool allows for deconvolution of experimental CD spectra into the structural feature patterns that are used to inform the "Rule Induction" method. Both bifunctional peptides were found to switch their conformation from an unordered state in aqueous buffers to their functionally relevant α-helical conformation in the presence of TFE. The theoretical CD

spectra determined from the PDB model files more closely represented the 90% TFE environment. This suggests that the computational structural predictions are more accurate for environments similar to the conditions in which the peptides act as a film. The results from the deconvolution using BeStSel for TiBP-AMPA and TiBP-GL13K are depicted in Figure 3-4.

Theoretical Surface Coverage Determination

The concentration of bifunctional peptides theoretical needed to provide 100% surface coverage when applied onto an implant-mimicking titanium disc surface was estimated by measuring the dimensions of the binding peptide domain to obtain a theoretical "footprint" area. The resulting area was used to determine the concentration of peptide molecules required to cover a 10 mm diameter titanium implant disc (

Table 3-3). One limitation of the theoretical surface coverage concentration calculation is that the surface is assumed to be smooth; however, the surface roughness produced by blasting an implant with titanium dioxide to promote osseous integration would result in a greater surface area than what would be calculated. This limitation was overcome by using a multiple of the theoretical binding concentration, up to 6-times (6X), to achieve near 100% surface coverage after a two-minutes binding period. We focused on minimizing the time required to achieve complete surface functionalization by the bifunctional peptide because this will be important in translating this technology to a clinical application. The two-minute binding time frame represents a reasonable working time for application of the bifunctional peptide film in a clinical environment.

Table 3-3: Theoretical "footprint" calculation and concentrations .

	Theoretical Footprint			Conc.
	Length (Å)	Width (Å)	Area (Å²)	µM
TiBP-AMPA	19.8	16.6	329	111
TiBP-GL13K	14.7	11.8	173	211

Evaluation of Binding, Stability and Durability

The theoretical footprint concentration of each bifunctional peptide with a multiple of the binding concentration up to 6X was determined to result in near 100% surface coverage after incubation with a titanium implant disc for only two minutes at 37°C. Following incubation, the discs were washed to remove unbound or non-specifically bound peptide from the surface prior to imaging with a fluorescent microscope. The fluorescent images were then analyzed using a MATLAB script to determine the percentage of the implant disc covered by the bifunctional peptides. The initial binding for TiBP-AMPA resulted in 99% surface coverage after two minutes compared to 96% for TiBP-GL13K. This indicates that in a clinically achievable application, the bifunctional peptides are able to form an antibacterial film with near complete coverage of the implant surface. Representative fluorescent images for each bifunctional peptide are depicted in Figure 3-5, while the chart indicates the mean with standard deviation error bars for three replicate experiments.

The bifunctional peptide film could be applied to a new dental implant prior to implantation and subsequently during recall appointments for treatment to previously placed implants. Recently we demonstrated *in vitro,* a bifunctional peptide that retained

ability to bind to the implant surface after overnight incubation *in vitro* after bacterial fouling and cleaning using a commercially available electric toothbrush [120]. The re-binding of the bifunctional peptide to a fouled and cleaned surface represents the feasibility of applying this technology to existing implants at recall appointments where the bifunctional peptide can be reapplied. However, when rebinding the bifunctional peptide in the oral environment, the peptide will compete for the implant surface with serum and saliva proteins, even after the implant is cleaned using standard dental practices. Thus, the ability of the peptide film to functionalize the implant surface in the presence of serum proteins was determined by pre-mixing the peptide with varying concentrations of bovine serum albumin (BSA) followed by incubating the mixture on the titanium disc for 2 minutes at 37°C. The results of the competitive binding of the bifunctional peptide in the presence of 0.01% BSA are depicted in Figure 3-5. TiBP-AMPA achieved 80% surface coverage while TiBP-GL13K achieved 73% surface coverage. There was no statistical difference between the coverage achieved by the two bifunctional peptides coverage in competition with BSA.

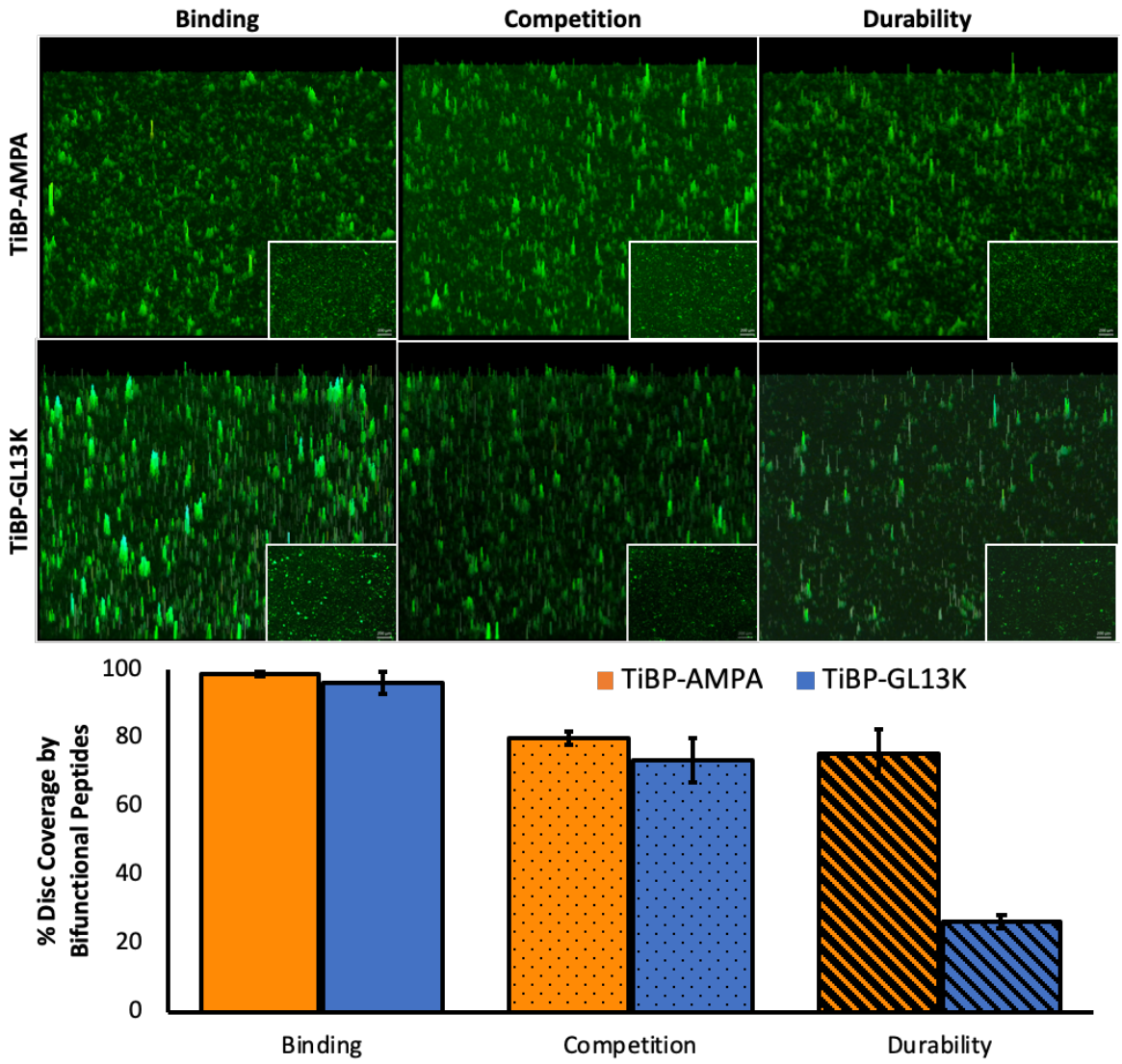

Figure 3-5: Fluorescent microscopy images of binding of bifunctional peptide to titanium implant discs, binding with competition from BSA, and durability following 1 minute of brushing with an electric toothbrush. The chart depicts the means and standard deviations of three replicate experiments for each bifunctional peptide in each condition. TiBP-AMPA binding was statistically significant compared to binding in competition with BSA and durability after 1-minute of brushing ($p < 0.05$). Statistical significance was determined for all conditions of TiBP-GL13K bifunctional peptide ($p < 0.05$). Statistical analysis was conducted using a one-way ANOVA.

The durability of the bifunctional peptide films was evaluated by brushing the functionalized implant discs with a commercially available electric toothbrush with a round

head slightly larger than the implant disc for one minute. The presence of bifunctional peptides was determined by fluorescently imaging the discs with FITC-labeled peptides before and after brushing. The durability of the TiBP-AMPA peptide film was significantly ($p < 0.05$) greater than that of the TiBP-GL13K peptide film. For TiBP-AMPA, 75% of the bifunctional peptide coating was retained compared to 27% for TiBP-GL13K (Figure 3-5).

Bifunctional Activities of the Designed Peptides

The binding and antimicrobial domain activities were evaluated by challenging the bifunctional peptide film applied to titanium implant discs with *S. mutans* bacteria for 24 hours. The FITC-labeled bifunctional peptides were visualized on the disc surface following 24 hours of bacterial challenge using a fluorescent microscope and the surface coverage was determined using MATLAB. The surface coverage was 84% for TiBP-AMPA and 60% for TiBP-GL13K. Representative fluorescent images of FITC-labeled bifunctional peptide on the implant disc and quantification of the percent surface coverage of three replicate experiments are contained in Figure 3-6.

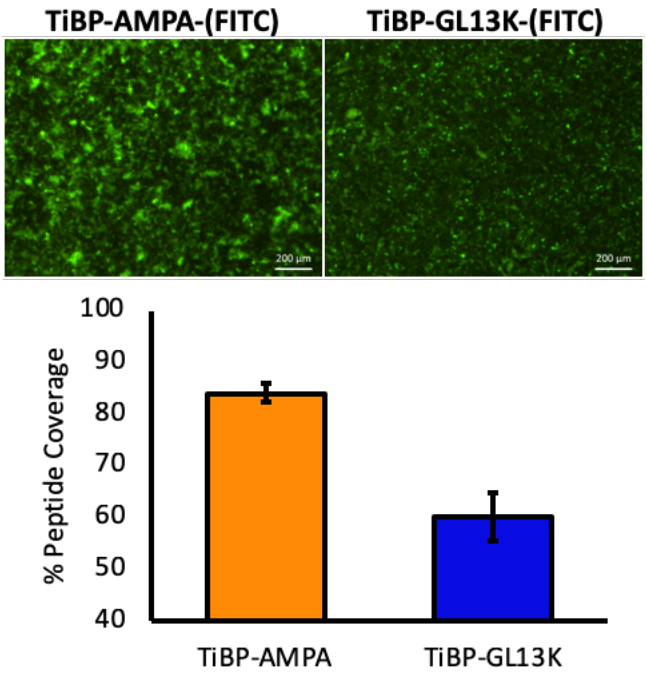

Figure 3-6: Visualization of FITC labeled bifunctional peptides using fluorescence microscopy after challenge by *S. mutans* for 24 hours. The percentage of peptide coverage was determined by evaluating images with a MATLAB script. The chart represents results obtained during three replicate experiments, of which, the fluorescence images are selected as representative of the whole. A statistically significant difference ($p < 0.05$) was found between the means for TiBP-AMPA and TiBP-GL13K coverage using a one-way ANOVA.

The percentage of α-helical secondary structure computationally predicted by the Chou-Fasman method, the secondary structure modeling and the experimental determination of secondary structure using CD supported our design prediction that TiBP-AMPA would outperform TiBP-GL13K in promotion of an antibacterial implant interface. We relied upon the previously established "rule" method [132] for the design of the bifunctional peptides in this manuscript took into the structural composition of the entire bifunctional peptide, not just the binding- or antimicrobial-domains. The rule method was trained on antimicrobial function with experimentally determined antimicrobial functions to identify secondary structural features in bifunctional peptides that promote formation of an effective interface for the prevention of implant associated infection.

The antimicrobial functional efficacy of TiBP-AMPA compared to TiBP-GL13K supported our design prediction. The use of propidium iodide (PI) staining to identify dead bacteria on the titanium disc surface showed 46% dead bacteria coverage for TiBP-AMPA, compared to 10% dead bacteria coverage for TiBP-GL13K. Sterilized bare discs were used as controls showed no dead bacteria. Representative fluorescent images and quantification of three replicate experiments are depicted in Figure 3-7.

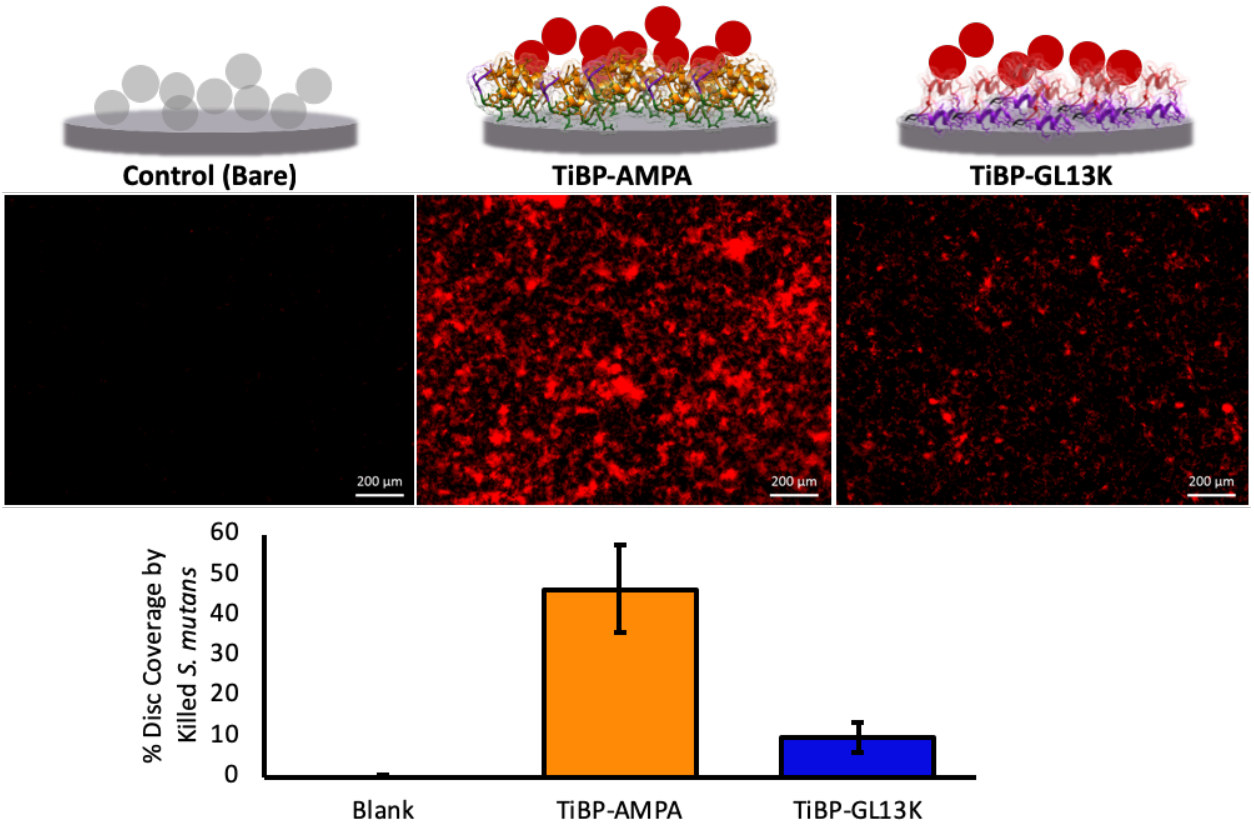

Figure 3-7: Fluorescence microscopy images and quantification of propidium iodide (PI) staining of dead *S. mutans* bacteria on implant discs after challenge for 24 hours. Dead bacteria appear with red fluorescence. The means and standard deviations are depicted in the chart for bare, sterilized titanium discs and discs functionalized by 2 minutes of bifunctional peptide binding at 37°C prior to bacterial challenge. Three replicate experiments were performed and a statistically significant difference ($p < 0.05$) was observed between means using ANOVA.

While one might postulate that this increase in antimicrobial function could due to the amount of bifunctional peptide remaining on the surface, e.g. 84% for TiBP-AMPA compared to 60% for TiBP-GL13K, the conservation of structure in the TiBP domain by the superimposed predicted secondary structures shown in Figure 3-3 suggests equal percentages of identity or relatedness for the binding domains. However, the analysis of backbone dynamics revealed that the antimicrobial domain of TiBP-AMPA was more highly ordered than that of TiBP-GL13K. The expected disordered region represented by the TiBP in both bifunctional peptides extends through the spacer, and much of the antimicrobial domain is disordered for TiBP-GL13K. This finding could affect the anchoring of the bifunctional peptide on the disc, as the disordered region of GL13K may be more available to interact with the implant surface nonspecifically. Additionally, the proposed mechanism of antimicrobial function is more dependent on the hydrophobicity and amphipathicity of the peptide without the additional effects attributed to the increased stability and greater number of α-helical secondary structure features in the AMPA compared to Gl13K. Secondary structure modeling revealed that the AMPA domain comprised two α-helical features joined by a turn compared to only one α-helical feature for GL13K.

The hydrophobic ratio of TiBP-AMPA was slightly greater (30%) than that of TiBP-GL13K (26%). More hydrophobic residues were aligned on the same face of TiBP-AMPA, with 10 residues being aligned for TiBP-AMPA compared to only 5 residues for TiBP-GL13K. With regard to hydrophobicity and amphipathicity, the design prediction based on the sequence and structure supported the experimental finding that TiBP-AMPA has greater antimicrobial activity than TiBP-Gl13K.

Overall, the antimicrobial peptide film property is observed to be dependent on the extent of the α-helical secondary structural features. Peptide stability under competitive binding environment was observed to be related to the ordered structures observed from our analysis of backbone dynamics. Molecular recognition-based peptide self-assembly domain prevented removal of the peptide even under harsh washing conditions. Ordering seems to provide the TiBP-AMPA peptide a competitive advantage. It may be plausible to design TiBP-GL13K with a different spacer combination which would induce an ordering in the structure and enhance its competitive binding. Conformational design parameters are postulated to play a critical role in the peptide stability considering the anchoring domain of the bifunctional peptides are the same. Secondary structure may undergo major changes on the metal surfaces, however functional assembly behavior under the biologically challenged material interfaces may still have a folding preferential.

Taken together, our experimental results demonstrate that using computationally efficient, less resource intensive methods can be used to successfully predict the properties of bifunctional peptide prior to more costly and time-consuming experimental evaluation. The computational design approach was validated experimentally by assessing the binding and antimicrobial function of bifunctional peptides on a simulated implant surface. This technology and approach to design represents a novel strategy to improving and developing bifunctional peptide films to combat bacterial infection and prevent/treat peri-implant disease. Prior to clinical trials, the cytocompatibility and biocompatibility of the bifunctional peptides to human cells will need to be examined. Additionally, the incorporation of AMP sequences not previously explored as antimicrobial agents in bifunctional peptides represents an opportunity to develop more broad-spectrum antibacterial efficacy, as well as options for treatment of antibiotic resistant bacterial

strains. The predictive design approach developed here offers a method for evaluating the functional efficacy of AMP, spacer, and binding domain combinations based on analyses of the relationship between sequence, structure and function. Combining this approach with the recently developed soft epitaxial fit for the binding domain of the peptide to match the epitaxial sites on the implant surfaces would be another area to explore in order to tune the functionality at the solid-interface. This approach may also provide predictable-, rational-, peptide designapproaches for a wide range of hybrid interfaces by combining conformational and interface design aspects

CONCLUSION

We developed a predictive computational approach for designing bifunctional peptides that sought to correlate structure and function, e.g. antimicrobial activity and demonstrated that the resulting peptides show promise as a medicinal approach to addressing bacterial dysbiogenesis[133,134] that leads to peri-implant disease with a shortening of the useful life of dental implants. With over 3 million implants placed in the US alone and growing by 500,000 implants/year [59], a reduced service life ending in implant failure will adversely impact public health. The rapid (two minute) delivery of antimicrobial bifunctional peptide films was tested on dental implant surfaces mimicking the application sequence necessary for re-treatment of peri-implantitis in a dental office [104]. The designed functional peptides consisted of three domains, from the N'-terminus: titanium binding, spacer and antimicrobial.

While the antimicrobial peptides were varied, the binding and spacer domains were kept constant with the goal of demonstrating that a computational approach can predict the antimicrobial properties of the resulting bifunctional peptide films. The percentage of α-

helicity of the bifunctional peptides and their individual constituting domains were computationally predicted by the Chou-Fasman algorithm. The peptides were further analyzed using chimera secondary structure models and these secondary structure predictions were compared experimentally using CD spectroscopy. This predictive design approach considered the structure and function of the entire bifunctional peptide molecule. Three design methods were used here, namely sequence-based, *de novo* modeling, and experimental evaluation; all indicated that peptide incorporating the AMPA anti-microbial domain had greater helical content than the one containing the GL13K antimicrobial domain. This prediction was confirmed by the backbone dynamic data. This ensemble of structural analysis techniques formed the basis for the prediction that TiBP-AMPA would functionally outperform TiBP-GL13K as an antimicrobial peptide film. In particular, amphipathic and α-helicity were shown to be more prominent in ordered regions, which contribute to greater antimicrobial peptide film activity. The bifunctional peptides were evaluated experimentally for their potential to prevent and treat peri-implant disease. The bifunctional peptides were delivered in the clinically relevant manner (2 minute binding period), under competition with serum proteins. Their mechanical durability was tested, and they were empirically challenged with bacteria to confirm our computational predictions. The peptide films have been shown capable of rebinding ability through up to five cycles of bacterial fouling, cleaning and reapplication. These results demonstrate the success of our computational design approach and suggest that the TiBP-AMPA peptide has strong potential as a treatment for peri-implant disease due to its ability mitigate bacterial biofilm formation.

SUPPLEMENTARY INFORMATION

The hydrophobicity analyses of the bifunctional peptides were carried out using the antimicrobial peptide database calculator and predictor tool. TiBP-AMPA has a hydrophobic ratio of 30% with 10 hydrophobic residues aligned along the same surface of the α-helix. TiBP-GL13K revealed a hydrophobic ratio of 26%, slightly less than TiBP-AMPA with only 5 hydrophobic residues aligned on the same surface.

Figure 3-8: Bifunctional peptide hydrophobicity analysis using the Antimicrobial Peptide Database (APD) Calculator and Predictor tool.

Table 3-4: The minimum inhibitory concentration of the AMP domain in isolation. Peptides requiring amidation at the C'-terminus (GL13K and TiBP-GL13K) were synthesized using Rink-amide resin.

	MIC (μM)
AMPA	45
GL13K	64
TiBP-AMPA	64
TiBP-GL13K	128

Table 3-5: Fluorescence image quantification for percentage surface coverage of the images using ImageJ software. Reproduced from Wisdom, C.; Chen, C.; Yuca, E.; Zhou, Y.; Tamerler, C.; Snead, M. L., Repeatedly Applied Peptide Film Kills Bacteria on Dental Implants. JOM (1989) 2019, 71 (4), 1271-1280. DOI: 10.1007/s11837-019-03334-w.

Treatment Cycle	%Surface Coverage
Sterile	18.3
1X Foul	24.3
2X Foul	8.6
3X Foul	32.9
4X Foul	41.5

CHAPTER 4 - REPEATEDLY APPLIED PEPTIDE FILM KILLS BACTERIA ON DENTAL IMPLANT*

ABSTRACT

The rising use of dental implants has increased the prevalence of peri-implant disease that shortens their useful life. A growing view of peri-implant disease suggests that plaque accumulation and microbiome dysbiogenesis triggers a host immune inflammatory response destroying soft and hard tissues supporting the implant. The incidence of peri-implant disease is difficult to estimate, but with over 3 million implants placed in the US alone, and the market growing by 500,000 implants/year such extensive use demands additional interceptive approaches. We report a water-based, non-surgical approach to address peri-implant disease using a bifunctional peptide film, which can be applied during the initial implant placement and later, reapplied to existing implants to reduce bacterial growth. Bifunctional peptides are based upon a titanium binding peptide (TiBP) optimally linked by a spacer peptide to an antimicrobial peptide (AMP). Dental implant surfaces covered with a bifunctional peptide film kills bacteria. Further, using a simple protocol for cleaning implant surfaces fouled by bacteria, the surface can be effectively re-coated with TiBP-AMP to regain an antimicrobial state. Fouling, cleansing, re-binding was confirmed for up to four cycles with a minimal loss of binding efficacy. Rebinding after fouling of a

---

* **Wisdom C**, Chen C, Yuca E, Zhou Y, Tamerler C, Snead ML. Repeatedly Applied Peptide Film Kills Bacteria on Dental Implants. JOM. 2019.

water-based film extends control over the oral microbiome composition providing a novel non-surgical treatment for dental implants.

INTRODUCTION

There is a continuing need to improve patient treatment based on the therapeutic advantages offered by titanium dental implants. However, a complex biofilm rapidly forms on the surface of any dental implant once it is placed in the oral cavity. Within several weeks, the biofilm consists of the typical subgingival bacterial species including keystone periodontal pathogens such as *P. gingivalis, A. actinomycetemcomitans, T. forsythia, T. denticola, and P. intermedia* [135]. The relative abundance of commensal bacterial species to periodontal pathogens shifts with dysbiosis and too often induces the host to mount an inflammatory response leading to peri-implant diseases starting with peri-implant mucositis and ending with peri-implantitis, resulting in the loss of soft and hard tissue anchoring the implant in the jaw and thus threatening the implant's useful life.

The expanded use of implants in dental treatment coupled with the rising prevalence of peri-implant disease threatens to shorten implant life and lead to implant failure in increasing numbers of patients [65,66]. Recent consensus on peri-implant disease points to plaque accumulation and microbial dysbiogenesis as the major factors triggering the host immune inflammatory response [67-69]. Millions of implants are placed yearly around the world, with 3 million placed in the US alone and rising at 500,000/annum [59]. Reduced service life and eventual implant failure will therefore have a growing adverse impact on public health with an increase in health care cost. On the other hand, an effective treatment for peri-implant disease would make the benefits of implants available to a wider-group of patients in need [136,137].

Despite a high success rate, within 5 years of placement, a small percentage (4-8%) of implants fail [8-10] and a higher percentage fail in patients with chronic illness, advanced age and/or poor periodontal health [137-140]. The Cochrane meta-analysis report estimated the

incidence of peri-implantitis as 1.6% after 3 years and 5.5% at 10 years [141,142]. In contrast, Derks and colleagues placed the incidence of peri-implantitis at ~14.5% after 9 years of service [143], while others identified clinically significant, non-linear bone loss as early as after 3 years of function in more than ~80% of patients [143]. With implant use growing, increasing implant loss has a profound financial health care cost with the potential loss of public confidence in the dental profession.

There is currently no definitive means for controlling and eliminating the bacterial biofilm on implants [75,144,145]. Current state-of-the art treatments for implants are similar to those for periodontal disease and include mechanical debridement and/or medicinal means intended to retard the biofilm. For implant surfaces, these include: abrasive cup polishing; abrasive air blasting; titanium brushes with cleansing agents such as sodium hypochlorite or povidone-iodine; chlorohexidine rinses; antibiotics; and antimicrobials. Each treatment can be used alone or in concert by dental professionals. Successful treatment for peri-implant disease must also recognize the need to maintain biocompatibility, osteogenic competency and cell viability at the implant surface to obtain favorable host cell responses [144-146]. Thus, a commonly held goal remains to control the oral microbiota in order to arrest/slow hard and soft tissue destruction by the host inflammatory response.

There have been numerous attempts to boost implant surface performance with biologically active signals [50,103,147-152]. However, the majority of them have required passive absorption or chemical coupling to the surface [153-155]. Absorption leads to leaching and poor performance. Covalent coupling also has limited success because coupling these agents (e.g., thiols, carboxylic acids, hydroxyl, guanidines, and amines) create hostile environments to bioactive molecules, leading to loss of bioactivity [153,156] and/or incorrect display of the bioactivity to the cellular environment. Moreover, these hostile coupling

environments can be used only during manufacturing and not at recall appointments, long after placement, when the longevity of the implant is threatened. Ideally, both strong affinity to the implant surface and maintenance of the antimicrobial state are required.

Peri-implantitis has become a growing concern in the community due to the increasing popularity of dental implants to restore form and function. Because at present, none of the non-surgical treatments result in a superior outcome, there is a lack of consensus with respect to predictable treatments for peri-implantitis, making treatment choices all but unmanageable for clinicians and patients. With the number of dental implants continuing to rise, there is an urgent need to identify a strategy that can further slow or even prevent peri-implantitis. Successful approaches will require novel and rational engineering design that can leverage the multi-faceted characteristics of biomolecules, as well as providing structural and functional properties at the material-tissue interfaces [157,158].

Using a combination of experimental and computational bioengineering approaches we engineered a bifunctional peptide to provide a biocompatible, water-based, easy-to-apply, durable, peptide film that possesses antimicrobial activity. The bifunctional peptide can be repeatedly applied at recall appointments for continued treatment of peri-implantitis to extend implant longevity. Reapplication offers a safe, inexpensive, water-based bifunctional peptide film to treat existing implants at recall appointments to arrest disease progression as a viable peri-implantitis treatment strategy compared to current state of the art treatments.

MATERIALS AND METHODS

Synthesis and Purification of Bifunctional Peptides

Peptides were produced with an AAPPTec Focus XC automated solid phase peptide synthesizer using standard Fmoc chemistries and Wang resins. To remove the Fmoc protecting group, Wang resins preloaded with the first amino acid protected by a Fmoc group were treated with 20% piperidine in dimethylformamide (DMF). Fmoc deprotection was monitored by UV-absorbance and the deprotected resin was then washed with DMF to remove piperidine. Modified amino acids with protected side chains and Fmoc were solubilized in DMF at a concentration of 0.2M and added in 7-fold excess. In a separate measuring vessel, amino acids in solution were activated with 0.4M O-benzotriazole-N,N,N',N'-tetramethyl-uronium-hexafluoro-phosphate (HBTU) in DMF and 1M 4-methylmorpholine (NMM). The activated amino acid was then added to the reaction vessel and mechanically mixed under nitrogen gas for 45 minutes to couple the amino acid to the resin. Double-coupling was used for each amino acid in the sequences. After amino acid addition, the resin was washed with DMF and the protocol applied again for each subsequent amino acid.

Following synthesis, the resins with synthesized peptides were dried with ethanol to remove residual DMF. The peptides were cleaved from the resin and the side-chains were deprotected using Reagent K (TFA/thioanisole/H2O/phenol/ethanedithiol (87.5:5:5:2.5)) and precipitated by cold ether. Crude peptides were purified with RP-HPLC and then lyophilized and stored at -20°C.

Minimum Inhibitory Concentration (MIC)

The MIC of TiBP-AMP was determined spectrophotometrically against *S. mutans* bacteria. Bacteria were cultivated and grown to mid-log phase. Serial dilutions, beginning at 256μM peptide concentration, were added to wells containing a final bacterial concentration of $1x10^7$ CFU/mL in a 96 well plate and grown at 37°C for 24 hours. Absorbance at 600nm was monitored using a Cytation3 microplate reader. Control samples consisted of $1x10^7$ CFU/mL bacteria only.

Titanium Implant Disc Preparation

Coin-shaped titanium implant discs, 10mm in diameter and 0.5mm thick, made from grade 4 titanium (USC Engineering Shop) were lap polished and grit blasted with 180-220 micron titanium dioxide particles and cleaned following a published protocol [56]. Briefly the cleaning protocol was to sonicate the discs in water, 70% ethanol, 40% sodium hydroxide, 50% nitric acid followed by rinsing with water and autoclaving prior to use.

Bacterial Culture and Maintenance

Streptococcus mutans ATCC 700610 was cultured according to the ATCC protocol in Brain Heart Infusion (BHI) broth (BD Difco). Several drops of rehydrated frozen stock of the bacteria were streaked on a BHI agar plate and incubated for 24 hours at 37°C and 5% CO_2. A single colony was removed from the agar plate and used to inoculate 5 mL of appropriate media followed by incubation overnight. Bacteria were grown to mid-log phase with a final concentration of 10^7 CFU/mL.

Bifunctional Peptide Binding on Titanium Discs

New, sterile titanium discs were functionalized with bifunctional peptides by incubation of the disc with a peptide solution at 37°C. Specifically, 100µL of a 100µM concentration of bifunctional peptide for TiBP-AMP and C-AMP. Following incubation the discs were washed in a 24 well-plate by pipetting 400µL of DI onto the wall of a well containing the disc and then removing the H_2O. Each disc was washed three times. The same procedure was repeated for the re-binding step for disc fouled/cleaned of bacteria.

Fluorescent Imaging for Peptide Binding

Peptide binding was evaluated by pipetting 20µL of Pierce fluorometric peptide labeling reagent directly onto the previously peptide film coated disc surface and incubating at room temperature, protected from light for five minutes. The discs were washed by holding the disc with forceps and pipetting water at a 45° angle, allowing the water to flow across the disc face. The discs were transferred to glass microscope slide, inverted, and imaged using an inverted fluorescent microscope (Zeiss Axioplus). The fluorescent images were saved both as a 2D representation, and a 3D representation in which the z-axis height corresponds to fluorescent intensity. Peptide binding was quantified as percent surface coverage using ImageJ software version 1.52a.

Peptide Film Antibacterial Function on Titanium Discs

Peptide functionalized discs were evaluated for antibacterial efficacy against *S. mutans* using the BacLight Live/Dead assay kit to differentiate living from dead bacteria present on the disc surface with selected bifunctional peptides compared to a water control. *S. mutans* (ATCC 700610) bacteria were grown and cultivated according to ATCC

protocols. 400µL of $1x10^7$ CFU/mL *S. mutans* bacteria were incubated with the functionalized discs for 4 hours, then washed with 0.85% NaCl, according to manufacture recommendations, to remove any phosphates that could interfere with the Live/Dead stains. A solution of 30% stain (1:1 ratio of PI to SYTO9) in 70% 0.85% NaCl solution was used to stain bacteria on the disc surface. The discs were then transferred to a glass microscope slide and inverted for fluorescence microscopy. Images of five unique locations on the discs were collected with 10X magnification.

Implant Disc Cleaning for Rebinding

Discs were cleaned to remove bacteria, peptide and salts using a method that is common to implant retreatment visit. An electric toothbrush with a round head slightly larger than the diameter of the disc was secured in a laboratory stand. A Petri dish filled with peri-plast wax was used as a base for insertion of 30 gauge needles in a triangle configuration surround the disc to prevent motion of the disc when the electric toothbrush was applied with 100g of force 10 Cm from the secured pivot point. A 1:10 solution of sodium hypochlorite was pipetted into the Petri dish and the disc was brushed for 2 minutes and then removed and washed thoroughly with water. The disc was then air dried in a sterile laminar flow hood in preparation of peptide rebinding. The rebinding protocol is identical to the initial binding protocol.

Retreatment Cycle Binding and Reapplication

A solution of 33µM of TiBP-AuBP in phosphate buffered saline was pipetted onto a titanium disc and incubated at room temperature for one hour. Discs were washed once with DI H_2O and then dried at room temperature. A solution of 50 nm gold nanoparticle

(AuNP) (Ted Pella Inc, USA) was incubated at room temperature on the peptide-functionalized disc for 20 minutes. The discs were washed once with DI H_2O and dried at room temperature. Next, a solution of 8 μM green fluorescent protein-gold binding peptide fusion (GFPuv-AuBP) was incubated on the surface for 20 minutes, washed, dried and imaged using a fluorescence microscope (Zeiss Axioplus). The same procedure was applied for four repetitions of fouling/cleansing. All images were analyzed with ImageJ software (version 1.52a).

Surface Profilometry

3D surface measurements of the discs were visualized using a white light profilometer (Veeco Wyko NT 1100 Optical Profiler). Pictures were taken at 5x, 10x and 50x magnification. Non-over-lapping pictures were taken of the disc. In order to obtain images from the same disc coordinates, a grid was etched onto a glass slide that repeatedly orients the disc in the same orientation and position. The profilometer was then manipulated to ensure the same region of the disc is imaged for consistency and reproducibility.

De Novo Peptide Structure Prediction and 3D Model Generation from Amino Acid Sequence

The de novo 3D structural modeling approach available through the online service, PEP-FOLD 3.5 was implemented to generate PDB models for the five best models of each bifunctional peptide amino acid sequence [4]. PEP-FOLD 3.5 generates 3D structural conformations of linear peptides between 5-50 amino acids and provides PDB models for the 5-best structures. PEP-FOLD 3.5 generates peptide structures by assigning one of 27

structural alphabet (SA) terms to fragments of four amino acids overlapping by three. The SA generalizes the secondary structure by assigning geometric descriptors emitted by the Hidden Markov model described by Maupetit, et. al. [5]. 3D models are then generated from the fragments using a course grained representation and refined by 30,000 Monte-Carlo steps. The chimeric peptide sequences were input into the PEP-FOLD 3.5 online service and 200 simulations were run assuming aqueous conditions and neutral pH. Once generated, the models were clustered and sorted using sOPEP (Optimized Potential for Efficient Structure Prediction) [7]. None biased modeling was applied.

3D Model Visualization and Recoloring

Protein Data Bank (PDB) files containing the secondary structure models generated by PEP-FOLD 3.5 were visualized and further analyzed by UCSF Chimera [8]. The structures were colored according to the peptide domains comprising the bifunctional peptides. The first functional domain was colored blue, the spacer was colored black, and the second functional domain was colored red. The structures were oriented so that the first functional domain was located at the bottom. The surface was added to the ribbon structure and a transparency of 80% was applied.

RESULTS

Antibacterial Activity in Solution

The bacterial growth curves of *S. mutans* bacteria grown in the presence of serial dilutions of TiBP-AMP are depicted in Figure 4-1. The minimum concentration of TiBP-AMP to inhibit *S. mutans* bacterial growth was found to be 64μM. The lowest

concentration evaluated, 8μM showed no bacterial inhibition, and in contrast, 256μM resulted in no growth of *S. mutans*.

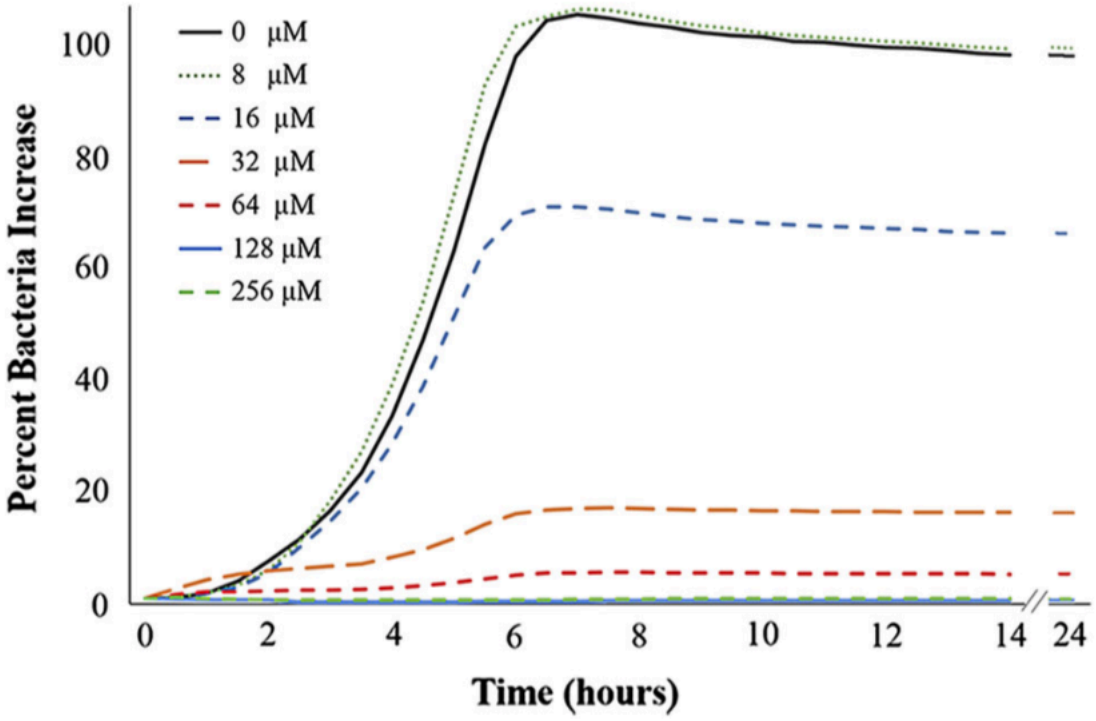

Figure 4-1:MIC of TiBP-AMP. Concentration of TiBP-AMP peptide in solution required to inhibit bacterial growth of *Streptococcus mutans.* Growth was measured every 30 min for 24 hours by absorbance at 600 nm and plotted as growth curves representing the increase of bacteria over time. The inhibitory concentration for TiBP-AMP was determined to be 64 μM.

Implant Disc Preparation and Cleansing

Discs were cleaned with a method common to periodontal therapy [159,160] and one that does not adversely affect clinical attachment. Hypochlorous acid (NaOCl) and a rotary electric toothbrush were used as a clinically relevant cleaning method to allow a rebinding of bifunctional peptide film to the implant surface.

Binding and Re-binding of the Bifunctional Peptide

The top panels of Figure 4-2 depict TiBP-AMP and Control-AMP (AMP without the TiBP domain) binding on titanium discs. Binding was quantified as a percent surface coverage and determined to be 46.8% for TiBP-AMP and 0.2% for the Control-AMP (Table 4-1). Re-binding following bacterial fouling and a clinically relevant cleaning procedure is shown in the middle panels of Figure 4-2. The cleaned disc was recoated with the same peptides and surface coverage for TiBP-AMP was determined to be 28.5% (Table 4-1) compared to 0.2% for Control-AMP (Table 4-1). After bacterial fouling, cleaned discs retained 60% of the original binding capacity. The absence of binding for the control bifunctional peptide to the cleaned discs demonstrates scant amounts of non-specific adherence of the peptide to bacterial debris.

Antibacterial Functionalization on Implant Discs

The discs were purposely inoculated with *S. mutans* to represent implant fouling in order to evaluate peptide film surface coverage for dental implant surfaces. The lower panels of Figure 4-2 show the difference in antibacterial properties between discs treated with the TiBP-AMP versus Control-AMP. The percent surface coverage of dead bacteria on the TiBP-AMP disc was 19.3% compared to 0.2% for the control (Table 4-2). There was a significant difference of 53.3% living bacteria on the control disc compared to 1.7% on the disc TiBP-AMP (Table 4-2).

Retreatment Cycle Binding and Reapplication

Figure 4-3 shows binding on titanium discs fouled up to 4 times. The bifunctional peptide, TiBP-AuBP was disclosed by incubation with gold nano-particles that bound to

the AuBP (gold binding peptide). A fusion protein with green fluorescent protein GFP_{uv}-AuBP was then used to identify peptides via the GFP fluorescent signal that were bound to the AuNPs on TiBP-AuBP film attached to the titanium disc surface. Minimal to no fluorescence was observed for bare titanium discs, for discs functionalized with TiBP-AuBP+AuNP, and no signal for discs functionalized with GFP_{uv}-AuBP fusion protein only. The fluorescence of the discs was measured using ImageJ and the results for TiBP-AuBP + AuNP + GFP_{uv}-AuBP are depicted in Table 4-3.

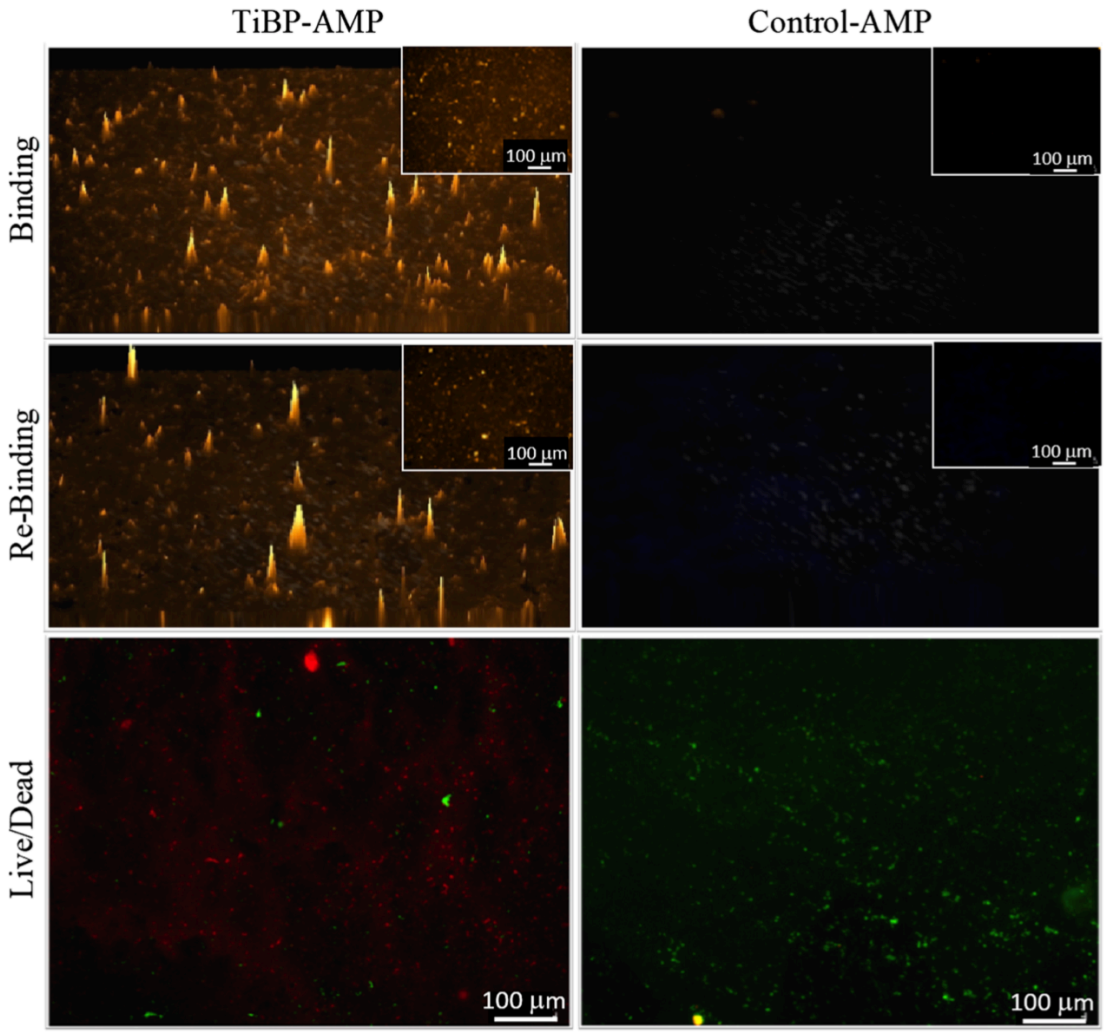

Figure 4-2: Fluorescence microscopy images of bifunctional peptide binding and antimicrobial activity on titanium implant discs. Binding and rebinding with 100 µM of either bifunctional peptide was identified with a fluorescent dye. In the larger 3D images, the z-axis height corresponds to fluorescence intensity, while the smaller insert images correspond to 2D representations. Rebinding was performed on a once-fouled *S. mutans* implant disc. The antibacterial properties of the bifunctional peptides against *S. mutans* are shown using a Live/Dead (L/D) assay to differentiate live (green) from dead (red) bacteria present on the disc surface. Scale bar = 100 µm.

De Novo Secondary Structure Generation

Secondary structures were generated for the three bifunctional peptides studied herein. The secondary structures for TiBP-AMP, Control-AMP, and TiBP-AuBP are depicted in Figure 4-4. The domains were recolored, so that blue indicates the first

functional domain (TiBP or Control), black indicates the spacer, and red indicates the second functional domain (AMP or AuBP).

Table 4-1: Quantitative results for the binding and rebinding of the bifunctional peptides shown in Figure 4-2

	TiBP-AMP (%)	Control-AMP (%)
Bind	46.8	0.2
Rebind	28.5	0.2

Results represent the percentage surface coverage of the peptide measured by ImageJ software analysis. Approximately 60% of the initial binding to a sterile implant disc was preserved on rebinding to a one-time *S. mutans*-fouled implant disc.

Titanium Disc Surface Topography

Surface topography characterization is summarized in Figure 4-5. The average roughness, RMS, and range are reported for bacteria fouled titanium discs after cleaning and for the TiBP-AMP after re-binding to the titanium discs. There was no significant change in the surface topography characteristics among the samples.

Table 4-2: Quantitative results from the live/dead images of *S. mutans* bacteria on implant discs treated with bifunctional peptides shown in Figure 4-2.

	TiBP-AMP (%)	Control-AMP (%)
Live	1.7	53.3
Dead	19.3	0.2
Total coverage	21.0	53.5

Results represent the percentage surface coverage of live and dead bacteria measured by ImageJ software analysis. TiBP-AMP resulted in a more effective antibacterial and anti-biofouling surface, represented by a higher percentage coverage of dead bacteria and lower total percentage of bacterial coverage on the surface.

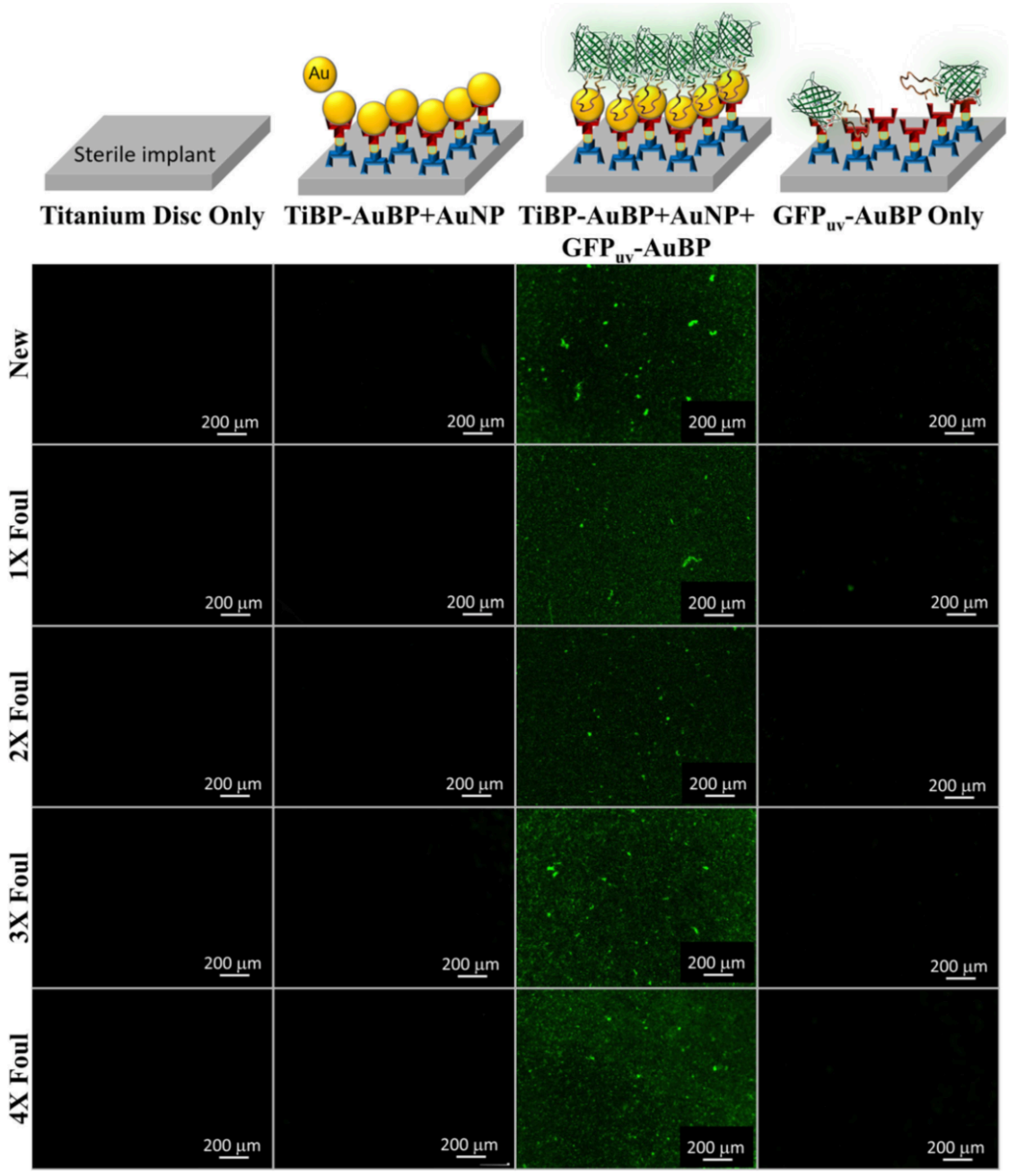

Figure 4-3: Fluorescence microscopy images of binding/rebinding on implant discs fouled multiple times by bacteria. A bifunctional peptide composed of the titanium binding peptide (TiBP) and a gold binding peptide (AuBP) was bound to the titanium disc and to gold nanoparticles (AuNP). A fusion protein, green fluorescent protein (GFPuv), fused to AuBP was subsequently bound to the AuNP immobilized on the titanium surface by the TiBP-AuBP bifunctional peptide. Schematics at the top of the figure represent the layer-by-layer assembly procedure used for imaging. After each addition, the surfaces were washed to remove any non-specifically bound peptides. Fluorescence images were obtained at each step and are shown. The procedure was repeated for multiple rounds of fouling to model multiple retreatment visits for implant surfaces affected by peri-implant disease. Scale bar = 200 µm.

Table 4-3: Fluorescence microscopy image quantification by measuring the percentage surface coverage of the images using ImageJ software.

Treatment cycle	Surface coverage (%)
Sterile	18.3
1 × foul	24.3
2 × foul	8.6
3 × foul	32.9
4 × foul	41.5

The percent surface coverage of the TiBP-AuBP + AuNP + GFPuv-AuBP assembly on titanium discs is depicted for sterile new discs and for discs fouled and then cleaned for up to four retreatment cycles.

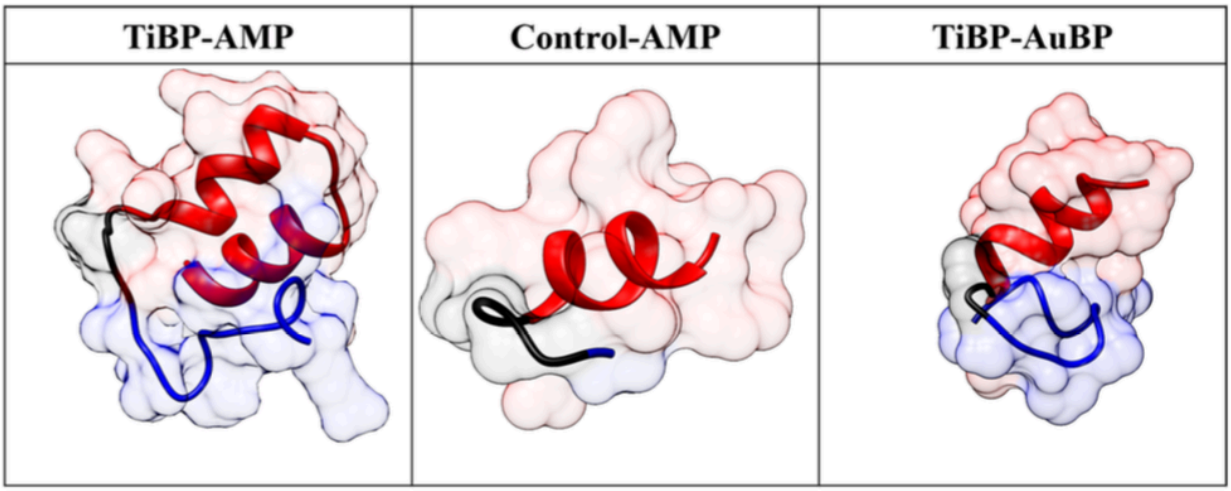

Figure 4-4: De novo secondary structures of the bifunctional peptides studied. The structures have been recolored according to the domains in each bifunctional peptide. In all structures, the titanium binding peptide is blue, the spacer peptide is black, and the antimicrobial peptide domain is red.

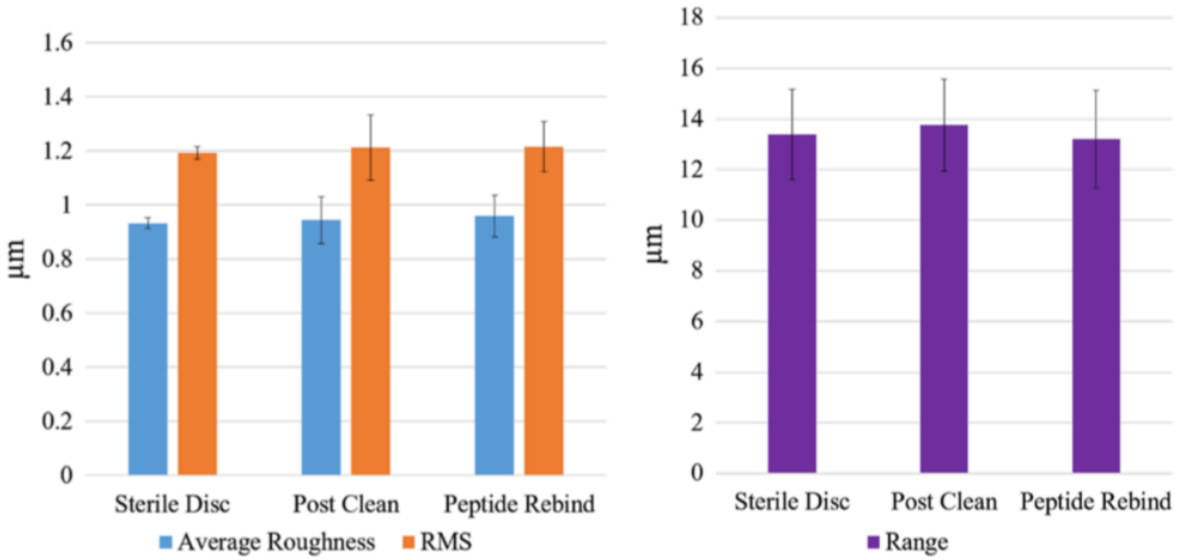

Figure 4-5: Surface topography characterization by optical profilometry . Optical profilometry images were collected and analyzed for sterile discs (Sterile), discs following bacterial fouling and the clinical cleaning procedure (Post Clean), and TiBP-AMP rebound to the fouled and cleaned disc surface. The lack of statistical difference (n = 5) for the average, RMS, and range of the roughness indicates that the surface topography prepared as an optimized surface for osteointegration was preserved through cleaning and rebinding.

DISCUSSION

In Solution Antibacterial Activity

The antibacterial activity of a TiBP-AMP was established. Critical to the success of the bifunctional peptide on the surface is the antimicrobial function of the AMP domain when joined to the anchoring domain created by a titanium binding peptide (TiBP) through an engineered spacer (Figure 4-4). The titanium binding peptide has been previously reported to effectively serve as a self-assembling anchor for bifunctional peptides [50,103,161]. Similarly, we have previously established the importance of engineering the design of the spacer to optimize the function of the antimicrobial peptide domain in the bifunctional peptide construct [161]. The spacer serves as a link between two functional domains that is designed to preserve the secondary structure for each individual domain, a parameter that is tightly linked to antimicrobial function. Here, a novel AMP domain obtained from the

literature was linked to the TiBP through a "spacer5" to create a bifunctional peptide as previously studied [161]. However, the antimicrobial, AMPA has not been used in a bifunctional peptide design and was selected through a rational design process based on previously determined antimicrobial "rules" [50]. The bifunctional peptide can be evaluated against other oral pathogens with significant influence in the initiation and progression of peri-implant disease. Other keystone periodontal pathogens that could be evaluated include *P. gingivalis, A. actinomycetemcomitans, T. forsythia, T. denticola, and P. intermedia*. As more data is obtained on the function of this peptide construct against oral pathogens, the same "rule" induction method can be applied to elucidate peptide secondary structure features that are predominant in effective peptides against bacteria in addition to *S. mutans.* The minimum inhibitory concentration for the TiBP-spacer5-AMPA bifunctional peptide was established at 64μM for an ATCC line of *S. mutans* (Figure 4-1).

Binding and Re-binding of the Bifunctional Peptide

TiBP-AMP is designed to incorporate a high-affinity titanium implant anchoring peptide with an antimicrobial peptide linked through a spacer designed to preserve the function of each peptide. The data demonstrates that the selected spacer design provides not only preserves antimicrobial activity, but also preserves robust anchoring activity to the implant surface through the TiBP domain as seen during repeated retreatment of cleansed bacteria fouled surfaces as would occur for implants already placed in the jaws (Figure 4-2, Table 4-1).

TiBP-AMP can be repeatedly applied to a bacteria fouled implant surface to deliver antimicrobial properties to address the etiopathogenesis for peri-implant disease. In contrast, the Control-AMP (without TiBP) shows minimal absorption to the surface of

bacteria fouled and cleansed titanium discs (Figure 4-2, Table 4-1). Low binding to fouled/cleaned titanium surfaces finding indicates that peptide binding is not due simply to non-specific adherence/absorption to the implant surface, nor to any bacteria debris (biopolymers) retained on the fouled surface. The data demonstrates that using maintenance procedures known and followed at professional recall appointments [159,160], that currently available anti-microbial peptide design can be successfully re-applied and is anchored to the surface of a previously fouled and cleaned implant surface.

Antibacterial Functionalization on Implant Discs

Antibacterial function and titanium anchoring function were both demonstrated simultaneously on discs functionalized with TiBP-AMP when challenged with *S. mutans* bacteria. The TiBP-AMP film successfully demonstrated an antibacterial function with 19.3% dead bacteria, compared to 0.2% for the Control-AMP. Additionally, the TiBP-AMP peptide film was antibiofouling with 21% total surface coverage by bacteria (living and dead) compared to 54% with the control peptide treated disc. Bifunctional peptides have previously been used as antibacterial surface agents; however, we demonstrate antibacterial and antibiofouling activity following re-binding with a procedure that could clinically be performed during a professional retreatment appointment. This technology is an advancement in the field over passively absorbed molecules subject to leaching and poor performance challenges [50,103,147-152]. A water-deliverery system for the bifunctional peptide completely eliminates the need for biologically hostile coupling environments typically required for chemically coupling the bioactive molecule [153-155]. The capacity to deliver a water-based bifunctional peptide to implants that have been previously placed in

the jaw is a paradigm shift, allowing potentially limitless retreatment opportunities to control oral biofilms during the life of the implant.

Retreatment Cycle Binding and Reapplication

A novel method for disclosing peptide anchored on the implant surface was demonstrated in Figure 4-3. This method ensures specific identification of the bifunctional peptide of interest on a titanium surface prepared for integration with the bone. This technique also ensures that the bifunctional peptide, TiBP-AuBP alone was identified avoiding noise from non-specific interactions with bacterial biopolymers on the disc surface. The specificity of detection was preserved following bacterial fouling for up to 4 cycles of fouling/cleansing. The quantitation of the peptides bound to the discs demonstrates that precise binding to the titanium surface is preserved. Furthermore, the data demonstrates that the amount of peptide bound generally increases slightly with each successive fouling cycle, with the exception of cycle 2. The demonstrated preservation of the TiBP to anchor to the surface strengthens the impact of this technology as a non-surgical, water based retreatment option for peri-implant disease. Multiple retreatment procedures can be performed, extending the lifetime of the implant.

De Novo Secondary Structure Generation

The secondary structures generated demonstrate preservation of the α-helix character of the antimicrobial domain, which has previously been linked to antimicrobial function. The engineered spacer is critical to preserving the function of the antimicrobial and binding domains.

Titanium Disc Surface Topography

Titanium implant discs were prepared by grit blasted with 180-220 micron titanium dioxide particles [54-56,60] and sterilized by following a widely used protocol similar to that used by implant manufactures to create "active osteointegration" surfaces [60]. Biocompatibility is an essential feature for all implant surfaces and preserving the surface properties is a mandatory design requirement. The average roughness, RMS and range parameters did not significantly change after fouling and cleaning for re-treatment, and after re-binding of the bifunctional peptide film (Figure 4-5). This result supports the advantage of this approach to not only create an antibacterial and anti-biofouling implant surface, but also one that is competent to support osteointegration and is similar to standards for surface topography currently favored by implant manufactures.

CONCLUSION

A water-based, non-surgical approach to address peri-implant disease using a bifunctional peptide film applied during the initial implant placement for new implants or at the time of retreatment for existing implants was demonstrated. Function of the TiBP and AMP domains linked by an engineered spacer in a bifunctional peptide was confirmed through identification of minimal inhibitory concentration in solution, as well as by surface antimicrobial activity. More so, this simple cleansing protocol likely preserved the biocompatibity of the titanium implant while reexposing the titanium surface after bacterial fouling to sufficiently permit rebinding of the bifunctional peptide. The re-bound bifunctional TiBP-AMP peptide film supported antibacterial and anti-biofouling activity over 4 fouling/cleaning cycles. This technology represents a paradigm shift in the

prevention of dental implant failure while adding to the range of bioactive molecules that can be used anchored to implant surfaces to improve their function.

CHAPTER 5 – CONCLUSION

The use of titanium dental implants is increasing and consequently the prevalence of implant failure and resulting diseases such as peri-implant disease. The failure of implants due to untreated and unresolved peri-implant disease will adversely impact public health, trigger increased health care costs, and result in tooth loss contributing to mortality in an aging population. The overall aim of this thesis was to develop a bio-enabled peptide film approach to combat implant failure by designing and engineering bifunctional peptides. The bifunctional peptide joins two independent biologically functional peptide domains on a single polypeptide chain through an engineered amino acid spacer. In this thesis, titanium binding peptide (TiBP) and three unique antimicrobial peptides (AMPs) were joined through a novel engineered amino acid spacer, GSGGG.

Several examples of bifunctional peptides on titanium medical implants can be found throughout the academic literature, with significant contributions coming from our group. Building upon the expertise demonstrated by our group to link RGD integrin binding peptide and antimicrobial peptides through a simple GGG spacer, this thesis demonstrates the importance of the spacer design by evaluating a longer and more rigid spacer, GSGGG. Peptide secondary structure is closely linked to function and preservation of the secondary structure of the functional domains is critical for peptide engineering. This understanding offers an opportunity to develop and engineer spacers tailored to improving bifunctional peptide efficacy. The bifunctional peptide evaluated in Chapter 2 of this thesis was composed of previously reported AMP and TiBP domains that were linked using the improved spacer design, Spacer5 (GSGGG). Computational and experimental peptide secondary structure studies revealed an improved conservation of the TiBP domain secondary structure and produced a higher percentage of 4- and 5-amino acid α-helix

structure with Spacer5 compared to the previously reported Spacer3. The addition of a serine and glycine in Spacer5 disrupted the α-helix at the spacer region and contributed to a shorter α-helix segment confined to the AMP domain. The bifunctional peptide with Spacer3 produced an α-helix structure that extended through the spacer and into the TiBP domain. Therefore, we hypothesized that Spacer5 would be more effective as a surface-active antimicrobial based on the "rules" we previously generated for bifunctional peptides. The "rules" indicated that 4- and 5-amino acid α-helix structure is a key contributing feature to antimicrobial function.

This hypothesis was tested by evaluating antimicrobial function in solution against *S. mutans* and *S. epidermidis* bacteria. *S. mutans* bacteria is common in dental implant infections, whereas *S. epidermidis* is common in orthopedic implant infections. The in-solution results supported the hypothesis for bifunctional peptide antimicrobial effectiveness against *S. mutans* with a 3-fold decrease in the minimum concentration required to inhibit bacterial growth (MIC). However, the MIC for the bifunctional peptide with Spacer5 did not improve against *S. epidermidis.*

Next, the hypothesis was tested by evaluating the bacterial attachment on titanium foils and stock titanium implant rods. The TiBP-Spacer5-AMP bifunctional peptide film compared to bare titanium foils reduced *S. mutans* and *S. epidermidis* attachment on the titanium foils by 6- and 33-fold, respectively. A more dramatic anti-biofouling effect was observed on the titanium implant rods with a 9-fold reduction in *S. mutans* bacterial attachment and a 48-fold reduction in *S. epidermidis* bacterial attachment.

Finally, host fibroblast cell response to the bifunctional peptide film was evaluated on titanium foils and implant rods. Fibroblast cell attachment was similar on bare titanium foils and foils with the bifunctional peptide film. However, the fibroblast cells attached to

the bifunctional peptide film coated foil spread more and showed improved viability measured by an MTT metabolic assay. On the titanium implant rods, the bifunctional peptide film resulted in greater numbers of cell attachment, spreading, and viability. This promising finding demonstrated that bifunctional peptide films offer not only the opportunity to prevent bacterial attachment, but to improve host cell attachment on clinically available titanium implant materials.

The results from Chapter 2 of this thesis provided a foundation and informed the direction for the rest of the work contained here. The key conclusions from Chapter 2 were confirmation of an improved spacer design that segregates antimicrobial and binding domain secondary structure, while allowing the two bio-functions to exist on the same polypeptide chain. This improved spacer design resulted in an increase in antimicrobial function in-solution and on the implant surface against *S. mutans*. The remainder of the thesis focuses on addressing prevention of infection and treating infection on dental implants where *S. mutans* is a common bacteria leading to infection and implant failure. Further, the evaluation of host fibroblast cell response supports using bifunctional peptide films to combat bacterial infection, while allowing host cell attachment, spreading, and viability that will be critical to the long-term integration and survivability of the implant. The findings in Chapter 2 provided additional support for the "rules" previously developed and aided in the design of bifunctional peptides that are presented in Chapter 3.

The focus of Chapter 3 was the rational design of bifunctional peptides with TiBP and Spacer5 that incorporated additional antimicrobial peptide domains available in the antimicrobial peptide database (APD). Antimicrobial peptides are promising alternatives to supplement or replace the current clinical standard for infection prevention and treatment, antibiotics. Concern due to the prevalence and difficulty in treating emerging

antibiotic resistant bacterial strains has spurred efforts by funding agencies to invest in antimicrobial research and development. Development of a rational design approach for bifunctional peptides is an opportunity to incorporate AMP sequences as they are discovered with improved antimicrobial efficacy, favorable host cell response, resistance to proteolytic degradation, and to tailor the bifunctional peptide to specific bacteria for a given application. There are currently over 3600 AMPs that have been discovered in the natural world or through *in silico* design. In Chapter 3, we selected two AMPs from the APD database, GL13K and AMPA, with proven antimicrobial activity against common dental pathogens and incorporated them into bifunctional peptides through a rational design approach considering the sequence-structure-function relationships. The predictive design approach consisted of three methods: 1) sequence-based, 2) *de novo* modeling, and 3) experimental evaluation.

The sequence-based approach used a computationally efficient well-established algorithm based on the probability of an amino acid to exist in a given secondary structure called the Chou-Fasman algorithm. The Chou-Fasman algorithm indicated that TiBP-Spacer5-AMPA would contain 69% α-helix structure compared to only 50% for TiBP-Spacer5-GL13K. Based on our "rules" for bifunctional peptide design and the correlation of α-helicity and antimicrobial function, the sequence-based prediction would indicate that TiBP-Spacer5-AMPA would have a greater antimicrobial activity. Additionally, the hydrophobicity and ampipathicity information determined from the amino acid sequences were studied using two tools. The Calculate and Predict tool from the APD indicated a hydrophobic ratio of 30% for TiBP-Spacer5-AMPA compared to 26% for TiBP-Spacer5-GL13K. Generation of helical wheels showed that TiBP-Spacer5-AMPA has 10 hydrophobic residues aligned along the same surface of the α-helix in the antimicrobial

peptide domain compared to only 5 for TiBP-Spacer5-GL13K. Hydrophobicity and ampipathicity are believed to allow the AMP to penetrate a bacterial lipid bilayer and disrupt the cell membrane leading to bacterial death. These analyses further support and add additional evidence for our prediction that TiBP-Spacer5-AMPA would be a more effective antimicrobial. A prediction of backbone dynamics from the amino acid sequence using DynaMine indicate conservation of the intrinsically disordered peptide region of the TiBP. These studies of the backbone dynamics indicate availability of the TiBP to interact with the implant surface for effective anchoring, while more ordered structure exists in the AMP domains for effective bacteria killing.

De novo modeling of the bifunctional peptides revealed two α-helixes joined by a turn in the AMPA domain compared to a short α-helix in the GL13K domain. This finding was of particular interest since we have established that short 4- and 5- amino acid α-helix features are important for antimicrobial function in bifunctional peptides. TiBP-Spacer5-AMPA containing two short helix structures could provide additional interaction and penetration of the bacterial cell membrane making it more effective at killing compared to the single feature in GL13K. The computational models were further studied using Chimera and the percent identity or similarity of the TiBP and AMP domains incorporated in bifunctional peptides compared to the independent domains was determined. The TiBP domain was 91.7% conserved in both bifunctional peptides. However, the AMPA domain was only 60% conserved compared to 92.3% for the GL13K domain. This result indicates that further work could be done to improve the spacer region linking TiBP and AMPA to preserve the secondary structure of the AMPA which is linked to antimicrobial function.

Finally, the bifunctional peptides were evaluated experimentally for their potential to prevent and treat peri-implant disease. The bifunctional peptides were delivered on a

clinically relevant time scale of two minutes to achieve binding and under competition with serum proteins. Both bifunctional peptides achieved near 100% binding within two minutes. In competition with serum proteins, TiBP-Spacer5-AMPA achieved 80% surface coverage compared to 73% surface coverage achieved by TiBP-Spacer5-GL13K. Mechanical durability of the bifunctional peptide films was tested by subjecting the peptide films to brushing with an electric toothbrush for one minute. TiBP-Spacer5-AMPA was better retained on the implant disc with 75% remaining after brushing compared to 27% of TiBP-Spacer5-GL13K remaining. This suggests that the TiBP-Spacer5-AMPA bifunctional peptide film is more durable in addition to the predicted antimicrobial advantages. Durability is critical in a clinical environment as the implant surface would be brushed and cleaned to aid in bacterial or food debris removal.

Two evaluations of the bifunctional peptide films in the presence of bacteria were conducted. First, a FITC label on the peptides was used to visualize the amount of peptide remaining on the surface after 24-hour challenge with *S. mutans*. 84% of the surface remained covered by the TiBP-Spacer5-AMPA film compared to only 60% for TiBP-Spacer5-GL13K. Finally, the antimicrobial efficacy on the implant disc surface was evaluated by staining dead bacteria with PI dye. The percentage of dead bacteria on implant discs with TiBP-Spacer5-AMA was 46% compared to 10% for TiBP-Spacer5-GL13K. These results demonstrate the success of our computational design approach and suggest that the TiBP-AMPA peptide has strong potential as a treatment for peri-implant disease due to its ability to mitigate bacterial biofilm formation.

In Chapter 4, we further evaluated TiBP-Spacer5-AMPA as a treatment and re-treatment option for peri-implantitis. We report a water-based, non-surgical approach to address peri-implant disease using a bifunctional peptide film, which can be applied during

the initial implant placement and later, reapplied to existing implants to reduce bacterial growth. The bifunctional peptide approach represents an improvement over non-specific binding of antimicrobials to the implant surface, as well as a water-based strategy that allows for retreatment without the harsh chemical treatment required for covalent immobilization of antibacterial agents on the implant surface. Further, we demonstrated a clinically relevant cleaning procedure for bacterial fouled discs using a rotary toothbrush that did not disrupt the titanium surface, thus preserving the biocompatibility of the implant material. We confirmed the surface topography preservation following fouling and cleaning using optical profilometry and did not observe a change in the average roughness of the implant surface. Our bifunctional peptide was able to re-bind to bacteria fouled and cleaned titanium implant discs up to four cycles with retention of 60% of the original binding capacity. Additionally, the antibacterial efficacy of the bifunctional peptide film re-bound to the fouled and cleaned implant surface was preserved.

The technology addresses the continuing need to improve patient treatment based on the therapeutic advantages offered by titanium dental implants by presenting a solution for treatment of peri-implant disease by controlling or eliminating the bacterial biofilm on implants. In Chapter 2, we develop the importance of spacer engineering linking a TiBP and AMP and relate the improved spacer design capable of better segregating and preserving the structure of the binding and antimicrobial domains is critical for improving function of each domain in the bifunctional peptide platform. In Chapter 3, we design novel bifunctional peptides by incorporating more effective AMPs from the Antimicrobial Peptide Database using a rational design approach and show the predictive ability of using less resource and cost intensive computational methods to design improved bifunctional peptides. In Chapter 4, we demonstrate the bifunctional peptide film as a treatment and re-

treatment option for new and already placed titanium dental implants with the capability of re-binding and bringing antimicrobial activity to the implant surface following bacteria fouling and a clinically relevant cleaning procedure. This technology represents a paradigm shift in the prevention of dental implant failure while adding to the range of bioactive molecules that can be used anchored to implant surfaces to improve their function.

REFERENCES

1 Health, U. D. o. & Services, H. in *NIH Technology Assessment Conference Summary. Bethesda, Maryland: National Institutes of Health, Consensus Development Program.*

2 Al-Radha, A. S. D., Dymock, D., Younes, C. & O'Sullivan, D. Surface properties of titanium and zirconia dental implant materials and their effect on bacterial adhesion. *Journal of dentistry* **40**, 146-153 (2012).

3 Gugwad, R., Reddy, G. S., Reddy, R. G., Bhatt, R. & Nagaral, S. C. Pure titanium as an implant material: Its biocompatibility and corrosion rate-An animal study. *Clinical Dentistry (0974-3979)* **7** (2013).

4 Gepreel, M. A.-H. & Niinomi, M. Biocompatibility of Ti-alloys for long-term implantation. *J Mech Behav Biomed* **20**, 407-415 (2013).

5 Verissimo, N. C. C., Geilich, B. M., Oliveira, H. G., Caram, R. & Webster, T. J. Reducing Staphylococcus aureus growth on Ti alloy nanostructured surfaces through the addition of Sn. *Journal of biomedical materials research. Part A*, doi:10.1002/jbm.a.35517 (2015).

6 Ridgeway, S. *et al.* Infection of the surgical site after arthroplasty of the hip. *Journal of Bone & Joint Surgery, British Volume* **87**, 844-850 (2005).

7 Olsen, M. A. *et al.* Risk factors for surgical site infection following orthopaedic spinal operations. *The Journal of Bone & Joint Surgery* **90**, 62-69 (2008).

8 Mudduganga dhar, B. C., Amarnath, G. S., Sonika, R., Chheda, P. S. & Garg, A. Meta-analysis of Failure and Survival Rate of Implant-supported Single Crowns, Fixed Partial Denture, and Implant Tooth-supported Prostheses. *J Int Oral Health* **7**, 11-17 (2015).

9 Moraschini, V., Poubel, L. A., Ferreira, V. F. & Barboza Edos, S. Evaluation of survival and success rates of dental implants reported in longitudinal studies with a follow-up period of at least 10 years: a systematic review. *Int J Oral Maxillofac Surg* **44**, 377-388, doi:10.1016/j.ijom.2014.10.023 (2015).

10 Derks, J. *et al.* Effectiveness of implant therapy analyzed in a Swedish population: early and late implant loss. *J Dent Res* **94**, 44S-51S, doi:10.1177/0022034514563077 (2015).

11 Pritchard, E. M., Valentin, T., Panilaitis, B., Omenetto, F. & Kaplan, D. L. Antibiotic-Releasing Silk Biomaterials for Infection Prevention and Treatment. *Advanced functional materials* **23**, 854-861 (2013).

12 Zilberman, M. & Elsner, J. J. Antibiotic-eluting medical devices for various applications. *Journal of Controlled Release* **130**, 202-215 (2008).

13 Bernthal, N. M. *et al.* Combined In vivo Optical and μCT Imaging to Monitor Infection, Inflammation, and Bone Anatomy in an Orthopaedic Implant Infection in Mice. *JoVE (Journal of Visualized Experiments)*, e51612-e51612 (2014).

14 Sadoghi, P. *et al.* Revision surgery after total joint arthroplasty: a complication-based analysis using worldwide arthroplasty registers. *J Arthroplasty* **28**, 1329-1332, doi:10.1016/j.arth.2013.01.012 (2013).

15 Rodríguez-Cano, A., Pacha-Olivenza, M.-Á., Babiano, R., Cintas, P. & González-Martín, M.-L. Non-covalent derivatization of aminosilanized titanium alloy implants: Silver-enhanced coating of antibacterial organics. *Surface and Coatings Technology* **245**, 66-73 (2014).

16 Peng, S. & Zhu, Y. Antimicrobial Activity of Ag+-Implanted Titanium Surface Modified with Covalent Graft of a Biocompatible Polymer. *Chemistry Letters* **43**, 355-356 (2014).

17 Hickok, N. J. & Shapiro, I. M. Immobilized antibiotics to prevent orthopaedic implant infections. *Advanced drug delivery reviews* **64**, 1165-1176 (2012).

18 Ketonis, C., Parvizi, J. & Jones, L. C. Evolving strategies to prevent implant-associated infections. *Journal of the American Academy of Orthopaedic Surgeons* **20**, 478-480 (2012).

19 Chen, X. *et al.* Dual action antibacterial TiO 2 nanotubes incorporated with silver nanoparticles and coated with a quaternary ammonium salt (QAS). *Surface and Coatings Technology* **216**, 158-165 (2013).

20 Gottenbos, B., van der Mei, H. C., Klatter, F., Nieuwenhuis, P. & Busscher, H. J. In vitro and in vivo antimicrobial activity of covalently coupled quaternary ammonium silane coatings on silicone rubber. *Biomaterials* **23**, 1417-1423 (2002).

21 He, G. *et al.* Addition of Zn to the ternary Mg-Ca-Sr alloys significantly improves their antibacterial property. *J Mater Chem B Mater Biol Med* **3**, 6676-6689, doi:10.1039/C5TB01319D (2015).

22 Lin, D.-J. *et al.* In vitro antibacterial activity and cytocompatibility of bismuth doped micro-arc oxidized titanium. *Journal of biomaterials applications* **27**, 553-563 (2013).

23 Pasupuleti, M., Schmidtchen, A. & Malmsten, M. Antimicrobial peptides: key components of the innate immune system. *Critical reviews in biotechnology* **32**, 143-171 (2012).

24 Hilchie, A. L., Wuerth, K. & Hancock, R. E. Immune modulation by multifaceted cationic host defense (antimicrobial) peptides. *Nature chemical biology* **9**, 761-768 (2013).

25 Cederlund, A., Gudmundsson, G. H. & Agerberth, B. Antimicrobial peptides important in innate immunity. *Febs J* **278**, 3942-3951 (2011).

26 Li, Y., Xiang, Q., Zhang, Q., Huang, Y. & Su, Z. Overview on the recent study of antimicrobial peptides: origins, functions, relative mechanisms and application. *Peptides* **37**, 207-215 (2012).

27 Yucesoy, D. *et al.* Chimeric Peptides as Implant Functionalization Agents for Titanium Alloy Implants with Antimicrobial Properties. *JOM* **67**, 754-766, doi:10.1007/s11837-015-1350-7 (2015).

28 Yazici, H. *et al.* Biological response on a titanium implant-grade surface functionalized with modular peptides. *Acta Biomater.* **9**, 53415352, doi:10.1016/j.actbio.2012.11.004 (2013).

29 Yazici, H. *et al.* Engineered Chimeric Peptides as Antimicrobial Surface Coating Agents toward Infection-Free Implants. *ACS Appl Mater Interfaces* **8**, 5070-5081, doi:10.1021/acsami.5b03697 (2016).

30 Tamerler, C. & Sarikaya, M. Molecular biomimetics: utilizing nature's molecular ways in practical engineering. *Acta Biomater* **3**, 289-299, doi:10.1016/j.actbio.2006.10.009 (2007).

31 Tamerler, C. *et al.* Molecular biomimetics: GEPI-based biological routes to technology. *Biopolymers* **94**, 78-94, doi:10.1002/bip.21368 (2010).

32 Yucesoy, D. T. *et al.* Chimeric peptides as implant functionalization agents for titanium alloy implants with antimicrobial properties. *JOM (1989)* **67**, 754-766, doi:10.1007/s11837-015-1350-7 (2015).

33 Seker, U. O. *et al.* Adsorption behavior of linear and cyclic genetically engineered platinum binding peptides. *Langmuir* **23**, 7895-7900, doi:10.1021/la700446g (2007).

34 Fjell, C. D., Jenssen, H., Cheung, W. A., Hancock, R. E. & Cherkasov, A. Optimization of antibacterial peptides by genetic algorithms and cheminformatics. *Chemical biology & drug design* **77**, 48-56, doi:10.1111/j.1747-0285.2010.01044.x (2011).

35 Zhou, Y., Snead, M. L. & Tamerler, C. Bio-inspired hard-to-soft interface for implant integration to bone. *Nanomedicine* **11**, 431-434, doi:10.1016/j.nano.2014.10.003 (2015).

36 Wilkins, M. R. *et al.* Protein identification and analysis tools in the ExPASy server. *Methods in molecular biology* **112**, 531-552 (1999).

37 Chaudhury, S., Lyskov, S. & Gray, J. J. PyRosetta: a script-based interface for implementing molecular modeling algorithms using Rosetta. *Bioinformatics* **26**, 689-691, doi:10.1093/bioinformatics/btq007 (2010).

38 Leaver-Fay, A. *et al.* Rosetta3: An Object-Oriented Software Suite for the Simulation and Design of Macromolecules. *Methods in enzymology* **487**, 545-574, doi:10.1016/B978-0-12-381270-4.00019-6 (2011).

39 Pettersen, E. F. *et al.* UCSF Chimera--a visualization system for exploratory research and analysis. *J Comput Chem* **25**, 1605-1612, doi:10.1002/jcc.20084 (2004).

40 Pawlak, Z. ROUGH SET THEORY AND ITS APPLICATIONS TO DATA ANALYSIS. *Cybernetics and Systems* **29**, 661-688, doi:10.1080/019697298125470 (1998).

41 Grzymala-Busse, J. W. & Rzasa, W. A Local Version of the MLEM2 Algorithm for Rule Induction. *Fundamenta Informaticae* **100**, 99-116, doi:10.3233/FI-2010-265 (2010).

42 Wiedemann, C., Bellstedt, P. & Görlach, M. CAPITO—a web server-based analysis and plotting tool for circular dichroism data. *Bioinformatics*, doi:10.1093/bioinformatics/btt278 (2013).

43 Raussens, V., Ruysschaert, J. M. & Goormaghtigh, E. Protein concentration is not an absolute prerequisite for the determination of secondary structure from circular dichroism spectra: a new scaling method. *Analytical biochemistry* **319**, 114-121 (2003).

44 Socransky, S., Haffajee, A., Lindhe, J., Karring, T. & Lang, N. Clinical periodontology and implant dentistry. (2008).

45 Montanaro, L. *et al.* Scenery of Staphylococcus implant infections in orthopedics. *Future microbiology* **6**, 1329-1349 (2011).

46 Wimley, W. C. Describing the mechanism of antimicrobial peptide action with the interfacial activity model. *ACS Chem Biol* **5**, 905-917, doi:10.1021/cb1001558 (2010).

47 Fjell, C. D., Hiss, J. A., Hancock, R. E. & Schneider, G. Designing antimicrobial peptides: form follows function. *Nature reviews Drug discovery* **11**, 37-51 (2012).

48 Choi, H., Rangarajan, N. & Weisshaar, J. C. Lights, Camera, Action! Antimicrobial Peptide Mechanisms Imaged in Space and Time. *Trends in Microbiology* **24**, 111-122, doi:http://dx.doi.org/10.1016/j.tim.2015.11.004 (2016).

49 Li, M. *et al.* Toward a Molecular Understanding of the Antibacterial Mechanism of Copper-Bearing Titanium Alloys against Staphylococcus aureus. *Advanced Healthcare Materials* **5**, 557-566, doi:10.1002/adhm.201500712 (2016).

50 Yucesoy, D. T. *et al.* Chimeric Peptides as Implant Functionalization Agents for Titanium Alloy Implants with Antimicrobial Properties. *Jom* **67**, 754-766, doi:10.1007/s11837-015-1350-7 (2015).

51 Rampersad, S. N. Multiple applications of Alamar Blue as an indicator of metabolic function and cellular health in cell viability bioassays. *Sensors* **12**, 12347-12360, doi:10.3390/s120912347 (2012).

52 Costerton, J. W., Stewart, P. S. & Greenberg, E. P. Bacterial biofilms: a common cause of persistent infections. *Science* **284**, 1318-1322 (1999).

53 Aparicio, C., Gil, F. J., Fonseca, C., Barbosa, M. & Planell, J. A. Corrosion behaviour of commercially pure titanium shot blasted with different materials and sizes of shot particles for dental implant applications. *Biomaterials* **24**, 263-273 (2003).

54 Ronold, H. J., Ellingsen, J. E. & Lyngstadaas, S. P. Tensile force testing of optimized coin-shaped titanium implant attachment kinetics in the rabbit tibiae. *J Mater Sci Mater Med* **14**, 843-849 (2003).

55 Ronold, H. J., Lyngstadaas, S. P. & Ellingsen, J. E. A study on the effect of dual blasting with TiO2 on titanium implant surfaces on functional attachment in bone. *J Biomed Mater Res A* **67**, 524-530, doi:10.1002/jbm.a.10580 (2003).

56 Ronold, H. J., Lyngstadaas, S. P. & Ellingsen, J. E. Analysing the optimal value for titanium implant roughness in bone attachment using a tensile test. *Biomaterials* **24**, 4559-4564 (2003).

57 Norowski, P. A., Jr. & Bumgardner, J. D. Biomaterial and antibiotic strategies for peri-implantitis: a review. *J Biomed Mater Res B Appl Biomater* **88**, 530-543, doi:10.1002/jbm.b.31152 (2009).

58 Aparicio, C., Padros, A. & Gil, F. J. In vivo evaluation of micro-rough and bioactive titanium dental implants using histometry and pull-out tests. *J Mech Behav Biomed Mater* **4**, 1672-1682, doi:10.1016/j.jmbbm.2011.05.005 (2011).

59 Achermann G. in *Vision 2020: Simply doing more for dental professionals* http://www.straumann.com (The Straumann Group, Amsterdam, 2012).

60 Monjo, M. *et al.* Correlation between molecular signals and bone bonding to titanium implants. *Clin Oral Implants Res* **24**, 1035-1043, doi:10.1111/j.1600-0501.2012.02496.x (2013).

61 Orsini, G., Pagella, P. & Mitsiadis, T. A. Modern Trends in Dental Medicine: An Update for Internists. *Am J Med* **131**, 1425-1430, doi:10.1016/j.amjmed.2018.05.042 (2018).

62 Gungormus, M. *et al.* Cementomimetics-constructing a cementum-like biomineralized microlayer via amelogenin-derived peptides. *Int J Oral Sci* **4**, 69-77, doi:10.1038/ijos.2012.40 (2012).

63 Lopez-Piriz, R. *et al.* Current state-of-the-art and future perspectives of the three main modern implant-dentistry concerns: Aesthetic requirements, mechanical properties, and peri-implantitis prevention. *J Biomed Mater Res A* **107**, 1466-1475, doi:10.1002/jbm.a.36661 (2019).

64 Olivares-Navarrete, R. *et al.* Mediation of osteogenic differentiation of human mesenchymal stem cells on titanium surfaces by a Wnt-integrin feedback loop. *Biomaterials* **32**, 6399-6411, doi:10.1016/j.biomaterials.2011.05.036 (2011).

65 Tarnow, D. P. Increasing Prevalence of Peri-implantitis: How Will We Manage? *J Dent Res* **95**, 7-8, doi:10.1177/0022034515616557 (2016).

66 Valente, N. A. & Andreana, S. Peri-implant disease: what we know and what we need to know. *J Periodontal Implant Sci* **46**, 136-151, doi:10.5051/jpis.2016.46.3.136 (2016).

67 Salvi, G. E., Cosgarea, R. & Sculean, A. Prevalence and Mechanisms of Peri-implant Diseases. *J Dent Res* **96**, 31-37, doi:10.1177/0022034516667484 (2017).

68 Berglundh, T. *et al.* Peri-implant diseases and conditions: Consensus report of workgroup 4 of the 2017 World Workshop on the Classification of Periodontal and Peri-Implant Diseases and Conditions. *J Periodontol* **89 Suppl 1**, S313-S318, doi:10.1002/JPER.17-0739 (2018).

69 Caton, J. G. *et al.* A new classification scheme for periodontal and peri-implant diseases and conditions - Introduction and key changes from the 1999 classification. *Journal of Periodontology* **89**, S1-S8, doi:10.1002/Jper.18-0157 (2018).

70 Listgarten, M. A. & Lai, C. H. Comparative microbiological characteristics of failing implants and periodontally diseased teeth. *Journal of Periodontology* **70**, 431-437, doi:DOI 10.1902/jop.1999.70.4.431 (1999).

71 Hultin, M. *et al.* Microbiological findings and host response in patients with peri-implantitis. *Clin Oral Implan Res* **13**, 349-358, doi:DOI 10.1034/j.1600-0501.2002.130402.x (2002).

72 Quirynen, M. *et al.* Dynamics of initial subgingival colonization of 'pristine' peri-implant pockets. *Clin Oral Implan Res* **17**, 25-37, doi:10.1111/j.1600-0501.2005.01194.x (2006).

73 Dutzan, N. *et al.* A dysbiotic microbiome triggers TH17 cells to mediate oral mucosal immunopathology in mice and humans. *Sci Transl Med* **10**, doi:10.1126/scitranslmed.aat0797 (2018).

74 Derks, J. *et al.* Peri-implantitis - onset and pattern of progression. *J Clin Periodontol* **43**, 383-388, doi:10.1111/jcpe.12535 (2016).

75 Lang, N. P., Wilson, T. G. & Corbet, E. F. Biological complications with dental implants: their prevention, diagnosis and treatment. *Clin Oral Implants Res* **11 Suppl 1**, 146-155 (2000).

76 Carral, C. *et al.* Mechanical and chemical implant decontamination in surgical peri-implantitis treatment: preclinical "in vivo" study. *J Clin Periodontol* **43**, 694-701, doi:10.1111/jcpe.12566 (2016).

77 Wimley, W. C. & Hristova, K. Antimicrobial peptides: successes, challenges and unanswered questions. *J Membr Biol* **239**, 27-34, doi:10.1007/s00232-011-9343-0 (2011).

78 Hvistendahl, M. Public health. China takes aim at rampant antibiotic resistance. *Science* **336**, 795, doi:10.1126/science.336.6083.795 (2012).

79 Pruden, A. Balancing water sustainability and public health goals in the face of growing concerns about antibiotic resistance. *Environmental science & technology* **48**, 5-14 (2013).

80 Torres, M. D. T., Sothiselvam, S., Lu, T. K. & de la Fuente-Nunez, C. Peptide Design Principles for Antimicrobial Applications. *J Mol Biol*, doi:10.1016/j.jmb.2018.12.015 (2019).

81 Mao, J., Kuranaga, T., Hamamoto, H., Sekimizu, K. & Inoue, M. Rational design, synthesis, and biological evaluation of lactam-bridged gramicidin A analogues: discovery of a low-hemolytic antibacterial peptide. *ChemMedChem* **10**, 540-545, doi:10.1002/cmdc.201402473 (2015).

82 Salwiczek, M. *et al.* Emerging rules for effective antimicrobial coatings. *Trends Biotechnol* **32**, 82-90, doi:10.1016/j.tibtech.2013.09.008 (2014).

83 Raphel, J., Holodniy, M., Goodman, S. B. & Heilshorn, S. C. Multifunctional coatings to simultaneously promote osseointegration and prevent infection of orthopaedic implants. *Biomaterials* **84**, 301-314, doi:10.1016/j.biomaterials.2016.01.016 (2016).

84 Tobin, E. J. Recent coating developments for combination devices in orthopedic and dental applications: A literature review. *Adv Drug Deliv Rev* **112**, 88-100, doi:10.1016/j.addr.2017.01.007 (2017).

85 Fjell, C. D., Hiss, J. A., Hancock, R. E. & Schneider, G. Designing antimicrobial peptides: form follows function. *Nat Rev Drug Discov* **11**, 37-51, doi:10.1038/nrd3591 (2011).

86 Bayramov, D. F. & Neff, J. A. Beyond conventional antibiotics - New directions for combination products to combat biofilm. *Adv Drug Deliv Rev* **112**, 48-60, doi:10.1016/j.addr.2016.07.010 (2017).

87 Eckert, R. Road to clinical efficacy: challenges and novel strategies for antimicrobial peptide development. *Future Microbiol* **6**, 635-651, doi:10.2217/fmb.11.27 (2011).

88 Holmberg, K. V. *et al.* Bio-inspired stable antimicrobial peptide coatings for dental applications. *Acta Biomater* **9**, 8224-8231, doi:10.1016/j.actbio.2013.06.017 (2013).

89 Godoy-Gallardo, M. *et al.* Covalent immobilization of hLf1-11 peptide on a titanium surface reduces bacterial adhesion and biofilm formation. *Acta Biomater* **10**, 3522-3534, doi:10.1016/j.actbio.2014.03.026 (2014).

90 Chen, R., Willcox, M. D., Ho, K. K., Smyth, D. & Kumar, N. Antimicrobial peptide melimine coating for titanium and its in vivo antibacterial activity in rodent subcutaneous infection models. *Biomaterials* **85**, 142-151, doi:10.1016/j.biomaterials.2016.01.063 (2016).

91 Chouirfa, H., Bouloussa, H., Migonney, V. & Falentin-Daudre, C. Review of titanium surface modification techniques and coatings for antibacterial applications. *Acta Biomater* **83**, 37-54, doi:10.1016/j.actbio.2018.10.036 (2019).

92 Moussa, D. G., Fok, A. & Aparicio, C. Hydrophobic and antimicrobial dentin: A peptide-based 2-tier protective system for dental resin composite restorations. *Acta Biomater* **88**, 251-265, doi:10.1016/j.actbio.2019.02.007 (2019).

93 Moussa, D. G. *et al.* Dentin Priming with Amphipathic Antimicrobial Peptides. *J Dent Res*, 22034519863772, doi:10.1177/0022034519863772 (2019).

94 Sarikaya, M., Tamerler, C., Jen, A. K., Schulten, K. & Baneyx, F. Molecular biomimetics: nanotechnology through biology. *Nat Mater* **2**, 577-585, doi:10.1038/nmat964 (2003).

95 Peelle, B. R., Krauland, E. M., Wittrup, K. D. & Belcher, A. M. Design criteria for engineering inorganic material-specific peptides. *Langmuir* **21**, 6929-6933, doi:10.1021/la050261s (2005).

96 Heinz, H. *et al.* Nature of molecular interactions of peptides with gold, palladium, and Pd-Au bimetal surfaces in aqueous solution. *J Am Chem Soc* **131**, 9704-9714, doi:10.1021/ja900531f (2009).

97 Puddu, V., Slocik, J. M., Naik, R. R. & Perry, C. C. Titania binding peptides as templates in the biomimetic synthesis of stable titania nanosols: insight into the role of buffers in peptide-mediated mineralization. *Langmuir* **29**, 9464-9472, doi:10.1021/la401777x (2013).

98 Walsh, T. R. & Knecht, M. R. Biointerface Structural Effects on the Properties and Applications of Bioinspired Peptide-Based Nanomaterials. *Chem Rev* **117**, 12641-12704, doi:10.1021/acs.chemrev.7b00139 (2017).

99 Tamerler, C. & Sarikaya, M. Genetically designed Peptide-based molecular materials. *ACS Nano* **3**, 1606-1615, doi:10.1021/nn900720g (2009).

100 Kacar, T. *et al.* Directed self-immobilization of alkaline phosphatase on micro-patterned substrates via genetically fused metal-binding peptide. *Biotechnol Bioeng* **103**, 696-705, doi:10.1002/bit.22282 (2009).

101 Gungormus, M. *et al.* Self assembled bi-functional peptide hydrogels with biomineralization-directing peptides. *Biomaterials* **31**, 7266-7274, doi:10.1016/j.biomaterials.2010.06.010 (2010).

102 VanOosten, S. K. *et al.* Biosilver nanoparticle interface offers improved cell viability. *Surf Innov* **4**, 121-132, doi:10.1680/jsuin.16.00010 (2016).

103 Yazici, H. *et al.* Biological response on a titanium implant-grade surface functionalized with modular peptides. *Acta Biomaterialia* **9**, 5341-5352, doi:10.1016/j.actbio.2012.11.004 (2013).

104 Wisdom, C. *et al.* Repeatedly Applied Peptide Film Kills Bacteria on Dental Implants. *JOM (1989)* **71**, 1271-1280, doi:10.1007/s11837-019-03334-w (2019).

105 Warotayanont, R., Zhu, D., Snead, M. L. & Zhou, Y. Leucine-rich amelogenin peptide induces osteogenesis in mouse embryonic stem cells. *Biochem Biophys Res Commun* **367**, 1-6 (2008).

106 Warotayanont, R., Frenkel, B., Snead, M. L. & Zhou, Y. Leucine-rich amelogenin peptide induces osteogenesis by activation of the Wnt pathway. *Biochem Biophys Res Commun*, 558-563 (2009).

107 Wisdom, C., VanOosten, S.K., Boone, K.W., Khvostenko, D., Arnold, P.M., Snead, M.L., and Tamerler, C. Controlling the Biomimetic Implant Interface: Modulating Antimicrobial Activity by Spacer Design. *Journal of Molecular and Engineering Materials* **4**, 164005-164001- 116405-164015, doi:10.1142/S2251237316400050 (2016).

108 Micsonai, A. *et al.* BeStSel: a web server for accurate protein secondary structure prediction and fold recognition from the circular dichroism spectra. *Nucleic Acids Res* **46**, W315-W322, doi:10.1093/nar/gky497 (2018).

109 Wiedemann, C., Bellstedt, P. & Gorlach, M. CAPITO--a web server-based analysis and plotting tool for circular dichroism data. *Bioinformatics* **29**, 1750-1757, doi:10.1093/bioinformatics/btt278 (2013).

110 Thevenet, P. *et al.* PEP-FOLD: an updated de novo structure prediction server for both linear and disulfide bonded cyclic peptides. *Nucleic Acids Research* **40**, W288-W293, doi:10.1093/nar/gks419 (2012).

111 Shen, Y. M., Maupetit, J., Derreumaux, P. & Tuffery, P. Improved PEP-FOLD Approach for Peptide and Miniprotein Structure Prediction. *J Chem Theory Comput* **10**, 4745-4758, doi:10.1021/ct500592m (2014).

112 Maupetit, J., Derreumaux, P. & Tuffery, P. PEP-FOLD: an online resource for de novo peptide structure prediction. *Nucleic Acids Research* **37**, W498-W503, doi:10.1093/nar/gkp323 (2009).

113 Cilia, E., Pancsa, R., Tompa, P., Lenaerts, T. & Vranken, W. F. The DynaMine webserver: predicting protein dynamics from sequence. *Nucleic Acids Res* **42**, W264-270, doi:10.1093/nar/gku270 (2014).

114 Pettersen, E. F. *et al.* UCSF chimera - A visualization system for exploratory research and analysis. *Journal of Computational Chemistry* **25**, 1605-1612, doi:10.1002/jcc.20084 (2004).

115 Bulheller, B. M. & Hirst, J. D. DichroCalc--circular and linear dichroism online. *Bioinformatics* **25**, 539-540, doi:10.1093/bioinformatics/btp016 (2009).

116 Wiedemann, C., Bellstedt, P. & Gorlach, M. CAPITO-a web server-based analysis and plotting tool for circular dichroism data. *Bioinformatics* **29**, 1750-1757, doi:10.1093/bioinformatics/btt278 (2013).

117 Ji, S., Li, W., Zhang, L., Zhang, Y. & Cao, B. Cecropin A-melittin mutant with improved proteolytic stability and enhanced antimicrobial activity against bacteria and fungi associated with gastroenteritis in vitro. *Biochem Biophys Res Commun* **451**, 650-655, doi:10.1016/j.bbrc.2014.08.044 (2014).

118 Chen, X., Hirt, H., Li, Y., Gorr, S. U. & Aparicio, C. Antimicrobial GL13K peptide coatings killed and ruptured the wall of Streptococcus gordonii and prevented formation and growth of biofilms. *PLoS One* **9**, e111579, doi:10.1371/journal.pone.0111579 (2014).

119 Wisdom, C. *et al.* Controlling the Biomimetic Implant Interface: Modulating Antimicrobial Activity by Spacer Design. *Journal of Molecular and Engineering Materials* (2016).

120 Wisdom, C. *et al.* Controlling the Biomimetic Implant Interface: Modulating Antimicrobial Activity by Spacer Design. *J Mol Eng Mater* **4**, doi:10.1142/S2251237316400050 (2016).

121 Zhu, X. *et al.* Characterization of antimicrobial activity and mechanisms of low amphipathic peptides with different alpha-helical propensity. *Acta Biomater* **18**, 155-167, doi:10.1016/j.actbio.2015.02.023 (2015).

122 Wang, J. *et al.* Antimicrobial peptides: Promising alternatives in the post feeding antibiotic era. *Med Res Rev* **39**, 831-859, doi:10.1002/med.21542 (2019).

123 Cilia, E., Pancsa, R., Tompa, P., Lenaerts, T. & Vranken, W. F. From protein sequence to dynamics and disorder with DynaMine. *Nat Commun* **4**, 2741, doi:10.1038/ncomms3741 (2013).

124 Schwarz, F., Derks, J., Monje, A. & Wang, H. L. Peri-implantitis. *J Periodontol* **89 Suppl 1**, S267-S290, doi:10.1002/JPER.16-0350 (2018).

125 Chapple, I. L. C. *et al.* Periodontal health and gingival diseases and conditions on an intact and a reduced periodontium: Consensus report of workgroup 1 of the 2017 World Workshop on the Classification of Periodontal and Peri-Implant Diseases and Conditions. *J Periodontol* **89 Suppl 1**, S74-S84, doi:10.1002/JPER.17-0719 (2018).

126 Delak, K. *et al.* The tooth enamel protein, porcine amelogenin, is an intrinsically disordered protein with an extended molecular configuration in the monomeric form. *Biochemistry* **48**, 2272-2281, doi:10.1021/bi802175a (2009).
127 Lacruz, R. S. *et al.* Structural analysis of a repetitive protein sequence motif in strepsirrhine primate amelogenin. *PLoS One* **6**, e18028, doi:10.1371/journal.pone.0018028 (2011).
128 Wald, T. *et al.* Intrinsically disordered enamel matrix protein ameloblastin forms ribbon-like supramolecular structures via an N-terminal segment encoded by exon 5. *J Biol Chem* **288**, 22333-22345, doi:10.1074/jbc.M113.456012 (2013).
129 Lamiable, A. *et al.* PEP-FOLD3: faster de novo structure prediction for linear peptides in solution and in complex. *Nucleic Acids Res* **44**, W449-454, doi:10.1093/nar/gkw329 (2016).
130 Wimley, W. C. Describing the Mechanism of Antimicrobial Peptide Action with the Interfacial Activity Model. *ACS chemical biology* **5**, 905-917, doi:10.1021/cb1001558 (2010).
131 Kabsch, W. & Sander, C. Dictionary of protein secondary structure: pattern recognition of hydrogen-bonded and geometrical features. *Biopolymers* **22**, 2577-2637, doi:10.1002/bip.360221211 (1983).
132 Boone, K., Camarda, K., Spencer, P. & Tamerler, C. Antimicrobial peptide similarity and classification through rough set theory using physicochemical boundaries. *BMC Bioinformatics* **19**, 469, doi:https://doi.org/10.1186/s12859-018-2514-6 (2018).
133 Socransky, S. S. & Haffajee, A. D. The bacterial etiology of destructive periodontal disease: current concepts. *J Periodontol* **63**, 322-331 (1992).
134 Haffajee, A. D. & Socransky, S. S. Microbial etiological agents of destructive periodontal diseases. *Periodontol 2000* **5**, 78-111 (1994).
135 Listgarten, M. A. The structure of dental plaque. *Periodontol 2000* **5**, 52-65 (1994).
136 Karoussis, I. K., Kotsovilis, S. & Fourmousis, I. A comprehensive and critical review of dental implant prognosis in periodontally compromised partially edentulous patients. *Clin Oral Implants Res* **18**, 669-679, doi:10.1111/j.1600-0501.2007.01406.x (2007).
137 Kotsovilis, S., Karoussis, I. K. & Fourmousis, I. A comprehensive and critical review of dental implant placement in diabetic animals and patients. *Clin Oral Implants Res* **17**, 587-599, doi:10.1111/j.1600-0501.2005.01245.x (2006).
138 Bryant, S. R. & Zarb, G. A. Outcomes of implant prosthodontic treatment in older adults. *J Can Dent Assoc* **68**, 97-102. (2002).
139 Koldsland, O. C., Scheie, A. A. & Aass, A. M. Prevalence of peri-implantitis related to severity of the disease with different degrees of bone loss. *J Periodontol* **81**, 231-238, doi:10.1902/jop.2009.090269 (2010).
140 Greenstein, G., Cavallaro, J., Jr. & Tarnow, D. Dental implants in the periodontal patient. *Dent Clin North Am* **54**, 113-128, doi:S0011-8532(09)00073-1 [pii] 10.1016/j.cden.2009.08.008 (2010).
141 Esposito, M., Grusovin, M. G., Tzanetea, E., Piattelli, A. & Worthington, H. V. Interventions for replacing missing teeth: treatment of perimplantitis. *Cochrane Database Syst Rev*, CD004970, doi:10.1002/14651858.CD004970.pub4 (2010).
142 Esposito, M., Ardebili, Y. & Worthington, H. V. Interventions for replacing missing teeth: different types of dental implants. *Cochrane Database Syst Rev*, CD003815, doi:10.1002/14651858.CD003815.pub4 (2014).
143 Derks, J. *et al.* Effectiveness of Implant Therapy Analyzed in a Swedish Population: Prevalence of Peri-implantitis. *J Dent Res* **95**, 43-49, doi:10.1177/0022034515608832 (2016).
144 Esposito, M., Grusovin, M. G. & Worthington, H. V. Interventions for replacing missing teeth: treatment of peri-implantitis. *Cochrane Database Syst Rev* **1**, CD004970, doi:10.1002/14651858.CD004970.pub5 (2012).

145 Grusovin, M. G., Coulthard, P., Worthington, H. V., George, P. & Esposito, M. Interventions for replacing missing teeth: maintaining and recovering soft tissue health around dental implants. *Cochrane Database Syst Rev*, CD003069, doi:10.1002/14651858.CD003069.pub4 (2010).
146 Louropoulou, A., Slot, D. E. & Van der Weijden, F. Influence of mechanical instruments on the biocompatibility of titanium dental implants surfaces: a systematic review. *Clin Oral Implants Res* **26**, 841-850, doi:10.1111/clr.12365 (2015).
147 Gitelman, A. & Rapaport, H. Bifunctional Designed Peptides Induce Mineralization and Binding to TiO2. *Langmuir* **30**, 4716-4724, doi:10.1021/la500310n (2014).
148 Vidal, G. *et al.* Enhanced cellular adhesion on titanium by silk functionalized with titanium binding and RGD peptides. *Acta Biomater* **9**, 4935-4943, doi:10.1016/j.actbio.2012.09.003 (2013).
149 Beyeler, M., Schild, C., Lutz, R., Chiquet, M. & Trueb, B. Identification of a fibronectin interaction site in the extracellular matrix protein ameloblastin. *Exp Cell Res* **316**, 1202-1212, doi:S0014-4827(09)00551-5 [pii]
10.1016/j.yexcr.2009.12.019 (2010).
150 Reyes, C. D., Petrie, T. A., Burns, K. L., Schwartz, Z. & Garcia, A. J. Biomolecular surface coating to enhance orthopaedic tissue healing and integration. *Biomaterials* **28**, 3228-3235, doi:10.1016/j.biomaterials.2007.04.003 (2007).
151 Auernheimer, J. *et al.* Titanium implant materials with improved riocompatibility through coating with phosphonate-anchored cyclic RGD peptides. *Chembiochem* **6**, 2034-2040, doi:10.1002/cbic.200500031 (2005).
152 Schliephake, H. *et al.* Effect of RGD peptide coating of titanium implants on periimplant bone formation in the alveolar crest - An experimental pilot study in dogs. *Clin Oral Implan Res* **13**, 312-319, doi:10.1034/j.1600-0501.2002.130312.x (2002).
153 Castner, D. G. & Ratner, B. D. Biomedical surface science: Foundations to frontiers. *Surf Sci* **500**, 28-60, doi:10.1016/s0039-6028(01)01587-4 (2002).
154 Tomsia, A. P. *et al.* Nanotechnology Approaches to Improve Dental Implants. *Int. J. Oral Maxillofac. Implants* **26**, 25-44 (2011).
155 Cranford, S. W., de Boer, J., van Blitterswijk, C. & Buehler, M. J. Materiomics: An -omics Approach to Biomaterials Research. *Advanced Materials* **25**, 802-824, doi:10.1002/adma.201202553 (2013).
156 Maia, F. R., Bidarra, S. J., Granja, P. L. & Barrias, C. C. Functionalization of biomaterials with small osteoinductive moieties. *Acta Biomater* **9**, 8773-8789, doi:10.1016/j.actbio.2013.08.004 (2013).
157 Koidou, V. P. *et al.* Peptide coatings enhance keratinocyte attachment towards improving the peri-implant mucosal seal. *Biomater Sci* **6**, 1936-1945, doi:10.1039/c8bm00300a (2018).
158 Wohlfahrt, J. C. *et al.* A novel non-surgical method for mild peri-implantitis- a multicenter consecutive case series. *Int J Implant Dent* **3**, 38, doi:10.1186/s40729-017-0098-y (2017).
159 Bizzarro, S., Van der Velden, U. & Loos, B. G. Local disinfection with sodium hypochlorite as adjunct to basic periodontal therapy: a randomized controlled trial. *J Clin Periodontol* **43**, 778-788, doi:10.1111/jcpe.12578 (2016).
160 Jurczyk, K., Nietzsche, S., Ender, C., Sculean, A. & Eick, S. In-vitro activity of sodium-hypochlorite gel on bacteria associated with periodontitis. *Clin Oral Investig* **20**, 2165-2173, doi:10.1007/s00784-016-1711-9 (2016).
161 Wisdom, C. *et al.* Controlling the Biomimetic Implant Interface: Modulating Antimicrobial Activity by Spacer Design. *Journal of molecular and engineering materials* **4**, 1640005 (2016).

APPENDIX A - PUBLICATIONS, PATENTS, AND PRESENTATIONS

PUBLICATIONS

- Wisdom C., Zhou, Y., Chen, C., Tamerler, C., and Snead, M.L. Mitigation of peri-implantitis by rational design of bifunctional peptides with antimicrobial properties. ACS Biomaterials Science & Engineering. ACS Biomaterials Science and Engineering. (2019)
- Wisdom, C., Chen, C., Yuca, E., Zhou, Y., Tamerler, C., & Snead, M. L. (2019). Repeatedly Applied Peptide Film Kills Bacteria on Dental Implants. JOM, 1-10.
- Wu, X., Mahalingam, S., VanOosten, S. K., Wisdom, C., Tamerler, C., & Edirisinghe, M. (2017). New generation of tunable bioactive shape memory mats integrated with genetically engineered proteins. Macromolecular bioscience, 17(2), 1600270.
- Wisdom, C., VanOosten, S. K., Boone, K. W., Khvostenko, D., Arnold, P. M., Snead, M. L., & Tamerler, C. (2016). Controlling the Biomimetic Implant Interface: Modulating Antimicrobial Activity by Spacer Design. Journal of molecular and engineering materials, 4(01), 1640005.

PATENTS

- Tamerler-Behar, C., Wisdom, E.C., Boone, K., 2019. Chimeric peptide for biomimetic implant interface. International Patent WO2019040517A1.
- Tamerler-Behar, C., Wisdom, E.C., Snead, M.L., 2019. Mitigation of Peri-Implantitis by Design and Stability of Bifunctional Peptides with Antimicrobial Properties. U.S. Patent Application 62/897,355.

- Carmarda, K., Tamerler, C., Boone, K., Wisdom, C., Spencer, P. Antimicrobial peptide design through rough set theory rule induction by physicochemical properties with a codon-based genetic algorithm. Provisional Application Number 62/773976. Filed November 30, 2018.
- Wisdom C., Tamerler, C. (KU) and Snead, M.L. (USC) , provisional filed, 2018

CONFERENCES AND PRESENTATIONS

- Wisdom, C., VanOosten, S., Boone, D., Arnold, P., Snead, M., Tamerler, C., Modulation of Antimicrobial Peptide Activity at the Medical Implant Interface through Chimeric Peptide Spacer Design. Bio-Nano Interfaces and Engineering Applications — Bio-Nano Interfaces: Biomedical Applications Section. The Minerals, Metals and Materials Annual Meeting, San Diego, CA, 2017.
- Wisdom, C., VanOosten, S., Boone, K., Khvostenko, D., Arnold, P., Snead, M., Tamerler, C., Biomimicking Biological Interfaces by Engineered Multi-Functional Peptides to Prevent Implant-Associated Infections, Capitol Graduate Research Summit, Topeka, KS, 2017. 1st Place Research Award, 1st Place Innovation Award
- Wisdom, C., VanOosten, S., Boone, K., Khvostenko, D., Arnold, P., Snead, M., Tamerler, C., Controlling the Biomimetic Implant Interface: Modulating Antimicrobial Activity by Spacer Design, University of Kansas Graduate Engineering Association Poster Competition, Lawrence, KS, 2016. 2ndPlace
- Wisdom, C., Lietz, R., Boone, D., Tamerler, C., Developing Bio-Nano Implant Interfaces through Chimeric Antimicrobial and Binding Peptide Design, University of Kansas School of Engineering Poster Session, Lawrence, KS, 2016.